8-2002

Correlation and Prediction of Fatigue Crack Growth Rate for different R-Ratios

Sudip Dinda

CORRELATION AND PREDICTION OF FATIGUE CRACK GROWTH RATE FOR DIFFERENT R-RATIOS

by

Sudip Dinda

A Thesis
Submitted to the
Faculty of The Graduate College
In partial fulfillment of the
requirements for the
Degree of Master of Science in Engineering(Mechanical)
Department of Mechanical and Aeronautical Engineering

Western Michigan University
Kalamazoo, Michigan
August 2002

ACKNOWLEDGMENTS

First of all I would like to thank the members of my thesis committee, Dr Daniel Kujawski, Dr Philip Guichelaar, Dr Judah Ari-Gur for taking the time to review my work. I would specially like to thank Dr Daniel Kujawski for guiding me through the entire course of my work.
I also like to thank Stoyan Stoychev and Byung-Joo Kim for their help.
I would also like to thank Nathan Mc Laughlin for his help in data analyses associated with the "master curve" approach.
Finally I must thank my family members who have always encouraged me in my work.

CORRELATION AND PREDICTION OF FATIGUE CRACK GROWTH RATE FOR DIFFERENT R-RATIOS

Sudip Dinda, M.S.E.

Western Michigan University, 2002

The prediction of fatigue crack growth rate of a structural material is an important aspect by which we can predict the critical or safe crack length and, therefore, avoid the sudden failure of components and structures.

There are numerous models which claim to predict the fatigue crack growth rate, but with the exception of the highly published "crack closure methodology" no other model lived up to the expectation of correlating the fatigue crack growth data or predicting the fatigue crack growth rate for different R-ratios.

In order to find an effective solution to the above problem a study has been conducted to discuss the difficulties associated with the existing crack closure, ΔK_{eff} methodology. A simplified fatigue crack driving force parameter, $K^* = K_{max}{}^{\alpha} (\Delta K^+)^{(1-\alpha)}$ is proposed to predict the crack growth rate for different R – ratios.

A validation on the effectiveness of the proposed crack growth parameter K^* relative to the existing crack closure approach, ΔK_{eff}, is done based on published experimental data.

In addition, another model is developed called the "master curve" approach, which also predicts the R-ratio effects on crack growth rate.

TABLE OF CONTENTS

Table of Contents-Continued

LIST OF TABLES

LIST OF FIGURES

List of Figures-continued

List of Figures-continued

1. INTRODUCTION

Fracture and fatigue are problems that are associated with load application to structures and materials. These problems have direct relation to engineering design from the time of its origin.
The systematic study of fatigue was initiated by Wohler [1], in the period of 1858-1860. He introduced the concept of the fatigue curve, which was used to define fatigue limit.

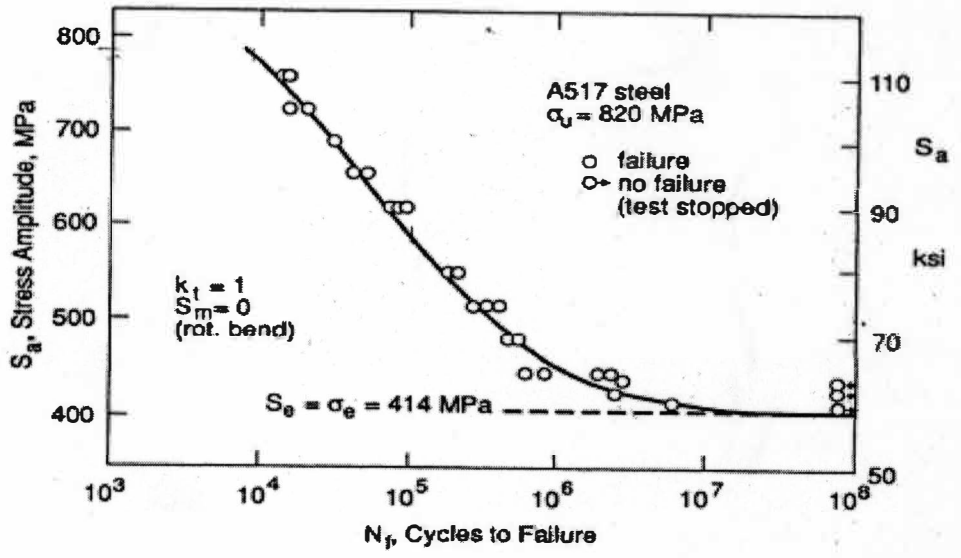

Figure 1. S-N curve for unnotched specimen of a steel specimen [2].

Some of the applications and discoveries in the field of fracture mechanics over the past few decades are listed below.
In 1956 Wells [3] used fracture mechanics to show that the fuselage failures in several Comet jet aircraft resulted from fatigue cracks reaching a critical size.
In 1957 Winne and Wundt [4] applied Irwin's energy release rate approach to predict the failure of large motors in steam turbines.

Around the year 1960 the fundamentals of linear elastic fracture mechanics (LEFM) were fairly well established and researchers turned their attention to crack tip plasticity.
Wells [5] attempted to apply LEFM to low carbon and medium strength structural steels. These materials were too ductile for LEFM but Well's [5] noticed that the crack faces moved apart with plastic deformation. This observation led to the development of the parameter known as the "crack tip opening displacement (CTOD)'.
In 1968 Rice [6] developed a parameter called J integral, which is used to characterize nonlinear material behavior ahead of the crack.
Much of the theoretical foundation of dynamic fracture mechanics was developed in the period between 1960 and 1980, when significant contributions were made by number of researchers.

1.1 FATIGUE OF MATERIALS

Fatigue of materials or structural components means damage and fracture of the structural component due to repeatedly applied stresses.
Fatigue can be classified into high cycle fatigue (HCF) and low cycle fatigue (LCF) [7].
HCF is usually accompanied by small-localized plastic deformation, while the main part of the body is deformed elastically. HCF is caused by high number of cycles, typically in the millions.
LCF is usually accompanied by elasto-plastic deformation in the bulk of the body. LCF is caused by small number of cycles typically in the thousands or less.

1.2 FATIGUE FAILURE MECHANISMS

Fatigue failure occurs due to the accumulation of damage at the localized region or regions in a material due to alternating loads, which leads to the formation of cracks and their subsequent propagation.
The sites for a crack initiation in a material under loading condition are pre-existing highly stressed regions like notches, pits and scratches.
When a crack grows to such an extent that the remaining net section is insufficient to carry the applied load, a sudden fracture takes place.
Fatigue crack surface usually has three predominant features, a crack initiation site, a crack growth surface area with distinct features, and a final fractured surface; these are shown in Fig.2.

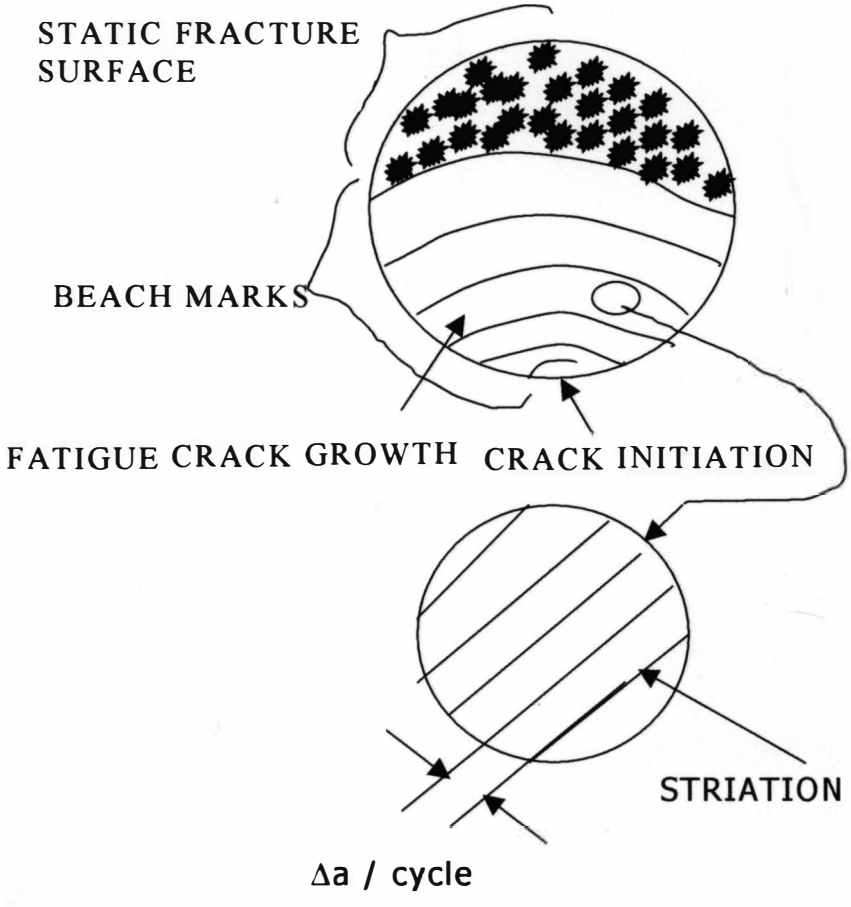

Figure 2. Features of a fatigue cracked surface.

In the absence of internal flaws the fatigue crack usually initiates at the surface of a specimen and its initial growth is generally in the direction of maximum shear stress.

1.3. CRACK GROWTH RATE

Fracture mechanics is important in life prediction of components that are subjected to time-dependent crack growth mechanism such as fatigue or stress corrosion cracking.

Crack growth can be caused by cyclic loading a behavior called fatigue crack growth. The rate of cracking can be correlated with fracture mechanics parameter such as stress intensity factor.

Failure for critical crack size can be computed if the fracture toughness is known[8].

Fatigue crack growth in metals can be described by the relationship

$$da/dN=C(\Delta K)^m \qquad (1\text{-}1)$$

where da/dN is the crack growth per cycle, ΔK is the stress intensity factor(SIF) range; C and m are material constants.

Assuming the applied loading is cyclic with constant loads P_{max} and P_{min}, the corresponding gross stresses are S_{max} and $S_{min,}$ the stress intensity factor range is given by the relationship

$$\Delta K=F\Delta S\ (\pi a)^{0.5} \qquad (1\text{-}2)$$

where

ΔK: Stress intensity factor range,

F: geometry factor, F=F(a/b),

ΔS: Gross stress range, $\Delta S = S_{max} - S_{min,}$

a: crack length,

b: component width.

The crack growth behavior for a given material can be described by the relationship that exist between da/dN and ΔK in a log-log plot as shown in

to approach a vertical asymptote denoted by ΔK_{th} which is called the threshold SIF range. This quantity is interpreted as a lower limiting value of ΔK below which the crack growth does not ordinarily occur. At high growth rates the curve again becomes steep due to rapid unstable crack growth just prior to final failure of the material, this is called the static failure region of the curve.

In the intermediate region of the curve the crack growth rate, da/dN is almost linear to ΔK and this region is called the Paris region. The Paris region is almost a straight-line plot in the log-log scale and can be represented by the equation, $da/dN=C(\Delta K)^m$ (define in page.4).

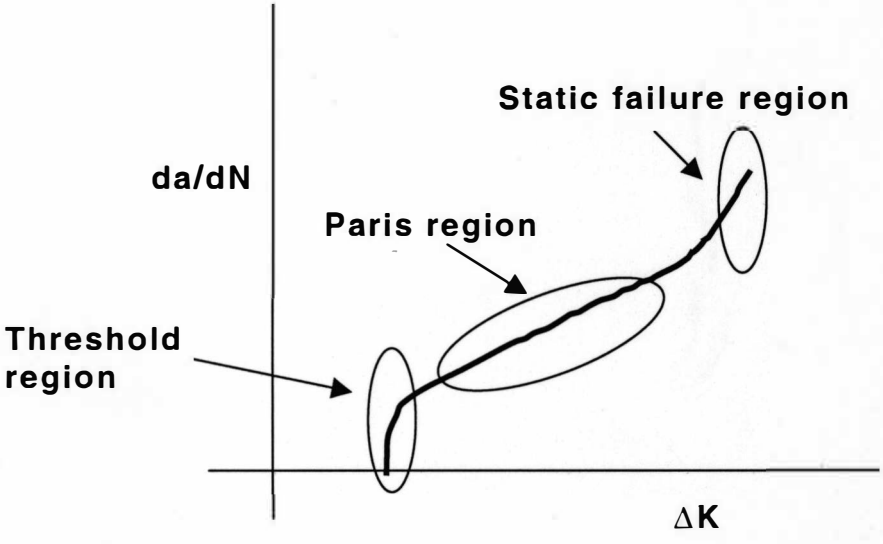

Figure 3. Illustration of fatigue crack growth rate over a wide range of stress intensities.

1.4. EFFECTS OF R-RATIOS ON FATIGUE CRACK GROWTH RATE

R-ratio is also known as the load ratio, which is defined as the ratio of K_{min}/K_{max}, where K_{min} is the minimum stress intensity factor and K_{max} is the maximum stress intensity factor.

An increase in the R-ratio of the cyclic loading causes growth rates for a given ΔK to be higher; this can be seen in Fig.4.

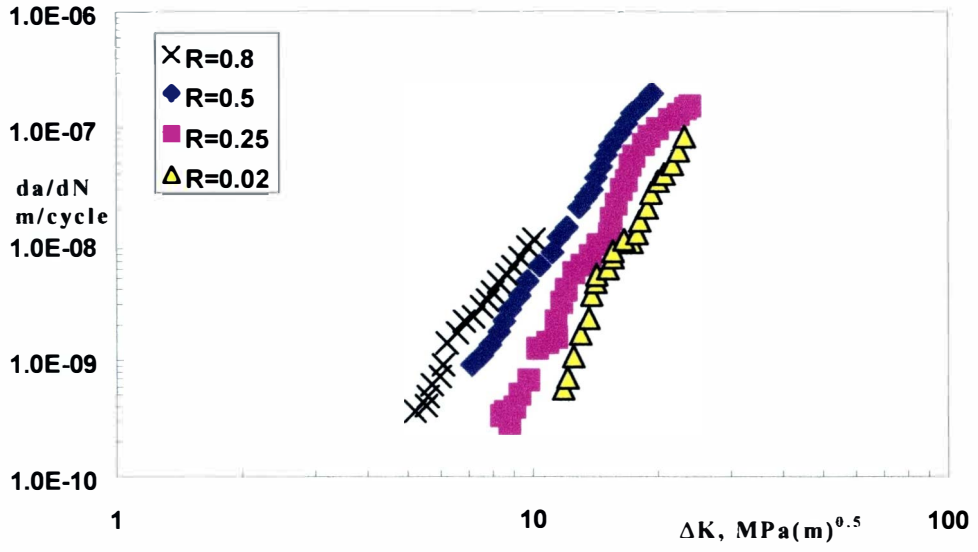

Figure 4. Fatigue crack growth data [9] of Ti 6-Al-4V as a function of ΔK.

1.5. DAMAGE TOLERANCE METHOD

Damage tolerance allows a sub critical flaw to remain in a structure. Consider a flaw in a structure that grows with time (e.g. fatigue crack or stress corrosion crack) as illustrated in the Fig.5.

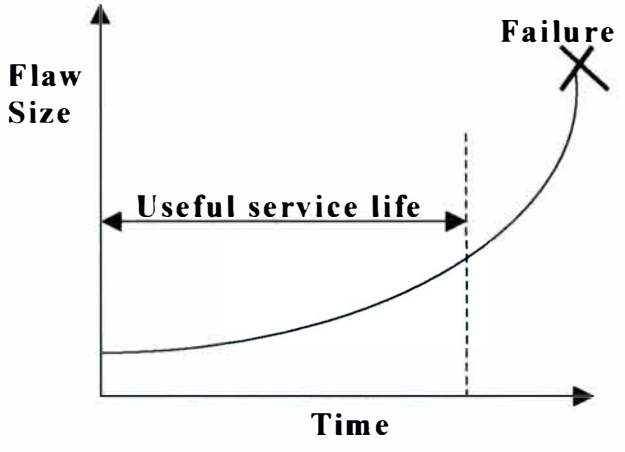

Figure 5. Damage tolerance approach.

The initial crack size is inferred from nondestructive evaluation (NDE) technique and the critical crack size is computed from applied stress and fracture toughness. Normally, an allowable flaw size would be defined by dividing the critical size by a safety factor. The predicted service life of the structure can then be inferred by calculating the time required for the flaw to grow from its initial size to its maximum allowable size.

2. DRAWBACKS OR PITTFALLS OF EXISTING CRACK CLOSURE METHODOLOGY

In 1971 Elber [10] introduced the crack closure concept, which later was widely accepted as a critical mechanism responsible for R-ratio effects in metallic materials. The crack closure concept is based on the effective stress intensity factor range, which Elber[10] defined as

$$\Delta K_{eff} = K_{max} - K_{op} \qquad (2\text{-}1)$$

Where K_{max} is the stress intensity calculated for the maximum load P_{max}. K_{op} is the stress intensity value for the crack opening load P_{op}.

Elber's [10] effective stress intensity factor (SIF) range, ΔK_{eff}, is commonly estimated by using the ASTM standard E647 recommendation. According to this recommendation K_{op} is determined as the stress intensity associated with the load that causes a 2% deviation in the slope of the load-displacement curve [8].

The effective range ΔK_{eff} is then calculated using the above equation. The above approach postulates that the load range between the opening load P_{op}, and the maximum load P_{max} will affect the crack propogation during the load cycle. However, it is observed that for low R-ratio (e.g. R=0.1), ΔK_{eff} at threshold is lower than the applied ΔK for high stress ratio (R>0.8 or higher), where crack closure is usually absent.

This is illustrated by an example given below.

Let us assume that the data for crack growth rate in terms of da/dN vs ΔK are given.

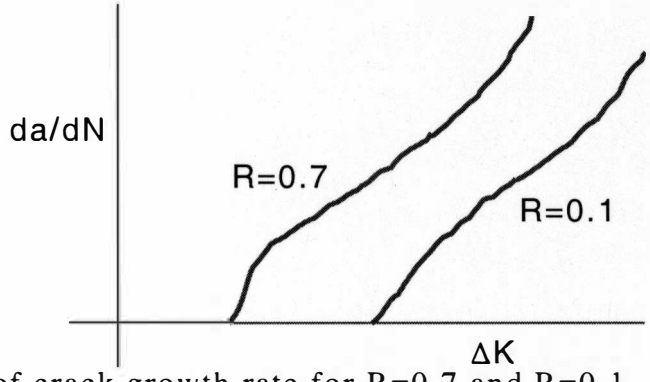

Figure 6. Illustration of crack growth rate for R=0.7 and R=0.1.

For example, at the threshold

for load ratio R=0.1; K_{max} =10 and K_{min} =1,

for load ratio R=0.7 ; K_{max} = 10 and K_{min} = 7.

Let the crack opening stress intensity factor K_{op} =6 as illustrated in Fig.7.

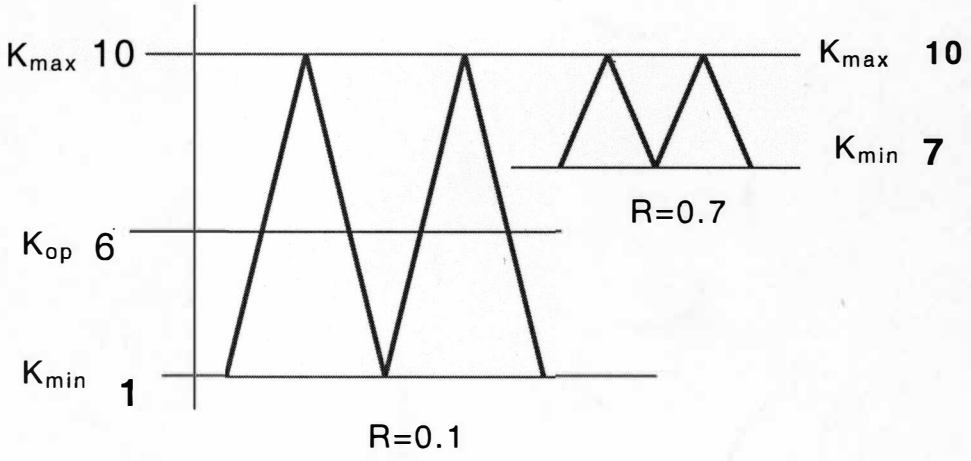

Figure 7. Load cycle diagram for R=0.7 and R=0.1.

Therefore :

For R=0.1 ; $K_{op} > K_{min}$; $\Delta K_{eff} = K_{max} - K_{op} = 4$

For R=0.7 ; $K_{cl} < K_{min}$; $\Delta K_{eff} = \Delta K_{app} = K_{max} - K_{min} = 3$

So theoretically the data should correlate in the form shown in Fig.8(a).

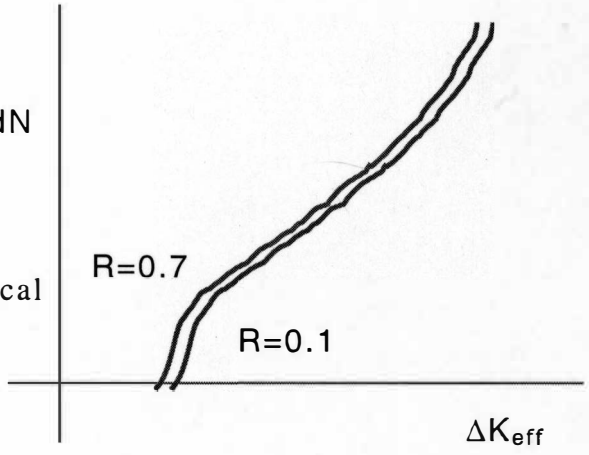

Figure 8(a). Expected theoretical correlation for the fatigue crack growth rate using ΔK_{eff} for R=0.7 and R=0.1

However, using "crack closure methodology", the correlation used in Fig.8(b) is usually obtained.

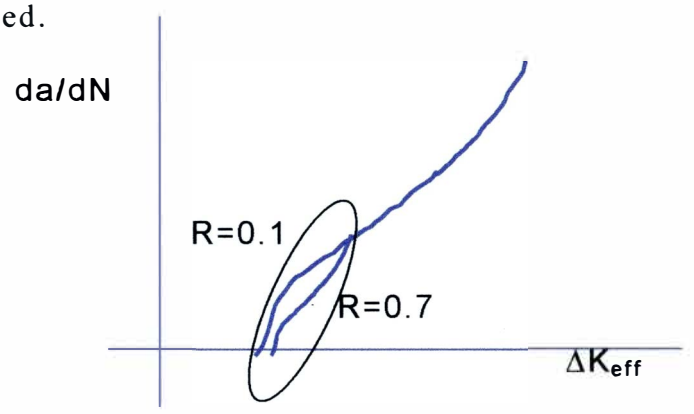

Figure 8(b). Correlation of the fatigue crack growth rate using ΔK_{eff} for R=0.7 and R=0.1.

Fig 8(b) indicates that at the threshold level (marked in the figure above) the crack growth rate for R=0.7 is lower than that of R=0.1. It is known, that higher load ratio results in higher crack growth rate, therefore at the threshold R=0.7 should yield a higher crack growth rate than R=0.1.
The above phenomenon is supported using experimental results for 2024-T3 Al alloy as depicted in Fig.9 and Fig.10.

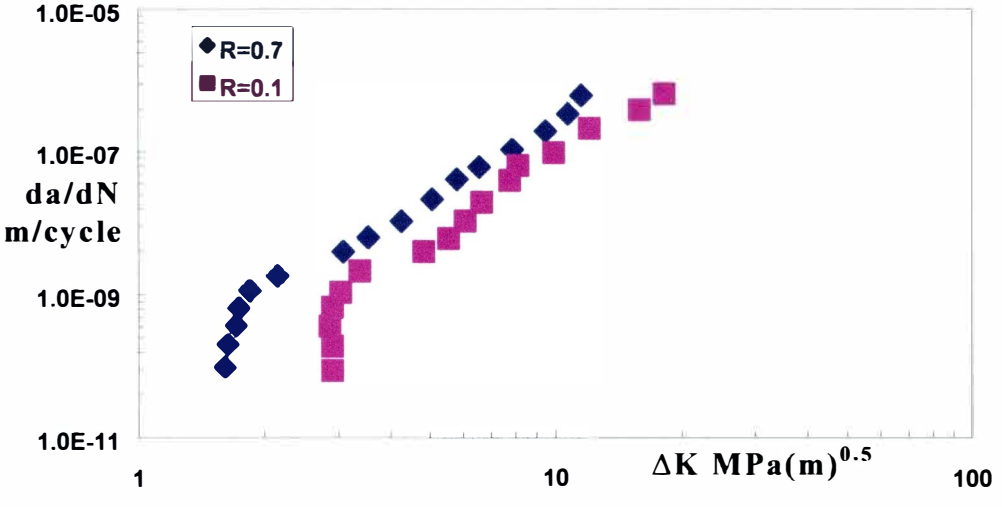

Figure 9. Fatigue crack growth data [11] of 2024-T3 aluminum alloy as a function of ΔK.

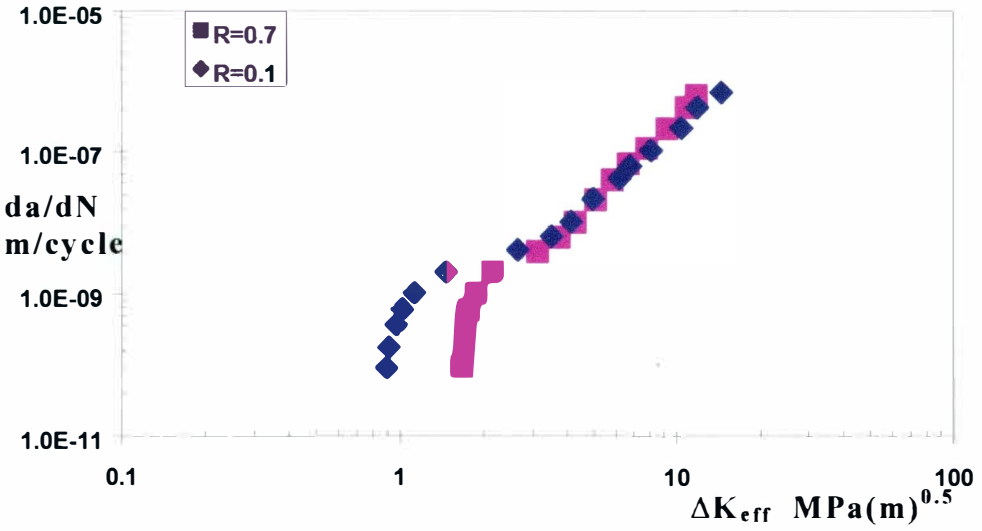

Figure 10. Fatigue crack growth data [11] of 2024-T3 aluminum alloy as a function of ΔK_{eff}.

The most important drawback of crack closure methodology is the difficulty in measuring the crack opening load.

The crack opening load depends on the measurement location and technique. From Fig.11 of load vs displacement curve one can see that there is a range on the curve where the crack is open.

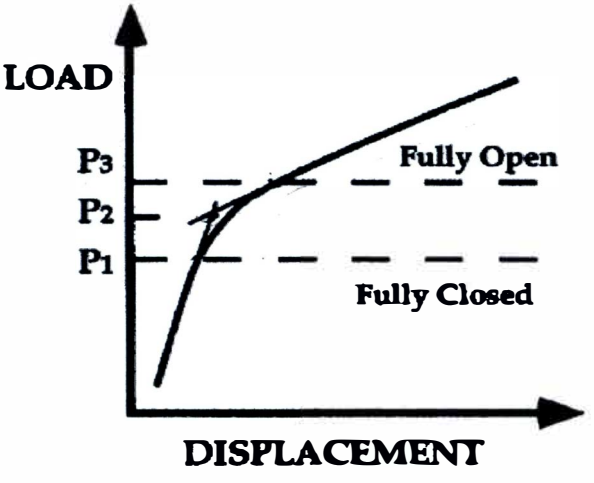

Figure 11. Load versus displacement curve[8].

Therefore, it is difficult to determine the actual load at which the crack is fully open. The load P_1 in Fig.11 represents the load at which the crack is fully closed and P_3 represents the load at which the crack is fully open, so the crack is basically open at some point between P_1 and P_2.

According to the ASTM recommendation, the stress intensity value for crack opening load K_{op} is determined as the stress intensity associated with the load that causes a 2% deviation in the slope of the load-displacement curve.

Also the stress intensity value for the crack opening load K_{op} changes with the material properties, geometry of the crack, specimen thickness and crack length[12].

According to Elber [10], ΔK_{eff} and ΔK can be related by the following relationship

$$U=\Delta K_{eff} / \Delta K \qquad (2\text{-}2)$$

where, U is the stress intensity ratio.

Therefore,

$$\Delta K_{eff} = U\Delta K, \text{ and} \qquad (2\text{-}3)$$

$$da/dN = C(U\Delta K)^m. \qquad (2\text{-}4)$$

Elber[10] postulated that U depends only on R- ratio, (e.g., U= 0.5+0.4R) which was an oversimplified assumption[13].

Other researchers observed that U depends on K_{max} , specimen thickness, microstructure, and load history.

Mc Clung [13], after doing extensive review, concluded that there are three distinct regimes of crack closure and U varies in all these three regions:

near the threshold U decreases with increasing K_{max}, in the Paris region U is independent of K_{max}, and at high ΔK values U decreases with increasing K_{max}.

So no single equation can describe closure in all the three regimes. This is a significant drawback of Elber crack closure assumption.

Donald[14] also showed that fatigue crack growth rate is not determined solely by ΔK_{eff} but also depends on K_{max}.

There are several other drawbacks associated with crack closure methodology, which Sadananda and Vasudevan [15] have discussed.

In spite of all these drawback and difficulties associated with the crack closure methodology researchers still prefer it since it correlates the R-ratio effectively into a single trend. But with simple mathematical transformation of the fatigue crack growth rate equation

$$da/dN = C(\Delta K)^m \quad (2\text{-}5)$$

one can also consolidate the data effectively into a single trend, without using the time consuming crack closure methodology.

Consider the crack growth rate data shown in Fig 12.

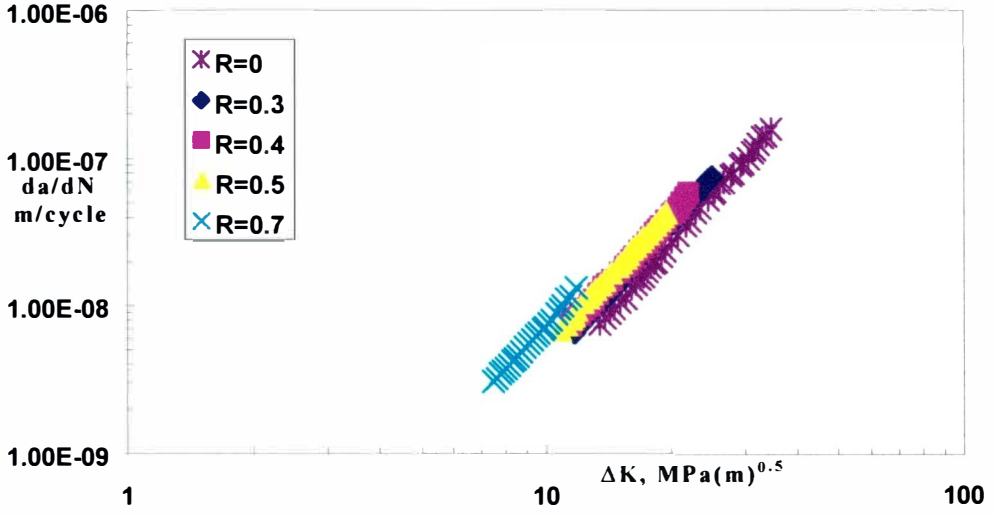

Figure 12. Fatigue crack growth data [16] of medium carbon structural steel as a function of ΔK.

The above Eq. 2-5 can be written as

$$da/dN = C_r(\Delta K_r)^m \quad (2\text{-}6)$$

where ΔK_r and C_r are the ΔK and the intercept of the R-ratio on which one wants to collapse all the other R-ratio effectively (e.i R=0.7).

For a given da/dN=constant

$$C(\Delta K)^m = C_r(\Delta K_r)^m, \text{ and} \quad (2\text{-}7)$$

$$\Delta K_r = \Delta K\,(C/C_r)^{1/m}. \quad (2\text{-}8)$$

Using the above formula (Eq. 2-8) all the R-ratios data can be collapsed effectively on R=0.7.

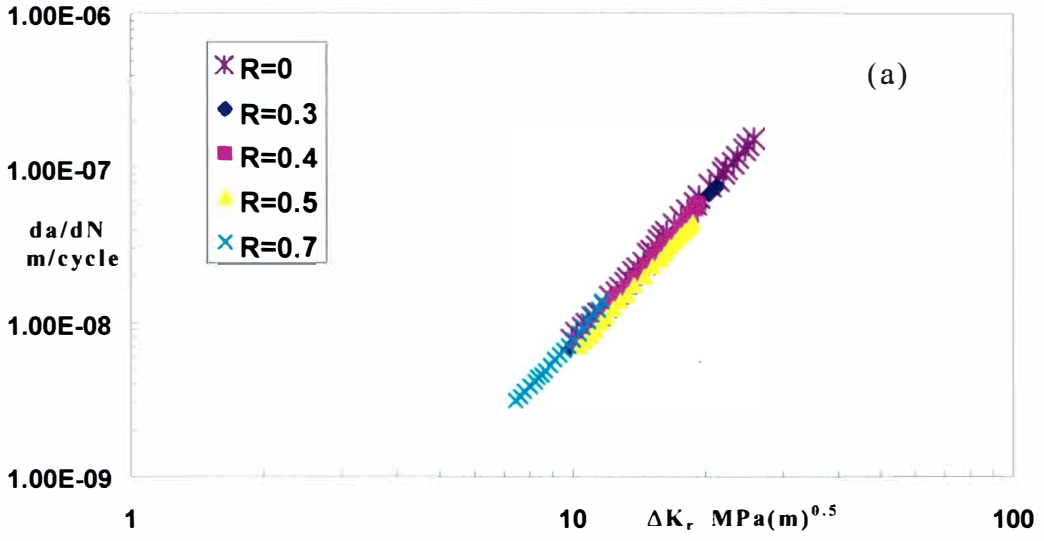

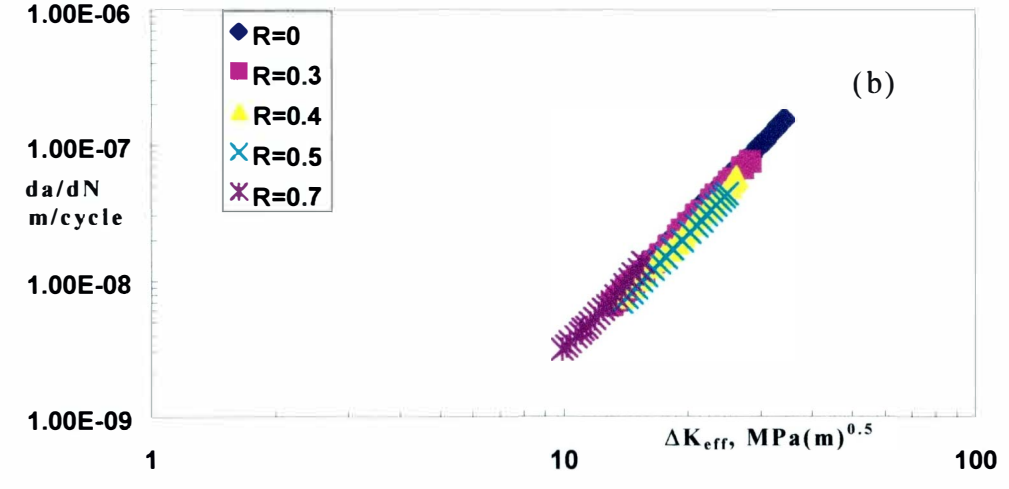

Figure 14. Fatigue crack growth data [16] of medium carbon structural steel as a function of (a)ΔK_r; (b) ΔK_{eff}.

Fig.14(a) shows the correlation obtained using Eq. 2-8 and Fig.14(b) depicts the correlation obtained using the crack closure methodology.

Figure 14(a) and 14(b) demonstrate that the above method is effective in collapsing the R-ratio data into a single line. Therefore it can be concluded that by collapsing the data effectively not necessarily proves that the crack closure method and corresponding ΔK_{eff} is sound.
With all these drawbacks and pitfalls that are enlisted above it was necessary to develop a simplified approach for R-ratio effects that will predict fatigue crack growth rate effectively..

3. METHODS FOR CORRELATING R-RATIO EFFECTS ON FATIGUE CRACK GROWTH

It is relevant that for ductile material the crack driving force is dominated by ΔK and for brittle materials by K_{max}[17]. In fact the contribution to fatigue crack driving force by ΔK and K_{max} also depends on the cyclic properties of the material, temperature and environment.

Taking all these effects into consideration a new fatigue crack driving force parameter was proposed [17], which takes into account of both ΔK and K_{max}, that is

$$K^* = (K_{max})^{\alpha} (\Delta K^+)^{1-\alpha} \qquad (3\text{-}1)$$

where α is the material parameter and K^+ is positive part of SIF range.

This is similar to modified Walker parameter [18]:

$$K = K_{max}^{(1-m)} \Delta K^{m} \qquad (3\text{-}2)$$

where m is the material parameter; K is the effective stress.

The equation proposed by Walker was valid only for positive R-ratios. However the fatigue crack driving force K* is valid for both positive and negative R-ratio.

It uses the ΔK^+ parameter, which takes into account of only the positive part of ΔK, assuming that for negative R-ratio the negative part of ΔK does not contribute to the crack growth.

The above generalization of the fatigue crack driving force K* is based on the following assumptions[17]:

(1) The damage at the crack tip process zone is an interplay of two damage processes, namely a monotonic damage due to K_{max} and a cyclic damage due to ΔK^+.

(2) The damage at the crack tip process zone is controlled by the elastic field around it.

(3) Existence of tensile stress in the process zone ($K_{max} > 0$) is a mandatory condition for the fatigue crack propagation.

3.1 METHODS FOR DETERMINATION OF MATERIAL PARAMETER α

3.1.1 FIRST METHOD

Let us consider the following relationship for K*

$$K^* = (K_{max})^{\alpha} (\Delta K^+)^{(1-\alpha)} \quad (3\text{-}3)$$

Taking log on both sides one gets

$\log K^* = \alpha \log K_{max} + (1-\alpha) \log (\Delta K^+)$,

$\alpha \log K_{max} = -(1-\alpha) \log (\Delta K^+) + \log K^*$, and finally

$$\log K_{max} = (-(1-\alpha) / \alpha) \log (\Delta K^+) + (1/\alpha) \log K^* \quad (3\text{-}4)$$

Equation 3-4 has the form of a straight line equation $y = mx+c$ (in log-log scale) where the slope m is equal to

$$m = -(1-\alpha) / \alpha. \quad (3\text{-}5)$$

The value of K_{max} can be calculated as

$$R \geq 0;\ K_{max} = \Delta K / (1-R);\ \Delta K^+ = \Delta K, \quad (3\text{-}6)$$

$$R \leq 0;\ K_{max} = \Delta K/(1-R) = \Delta K^+. \quad (3\text{-}7)$$

The value of α is determined from the slope of the log-log plot of K_{max} vs ΔK for constant da/dN. Subsequently, $\alpha_{average}$ is calculated from the various α values which corresponds to a particular da/dN. This $\alpha_{average}$ value is used in $K^* = (K_{max})^{\alpha} (\Delta K^+)^{(1-\alpha)}$ to calculate the fatigue crack driving force K*. The K* value is then used to correlate the R-ratio effects into a single trend, (refer to Fig.15 and Table 1).

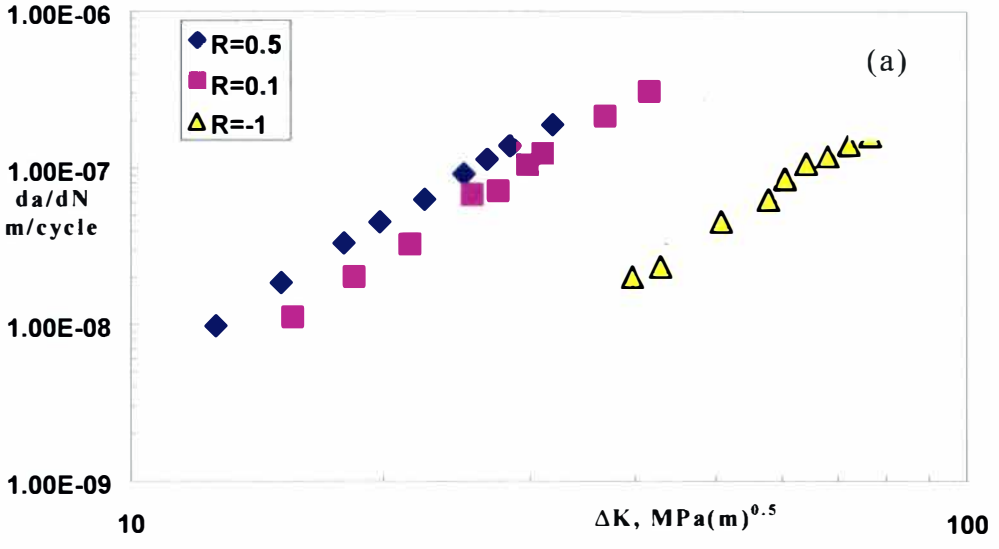

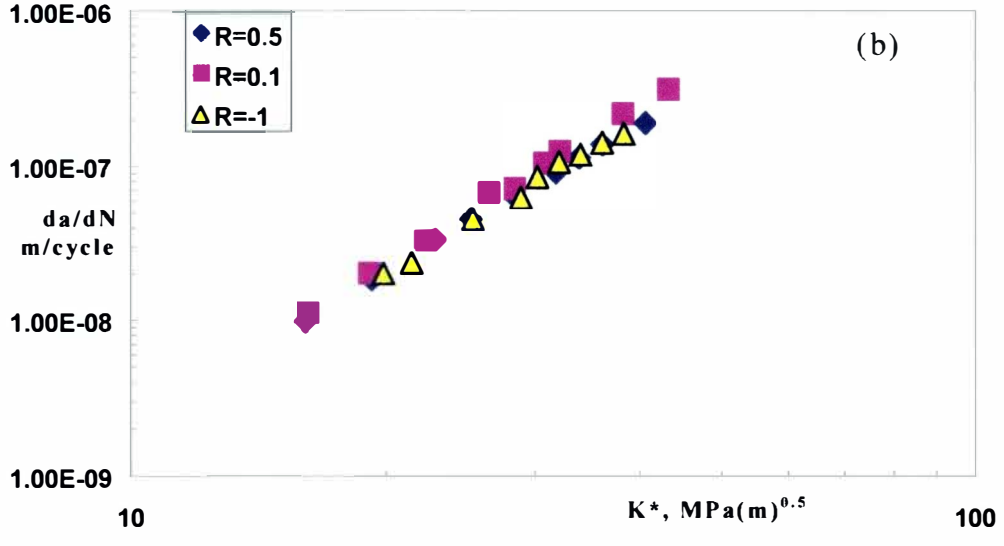

Figure 15. Fatigue crack growth data [19] of nickel based superalloy Udimet 720 as a function of (a) ΔK; (b) K*(first method).

Table 1. Calculation of α_{avg} for the first method for nickel based superalloy Udimet 720[19]

R	da/dN	ΔK	K_{max}	m	α
0.5	2E-08	15.502	31.003	-1.442	0.41
0.1	2E-08	18.66	20.734		
-1	2E-08	20.807	20.807		
0.5	3E-08	17.655	35.31	-1.595	0.385
0.1	3E-08	21.304	23.671		
-1	3E-08	23.301	23.301		
0.5	4E-08	19.115	38.231	-1.688	0.372
0.1	4E-08	22.9	25.444		
-1	4E-08	24.987	24.987		
0.5	5E-08	20.847	41.693	-1.789	0.359
0.1	5E-08	24.204	26.894		
-1	5E-08	26.924	26.924		
0.5	6E-08	22.68	45.361	-1.688	0.372
0.1	6E-08	25.521	28.357		
-1	6E-08	29.222	29.222		
0.5	7E-08	23.685	47.37	-2.044	0.329
0.1	7E-08	27.766	30.851		
-1	7E-08	30.006	30.006		
0.5	8E-08	24.616	49.232	-2.362	0.297
0.1	8E-08	28.857	32.063		
-1	8E-08	30.443	30.443		
0.5	9E-08	25.338	50.675	-2.307	0.302
0.1	9E-08	29.56	32.845		
-1	9E-08	31.487	31.487		
0.5	1E-07	26.081	52.161	-2.202	0.312
0.1	1E-07	30.063	33.403		
-1	1E-07	32.646	32.646		
				α_{avg}	0.349

3.1.2 SECOND METHOD

$K^* = (K_{max})\ (\Delta K^+)^{(1-\alpha)}$ (3-8)

since $K_{max} = \Delta K / (1-R)$,

therefore, $K^* = K_{max}(1-R)^{(1-\alpha)}$. (3-9)

Taking log on both sides yeilds

$\log K^* = \log K_{max} + (1-\alpha) \log (1-R)$

$\log K_{max} = (\alpha-1) \log (1-R) + \log K^*$ (3-10)

The Eq. 3-3 is in the form of a straight line equation $y= mx+c$ (in log-log scale) where the slope m is equal to

$m = \alpha-1$. (3-11)

Thus, α is determined from the slope of the log-log plot of K_{max} vs R for a constant da/dN.

The $\alpha_{average}$ is calculated from the various α values which corresponds to a particular da/dN.

Then, $\alpha_{average}$ value is used in $K^* = K_{max}(1-R)^{(1-\alpha)}$ to calculate the fatigue crack driving force K^*.

The above formula is for $R \geq 0$, whereas

for $R \leq 0$; $K_{max} = \Delta K^+ = K^*$. (3-12)

These K^* value is then used to collapse different R-ratio data into a single trend, (Refer to Fig.16 and Table 2.).

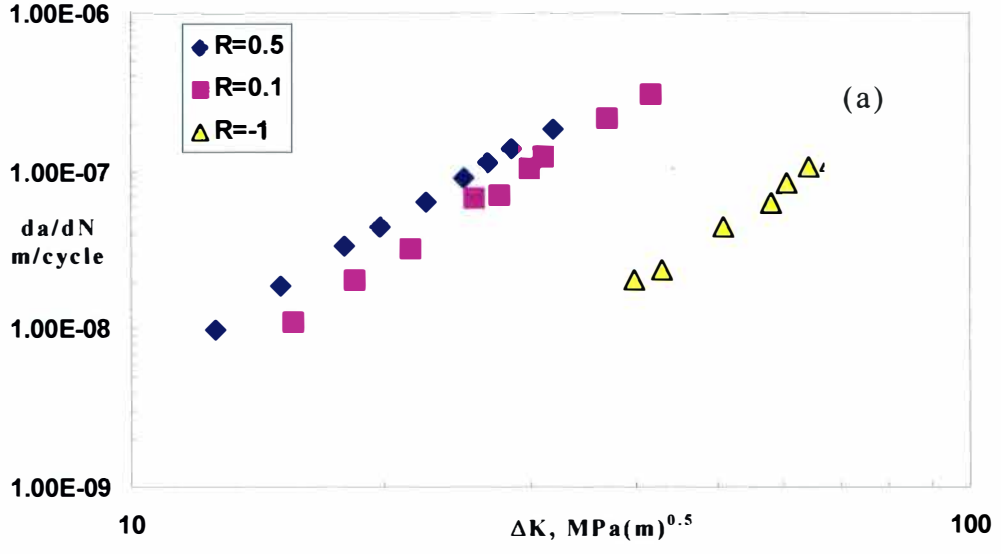

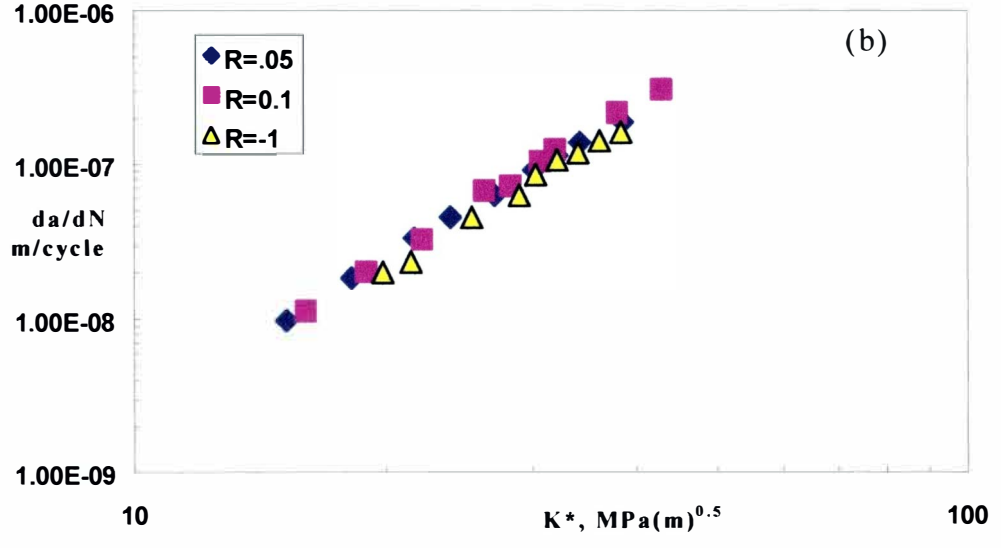

Figure 16. Fatigue crack growth data [19] of nickel based superalloy Udimet 720 as a function of (a) ΔK; (b) K*(second method).

Table 2. Calculation of α_{avg} for the second method for nickel based superalloy Udimet 720[19]

R	da/dN	ΔK	K_{max}	(1-R)	m	α
0.5	2E-08	15.501	31.003	0.5	-0.684	0.315
0.1	2E-08	18.660	20.7337	0.9		
-1	2E-08	20.807	20.807			
0.5	3E-08	17.654	35.309	0.5	-0.680	0.319
0.1	3E-08	21.303	23.670	0.9		
-1	3E-08	23.301	23.301			
0.5	4E-08	19.115	38.230	0.5	-0.692	0.307
0.1	4E-08	22.899	25.444	0.9		
-1	4E-08	24.987	24.987			
0.5	4E-08	20.846	41.693	0.5	-0.745	0.254
0.1	4E-08	24.204	26.893	0.9		
-1	4E-08	26.924	26.924			
0.5	6E-08	22.680	45.360	0.5	-0.799	0.200
0.1	6E-08	25.521	28.357	0.9		
-1	6E-08	29.221	29.221			
0.5	7E-08	23.685	47.370	0.5	-0.729	0.270
0.1	7E-08	27.766	30.851	0.9		
-1	7E-08	30.006	30.006			
0.5	8E-08	24.615	49.231	0.5	-0.729	0.270
0.1	8E-08	28.856	32.063	0.9		
-1	8E-08	30.443	30.443			
0.5	9E-08	25.337	50.672	0.5	-0.737	0.262
0.1	9E-08	29.560	32.844	0.9		
-1	9E-08	31.487	31.487			
0.5	1E-07	26.080	52.161	0.5	-0.758	0.241
0.1	1E-07	30.063	33.403	0.9		
-1	1E-07	32.645	32.645			
					α_{avg}	0.271

3.1.3. THIRD METHOD

Since a constant da/dN would result in the same crack driving force parameter K*,

therefore $K^* = (K_{max})^{\alpha} (\Delta K^+)^{(1-\alpha)}$; can be written as

$$\Delta K_1^+/(1-R_1) = \Delta K_2^+/(1-R_2). \quad (3\text{-}13)$$

The relation $K_{max} = \Delta K^+/(1-R)$ was used in the above re arrangement.

Taking log on both sides gets

$$\alpha = \log(\Delta K_1^+/\Delta K_2^+) / \log(1-R_1/1-R_2) \quad (3\text{-}14)$$

The α_{avg} is calculated from the various α values which correspond to a particular da/dN.

Then, α_{avg} value is used in $K^* = (K_{max})^{\alpha} (\Delta K+)^{(1-\alpha)}$ to calculate K*.

The above formula is for $R \geq 0$; whereas

for $R \leq 0$; $K^* = K_{max} = \Delta K^+$; where $K_{max} = \Delta K/(1-R)$. (3-15)

These K* value is then used to collapse different R-ratio data into a single trend, (Refer to Fig 17 and Table 3.).

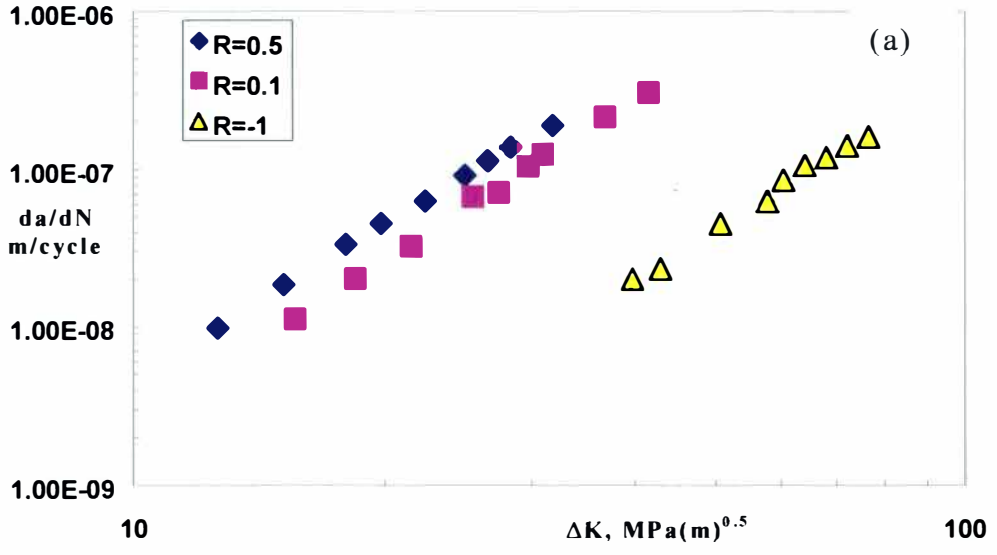

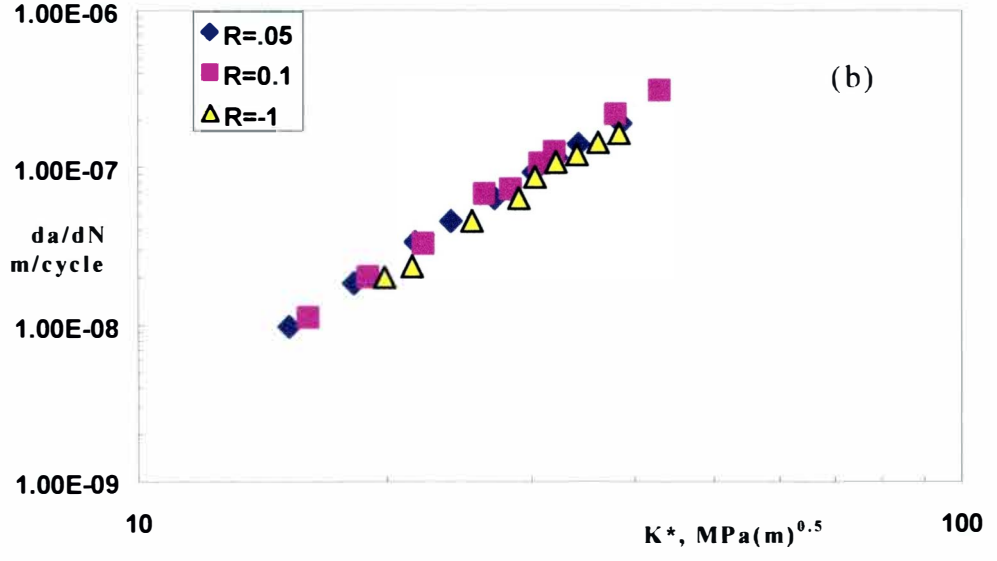

Figure 17. Fatigue crack growth data [19] of nickel based superalloy Udimet 720 as a function of (a) ΔK; (b) K*(third method).

Table 3. Calculation of α_{avg} for the third method for nickel based superalloy Udimet 720[19]

R	da/dN	ΔK	K_{max}	α
0.5	2E-08	15.501	31.003	0.316
0.1	2E-08	18.660	20.733	
-1	2E-08	20.807	20.807	
0.5	3E-08	17.654	35.309	0.32
0.1	3E-08	21.303	23.670	
-1	3E-08	23.301	23.301	
0.5	4E-08	19.115	38.230	0.307
0.1	4E-08	22.899	25.444	
-1	4E-08	24.987	24.987	
0.5	4E-08	20.846	41.693	0.254
0.1	4E-08	24.204	26.893	
-1	4E-08	26.924	26.924	
0.5	6E-08	22.680	45.360	0.201
0.1	6E-08	25.521	28.357	
-1	6E-08	29.221	29.221	
0.5	7E-08	23.685	47.370	0.27
0.1	7E-08	27.766	30.851	
-1	7E-08	30.006	30.006	
0.5	8E-08	24.615	49.231	0.27
0.1	8E-08	28.856	32.063	
-1	8E-08	30.443	30.444	
0.5	9E-08	25.337	50.675	0.262
0.1	9E-08	29.560	32.844	
-1	9E-08	31.487	31.487	
0.5	1E-07	26.080	52.161	0.242
0.1	1E-07	30.063	33.403	
-1	1E-07	32.645	32.645	
			α_{avg}	0.271

All the three methods shown above produce almost the same result. In fact, method two and method three are comparable because both are derived from the same formula $K^* = (K_{max})^{\alpha} (\Delta K^+)^{(1-\alpha)}$.
Therefore, it can be concluded that either the second or the third method could be used to calculate the fatigue crack driving force along with the first method.
Considerable amount of comparison has been done between the first and the second method in terms of the effectiveness of both methods in correlating the experimental data taken from various journal papers.
It was found that both methods give almost identical results, as can be seen from the various analyses that are listed in Appendix A.
Since the first and the second method yield similar results, further analyses of other materials have been conducted using the first method alone, and the results are listed in Appendix B.

4. PREDICTION OF CRACK GROWTH RATE USING K* APPROACH

Once the data taken from the literature is correlated using the fatigue crack driving force analysis as shown in Fig.18(b), one can then actually predict for other R –ratios using the best fit line for the correlated data. Using the points from the best fit line one can predict for other R-ratios. The above analysis is done by using statistical software known as Minitab.

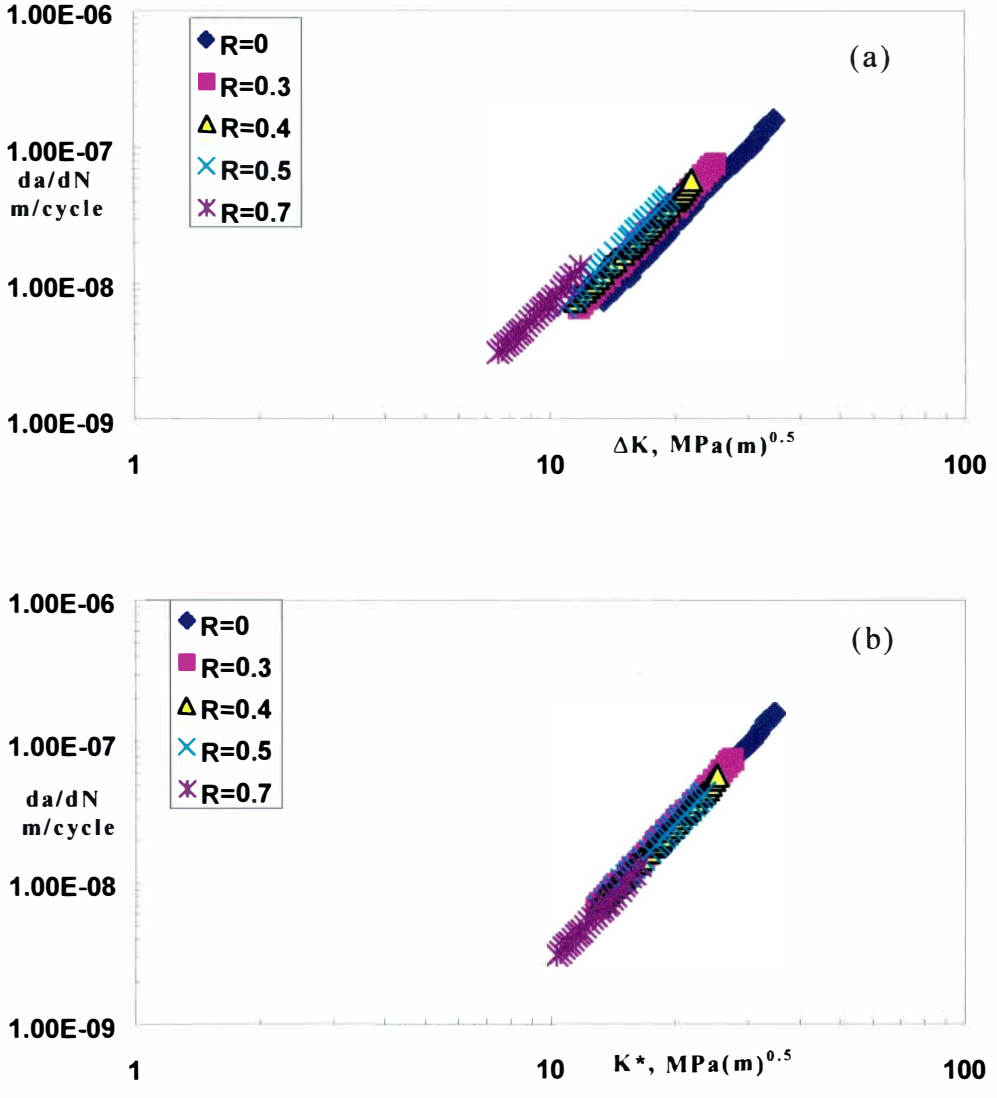

Figure 18. Fatigue crack growth data [16] of medium carbon structural steel as a function of (a) ΔK; (b) K*(first method).

A regression analysis is perform for the correlated data shown in Fig 18(b), X input is taken as log(K*) and R-ratios and the Y input as log (da/dN) as shown in Table 4.

Table 4. Regression analysis using minitab {X input is log(K*) and R-ratios, Y input is log (da/dN) }[16]

K*	Log(K*)	R	da/dN	Log(da/dN)	Reg eq	antilog (Reg eq)
1.03E+01	1.01E+00	0.7	3.09E-09	-8.51E+00	-8.51E+00	3.08E-09
1.06E+01	1.02E+00	0.7	3.23E-09	-8.49E+00	-8.48E+00	3.30E-09
1.07E+01	1.03E+00	0.7	3.49E-09	-8.46E+00	-8.46E+00	3.49E-09
1.09E+01	1.04E+00	0.7	3.63E-09	-8.44E+00	-8.44E+00	3.67E-09
1.11E+01	1.05E+00	0.7	3.77E-09	-8.42E+00	-8.41E+00	3.88E-09
1.13E+01	1.05E+00	0.7	3.97E-09	-8.40E+00	-8.39E+00	4.10E-09
1.15E+01	1.06E+00	0.7	4.23E-09	-8.37E+00	-8.36E+00	4.34E-09
1.17E+01	1.07E+00	0.7	4.39E-09	-8.36E+00	-8.34E+00	4.56E-09
1.18E+01	1.07E+00	0.7	4.56E-09	-8.34E+00	-8.32E+00	4.79E-09
1.21E+01	1.08E+00	0.7	4.89E-09	-8.31E+00	-8.29E+00	5.10E-09
1.23E+01	1.09E+00	0.7	5.24E-09	-8.28E+00	-8.26E+00	5.43E-09
1.26E+01	1.10E+00	0.7	5.57E-09	-8.25E+00	-8.24E+00	5.79E-09
1.28E+01	1.11E+00	0.7	5.88E-09	-8.23E+00	-8.21E+00	6.16E-09
1.31E+01	1.12E+00	0.7	6.30E-09	-8.20E+00	-8.18E+00	6.61E-09
1.33E+01	1.12E+00	0.7	6.54E-09	-8.18E+00	-8.16E+00	6.94E-09
1.36E+01	1.13E+00	0.7	6.90E-09	-8.16E+00	-8.13E+00	7.45E-09
1.37E+01	1.14E+00	0.7	7.17E-09	-8.14E+00	-8.11E+00	7.72E-09
1.40E+01	1.15E+00	0.7	7.63E-09	-8.12E+00	-8.09E+00	8.22E-09
1.43E+01	1.15E+00	0.7	8.05E-09	-8.09E+00	-8.06E+00	8.69E-09
1.47E+01	1.17E+00	0.7	8.82E-09	-8.05E+00	-8.02E+00	9.52E-09

Table 4-continued						
K*	Log(K*)	R	da/dN	Log(da/dN)	Reg eq	antilog (Reg eq)
1.30E+01	1.11E+00	0.5	6.85E-09	-8.16E+00	-8.18E+00	6.64E-09
1.35E+01	1.13E+00	0.5	7.45E-09	-8.13E+00	-8.13E+00	7.37E-09
1.38E+01	1.14E+00	0.5	8.11E-09	-8.09E+00	-8.10E+00	8.02E-09
1.41E+01	1.15E+00	0.5	8.56E-09	-8.07E+00	-8.07E+00	8.48E-09
1.42E+01	1.15E+00	0.5	9.38E-09	-8.03E+00	-8.05E+00	8.85E-09
1.48E+01	1.17E+00	0.5	1.05E-08	-7.98E+00	-8.00E+00	9.90E-09
1.52E+01	1.18E+00	0.5	1.13E-08	-7.95E+00	-7.96E+00	1.08E-08
1.54E+01	1.19E+00	0.5	1.20E-08	-7.92E+00	-7.94E+00	1.15E-08
1.58E+01	1.20E+00	0.5	1.29E-08	-7.89E+00	-7.91E+00	1.24E-08
1.63E+01	1.21E+00	0.5	1.39E-08	-7.86E+00	-7.87E+00	1.36E-08
1.66E+01	1.22E+00	0.5	1.49E-08	-7.83E+00	-7.84E+00	1.46E-08
1.73E+01	1.24E+00	0.5	1.68E-08	-7.77E+00	-7.79E+00	1.64E-08
1.79E+01	1.25E+00	0.5	1.84E-08	-7.73E+00	-7.74E+00	1.84E-08
1.82E+01	1.26E+00	0.5	1.96E-08	-7.71E+00	-7.71E+00	1.95E-08
1.87E+01	1.27E+00	0.5	2.11E-08	-7.67E+00	-7.68E+00	2.11E-08
1.90E+01	1.28E+00	0.5	2.23E-08	-7.65E+00	-7.65E+00	2.22E-08
1.93E+01	1.29E+00	0.5	2.43E-08	-7.61E+00	-7.63E+00	2.36E-08
1.97E+01	1.30E+00	0.5	2.54E-08	-7.59E+00	-7.60E+00	2.52E-08
2.02E+01	1.31E+00	0.5	2.74E-08	-7.56E+00	-7.56E+00	2.74E-08
2.06E+01	1.31E+00	0.5	2.92E-08	-7.54E+00	-7.54E+00	2.88E-08
2.11E+01	1.32E+00	0.5	3.08E-08	-7.51E+00	-7.50E+00	3.13E-08
2.16E+01	1.33E+00	0.5	3.32E-08	-7.48E+00	-7.47E+00	3.38E-08
2.20E+01	1.34E+00	0.5	3.56E-08	-7.45E+00	-7.44E+00	3.60E-08
2.29E+01	1.36E+00	0.5	4.06E-08	-7.39E+00	-7.39E+00	4.08E-08
1.42E+01	1.15E+00	0.4	9.45E-09	-8.02E+00	-8.05E+00	8.84E-09
1.46E+01	1.16E+00	0.4	1.01E-08	-8.00E+00	-8.01E+00	9.68E-09

Table 4-continued

K*	Log(K*)	R	da/dN	Log(da/dN)	Reg eq	antilog (Reg eq)
1.57E+01	1.20E+00	0.4	1.33E-08	-7.87E+00	-7.91E+00	1.23E-08
1.61E+01	1.21E+00	0.4	1.40E-08	-7.85E+00	-7.88E+00	1.32E-08
1.61E+01	1.21E+00	0.4	1.40E-08	-7.85E+00	-7.88E+00	1.32E-08
1.65E+01	1.22E+00	0.4	1.49E-08	-7.83E+00	-7.84E+00	1.43E-08
1.72E+01	1.24E+00	0.4	1.67E-08	-7.78E+00	-7.78E+00	1.65E-08
1.77E+01	1.25E+00	0.4	1.83E-08	-7.74E+00	-7.74E+00	1.81E-08
1.81E+01	1.26E+00	0.4	1.91E-08	-7.72E+00	-7.72E+00	1.91E-08
1.84E+01	1.26E+00	0.4	2.03E-08	-7.69E+00	-7.69E+00	2.02E-08
1.87E+01	1.27E+00	0.4	2.15E-08	-7.67E+00	-7.67E+00	2.12E-08
1.92E+01	1.28E+00	0.4	2.35E-08	-7.63E+00	-7.63E+00	2.33E-08
1.97E+01	1.29E+00	0.4	2.50E-08	-7.60E+00	-7.60E+00	2.51E-08
2.01E+01	1.30E+00	0.4	2.68E-08	-7.57E+00	-7.57E+00	2.70E-08
2.04E+01	1.31E+00	0.4	2.89E-08	-7.54E+00	-7.54E+00	2.85E-08
2.09E+01	1.32E+00	0.4	3.10E-08	-7.51E+00	-7.51E+00	3.06E-08
2.13E+01	1.33E+00	0.4	3.27E-08	-7.49E+00	-7.49E+00	3.24E-08
2.16E+01	1.33E+00	0.4	3.45E-08	-7.46E+00	-7.47E+00	3.40E-08
2.23E+01	1.35E+00	0.4	3.76E-08	-7.43E+00	-7.43E+00	3.75E-08
2.30E+01	1.36E+00	0.4	4.15E-08	-7.38E+00	-7.38E+00	4.17E-08
2.39E+01	1.38E+00	0.4	4.62E-08	-7.34E+00	-7.33E+00	4.69E-08
1.42E+01	1.15E+00	0.3	9.17E-09	-8.04E+00	-8.05E+00	8.86E-09
1.44E+01	1.16E+00	0.3	9.75E-09	-8.01E+00	-8.03E+00	9.30E-09
1.48E+01	1.17E+00	0.3	1.03E-08	-7.99E+00	-7.99E+00	1.02E-08
1.53E+01	1.18E+00	0.3	1.14E-08	-7.94E+00	-7.95E+00	1.13E-08
1.57E+01	1.20E+00	0.3	1.28E-08	-7.89E+00	-7.91E+00	1.23E-08
1.61E+01	1.21E+00	0.3	1.36E-08	-7.87E+00	-7.87E+00	1.35E-08
1.64E+01	1.21E+00	0.3	1.42E-08	-7.85E+00	-7.85E+00	1.42E-08

Table 4-continued

K*	Log(K*)	R	da/dN	Log(da/dN)	Reg eq	antilog (Reg eq)
1.76E+01	1.25E+00	0.3	1.79E-08	-7.75E+00	-7.75E+00	1.79E-08
1.78E+01	1.25E+00	0.3	1.93E-08	-7.71E+00	-7.73E+00	1.86E-08
1.82E+01	1.26E+00	0.3	2.02E-08	-7.69E+00	-7.71E+00	1.97E-08
1.84E+01	1.26E+00	0.3	2.11E-08	-7.67E+00	-7.69E+00	2.06E-08
1.89E+01	1.28E+00	0.3	2.34E-08	-7.63E+00	-7.65E+00	2.24E-08
1.94E+01	1.29E+00	0.3	2.46E-08	-7.61E+00	-7.61E+00	2.43E-08
1.96E+01	1.29E+00	0.3	2.56E-08	-7.59E+00	-7.60E+00	2.52E-08
2.00E+01	1.30E+00	0.3	2.79E-08	-7.56E+00	-7.57E+00	2.70E-08
2.04E+01	1.31E+00	0.3	2.96E-08	-7.53E+00	-7.54E+00	2.88E-08
2.22E+01	1.35E+00	0.3	3.67E-08	-7.44E+00	-7.43E+00	3.76E-08
2.24E+01	1.35E+00	0.3	3.82E-08	-7.42E+00	-7.41E+00	3.86E-08
2.30E+01	1.36E+00	0.3	4.18E-08	-7.38E+00	-7.37E+00	4.23E-08
2.35E+01	1.37E+00	0.3	4.52E-08	-7.35E+00	-7.35E+00	4.51E-08
2.39E+01	1.38E+00	0.3	4.84E-08	-7.32E+00	-7.32E+00	4.77E-08
2.68E+01	1.43E+00	0.3	7.15E-08	-7.15E+00	-7.16E+00	6.92E-08
2.74E+01	1.44E+00	0.3	7.49E-08	-7.13E+00	-7.13E+00	7.42E-08
13.40227	1.13E+00	0	7.51E-09	-8.12E+00	-8.12E+00	7.65E-09
13.78798	1.14E+00	0	8.30E-09	-8.08E+00	-8.08E+00	8.38E-09
14.18479	1.15E+00	0	8.89E-09	-8.05E+00	-8.04E+00	9.18E-09
14.49779	1.16E+00	0	9.60E-09	-8.02E+00	-8.01E+00	9.85E-09
14.98027	1.18E+00	0	1.06E-08	-7.97E+00	-7.96E+00	1.09E-08
15.47882	1.19E+00	0	1.12E-08	-7.95E+00	-7.92E+00	1.22E-08
15.95908	1.20E+00	0	1.30E-08	-7.88E+00	-7.87E+00	1.34E-08
16.38258	1.21E+00	0	1.40E-08	-7.85E+00	-7.84E+00	1.46E-08
16.74407	1.22E+00	0	1.51E-08	-7.82E+00	-7.81E+00	1.57E-08
17.07622	1.23E+00	0	1.58E-08	-7.80E+00	-7.78E+00	1.67E-08

Table 4-continued						
K*	Log(K*)	R	da/dN	Log(da/dN)	Reg eq	antilog (Reg eq)
18.07325	1.26E+00	0	1.94E-08	-7.71E+00	-7.70E+00	2.00E-08
18.31148	1.26E+00	0	1.99E-08	-7.70E+00	-7.68E+00	2.09E-08
18.83848	1.28E+00	0	2.18E-08	-7.66E+00	-7.64E+00	2.29E-08
20.64696	1.31E+00	0	3.01E-08	-7.52E+00	-7.51E+00	3.07E-08
21.56818	1.33E+00	0	3.51E-08	-7.46E+00	-7.45E+00	3.53E-08
22.04409	1.34E+00	0	3.76E-08	-7.43E+00	-7.42E+00	3.79E-08
22.72806	1.36E+00	0	4.31E-08	-7.37E+00	-7.38E+00	4.18E-08
23.28032	1.37E+00	0	4.62E-08	-7.34E+00	-7.35E+00	4.51E-08
24.37217	1.39E+00	0	5.26E-08	-7.28E+00	-7.28E+00	5.23E-08
28.02577	1.45E+00	0	7.90E-08	-7.10E+00	-7.09E+00	8.20E-08
29.1487	1.46E+00	0	8.93E-08	-7.05E+00	-7.03E+00	9.30E-08
29.53292	1.47E+00	0	9.21E-08	-7.04E+00	-7.01E+00	9.70E-08
30.44925	1.48E+00	0	9.95E-08	-7.00E+00	-6.97E+00	1.07E-07
31.12112	1.49E+00	0	1.09E-07	-6.96E+00	-6.94E+00	1.15E-07
31.60024	1.50E+00	0	1.14E-07	-6.94E+00	-6.92E+00	1.21E-07

Using the coefficients from Table 5, a regression equation is developed for da/dN, which is represented by last column in Table 4. The best-fit line is plotted for K* and da/dN(antilog reg eq) for the smallest R-ratio in this case it is R=0 (Fig.19) .

The reason is that at R=0, $K^* = K_{max} = \Delta K^+ = \Delta K$ (4-1)

So, basically all the R-ratios collapse on the R=0, in case for crack growth rate data which does not have the load ratio, R=0 the best fit line is calculated based on the smallest R-ratio

Table 5. ANOVA table{with the coefficients for the regression equation to determine the best fit line for the correlated data}

Regression Analysis			
Regression Statistics			
Multiple R	0.999226824		
R Square	0.998454245		
Adjusted R Square	0.998433906		
Standard Error	0.015411861		
Observations	155		
ANOVA			
	df	*SS*	*MS*
Regression	2	23.32068487	11.66034244
Residual	152	0.036103871	0.000237525
Total	154	23.35678874	
	Coefficients	*Standard Error*	*t Stat*
Intercept	-11.73894916	0.017191562	-682.8320128
K*	3.213654208	0.012584638	255.3632699
r	-0.044653683	0.00640131	-6.975709641

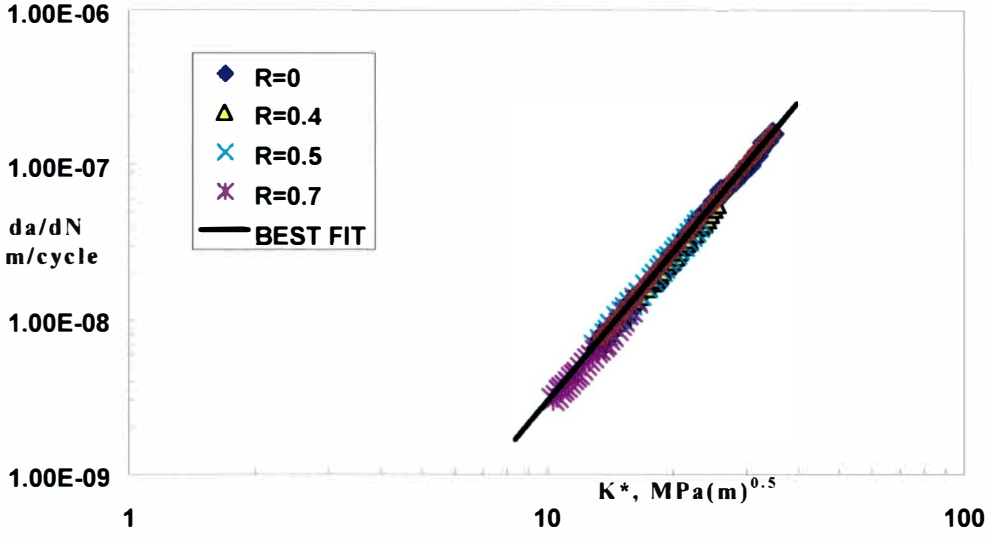

Figure 19. Fatigue crack growth data [16] of medium carbon structural steel as a function of K*(first method) with the best fit line.

Once the best-fit line is obtained for the correlated data in terms of the fatigue crack driving force K* one can predict da/dN curves for other R-ratios.

Table 6. Data of the best fit line in terms of da/dN and K*

K*	da/dN
13.40227	7.65E-09
13.78798	8.38E-09
14.18479	9.18E-09
14.49779	9.85E-09
14.98027	1.09E-08
15.47882	1.22E-08
15.95908	1.34E-08
16.38258	1.46E-08
16.74407	1.57E-08
17.07622	1.67E-08
17.41496	1.78E-08
17.7217	1.88E-08
18.07325	2.00E-08
18.31148	2.09E-08
18.83848	2.29E-08
19.21218	2.44E-08
19.89493	2.72E-08
20.64696	3.07E-08
21.56818	3.53E-08
22.04409	3.79E-08
22.72806	4.18E-08
23.28032	4.51E-08

Table 6-continued	
K*	da/dN
25.29344	5.89E-08
25.96464	6.41E-08
26.53756	6.88E-08
27.66116	7.86E-08
28.02577	8.20E-08
29.1487	9.30E-08
29.53292	9.70E-08
30.44925	1.07E-07
31.12112	1.15E-07
31.60024	1.21E-07
32.15683	1.27E-07
32.86638	1.37E-07
33.51836	1.46E-07

Using the above set of best-fit line data for medium carbon steel we can predict the crack growth rate for other R-ratios.

The fatigue crack driving force parameter K* is used to correlate all the fatigue crack growth data for all R-ratios into a single trend. Therefore, data for any other R-ratio will also fall into the same trend when they are correlated using fatigue crack driving force parameter K*. Thus the K* values of the best fit line are used to convert them to the corresponding ΔK values for the predicting R ratios, that is $\Delta K = K^* (1-R)$.

This can be shown by the following example in which the fatigue crack growth rate for R=-1 (third column) is predicted using the above procedure.

Table 7. Prediction of fatigue crack growth rate data for R=-1

K*	da/dN	Pred ΔK
13.40227	7.65E-09	26.80455
13.78798	8.38E-09	27.57597
14.18479	9.18E-09	28.36959
14.49779	9.85E-09	28.99557
14.98027	1.09E-08	29.96054
15.47882	1.22E-08	30.95763
15.95908	1.34E-08	31.91816
16.38258	1.46E-08	32.76516
16.74407	1.57E-08	33.48813
17.07622	1.67E-08	34.15244
17.41496	1.78E-08	34.82993
17.7217	1.88E-08	35.44341
18.07325	2.00E-08	36.1465
18.31148	2.09E-08	36.62296
18.83848	2.29E-08	37.67695
19.21218	2.44E-08	38.42435
19.89493	2.72E-08	39.78986
20.64696	3.07E-08	41.29393
21.56818	3.53E-08	43.13636
22.04409	3.79E-08	44.08818
22.72806	4.18E-08	45.45612
23.28032	4.51E-08	46.56064
24.37217	5.23E-08	48.74433
25.07358	5.73E-08	50.14716
25.29344	5.89E-08	50.58688
25.96464	6.41E-08	51.92928

Table 7-continued		
K*	da/dN	Pred ΔK
28.02577	8.20E-08	56.05155
29.1487	9.30E-08	58.29741
29.53292	9.70E-08	59.06585
30.44925	1.07E-07	60.8985
31.12112	1.15E-07	62.24224
31.60024	1.21E-07	63.20047
32.15683	1.27E-07	64.31366
32.86638	1.37E-07	65.73277
33.51836	1.46E-07	67.03672
34.483	1.60E-07	68.966

The predicted values of ΔK for R=-1 are plotted versus da/dN below in Fig.20 together with the experimental data. Figure 20 shows how the predicted crack growth rate is in comparison to the experimental data for other R-ratios.

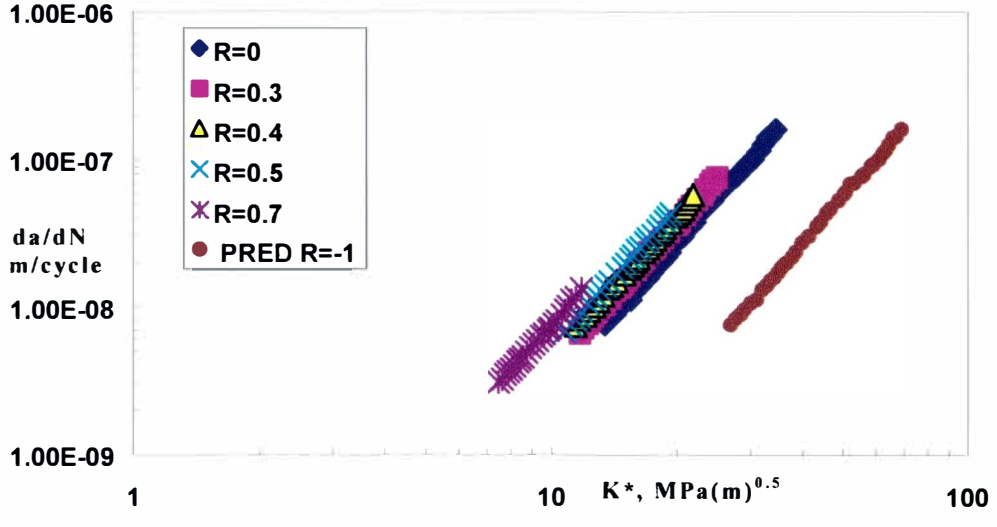

Figure 20. Fatigue crack growth data [16] of medium carbon structural steel as a function of ΔK along with the predicted crack growth data for R=-1.

Certain argument might arise to the extent of accuracy of this method in predicting the crack growth rate for other R-ratios. The only way to validate that is to do a prediction for an existing R-ratio from the experimental data shown in Fig.21.

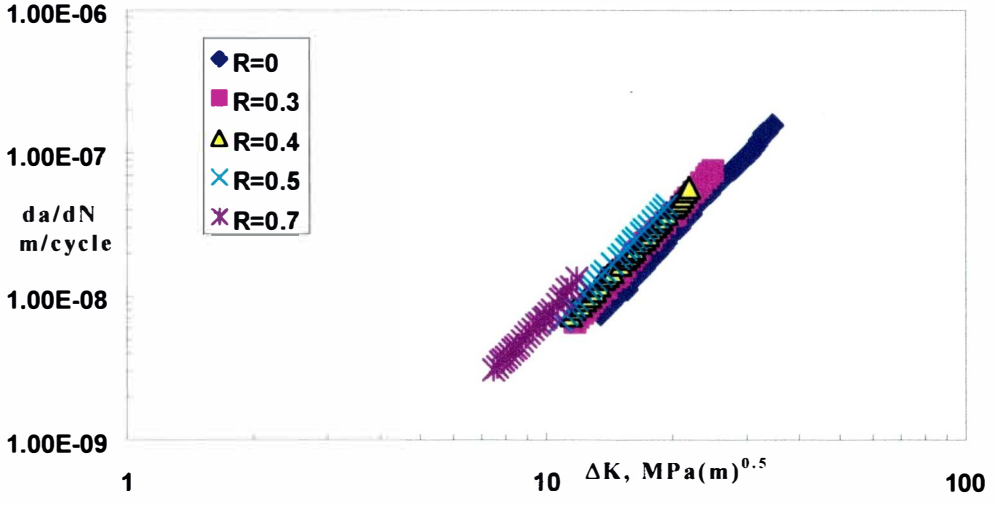

Figure 21. Fatigue crack growth data [16] of medium carbon structural steel as a function of ΔK.

Instead of using all the five R ratios in the analysis of K*, only four R-ratios that is R=0, 0.4, 0.5, and 0.7 were used. The crack growth rate for R=0.3 is predicted and compared wih experimental data.

Using the fatigue crack driving force parameter K* the data are correlated into a single trend and then ANOVA level-1 analysis is done to find out the best-fit line as shown in Fig.22.

The K* data from the best-fit line are used in predicting the fatigue crack growth rate for R=0.3 and then compared with the experimental value of crack growth rate obtained for R=0.3. The result is depicted in Fig.23. Similar kind of analysis is done for other materials and the results are listed in the Appendix C.

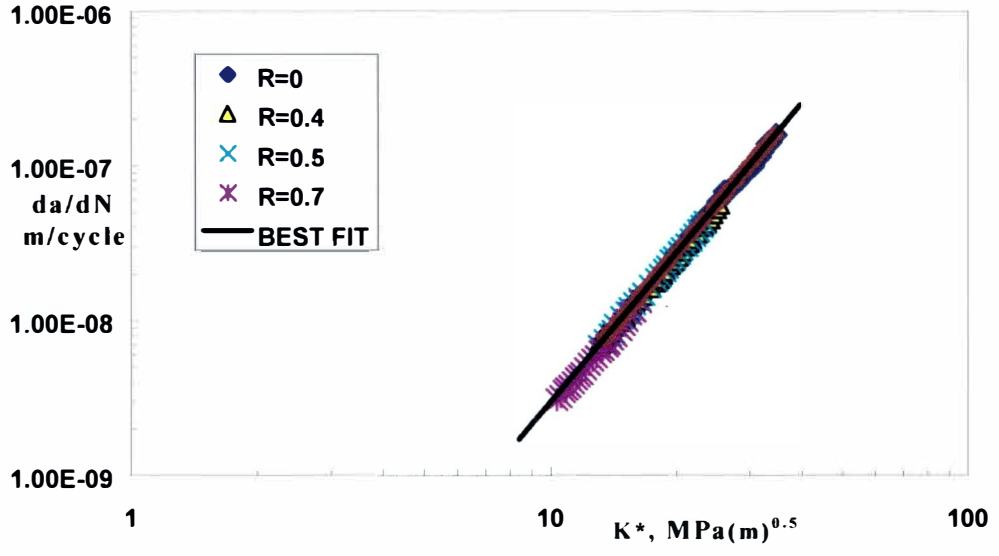

Figure 22. Fatigue crack growth data [16] of medium carbon structural steel as a function of K*(first method) with the best fit line for four of the existing five R-ratios.

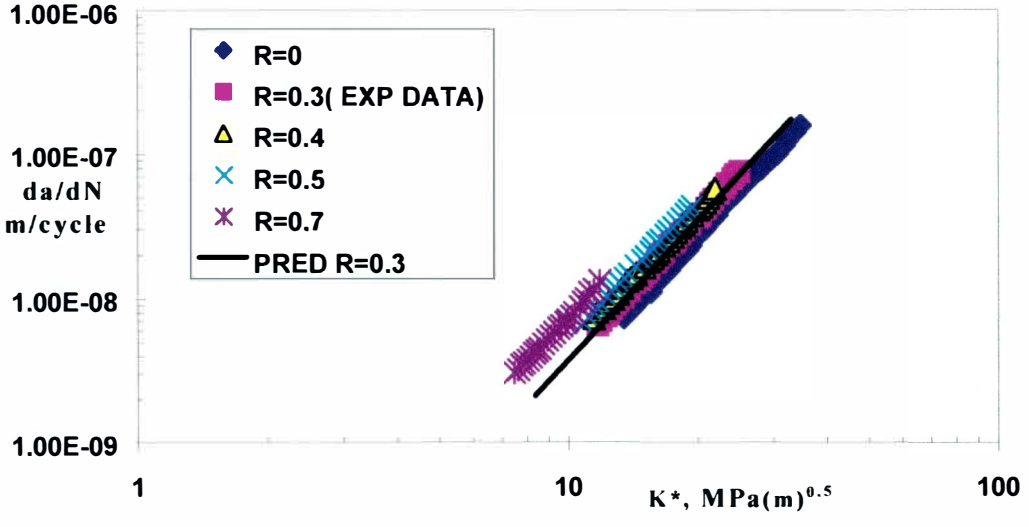

Figure 23. Fatigue crack growth data [16] of medium carbon structural steel as a function of ΔK showing the predicted and experimental result for R=0.3.

5. DETERMINATION OF THE BEST-FIT LINE FOR THE CORRELATED DATA

Sometimes the correlated data are not linear as shown in Fig.24. In such case the analysis for the best-fit line is slightly different from the previous analysis, as it is illustrated below.

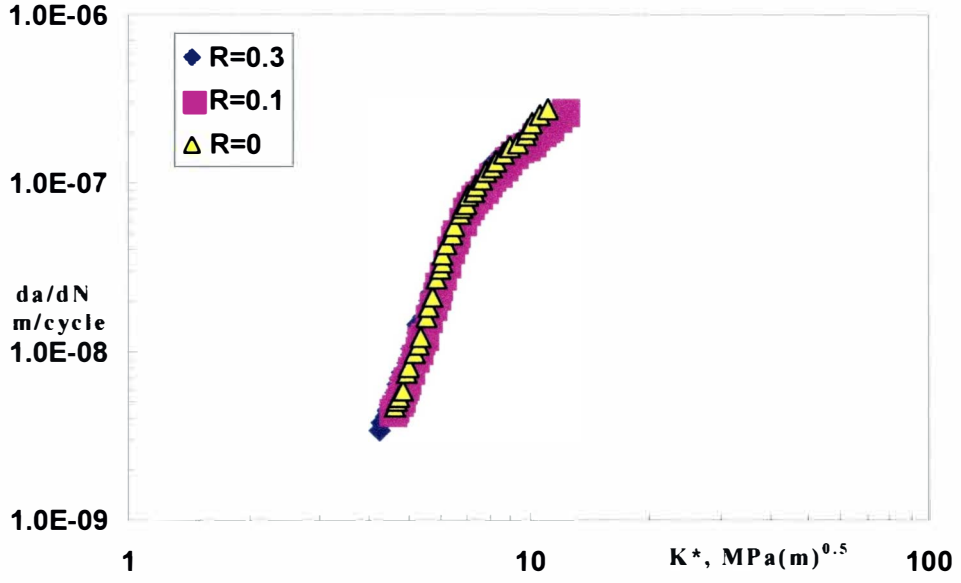

Figure 24. Fatigue crack growth data [20] of 7075-T651 as a function of K*.

From Table 8 a regression analysis is done for the data in which the X input is taken as log (K*), log (K*)^2,log (K*)^3 and R-ratio. The Y input as log(da/dN). The reason for taking log(K*) to the third power is to approximate the trend of the data as a polynomial trend.

Table 8. Regression analysis using minitab [20].

Log (da/dN)	da/dN	R	Log (K*)^3	Log (K*)^2	Log K*	K*	Reg eq	Antilog (reg eq)
-8.321	4.77E-09	0	0.297	0.445	0.667	4.64E+00	-8.283	5.2E-09
-8.287	5.17E-09	0	0.299	0.447	0.669	4.66E+00	-8.27	5.4E-09
-8.257	5.53E-09	0	0.31	0.458	0.676	4.75E+00	-8.215	6.1E-09
-8.223	5.98E-09	0	0.32	0.468	0.684	4.83E+00	-8.161	6.9E-09
-8.125	7.51E-09	0	0.337	0.484	0.696	4.96E+00	-8.08	8.3E-09

Table 8-continued								
Log (da/dN)	da/dN	R	Log (K*)^3	Log (K*)^2	Log K*	K*	Reg eq	Antilog (reg eq)
-7.957	1.10E-08	0	0.38	0.525	0.724	5.30E+00	-7.885	1.3E-08
-7.908	1.24E-08	0	0.389	0.533	0.73	5.37E+00	-7.847	1.4E-08
-7.79	1.62E-08	0	0.415	0.556	0.746	5.57E+00	-7.747	1.8E-08
-7.726	1.88E-08	0	0.424	0.565	0.751	5.64E+00	-7.711	1.9E-08
-7.662	2.18E-08	0	0.437	0.576	0.759	5.74E+00	-7.663	2.2E-08
-7.554	2.79E-08	0	0.458	0.594	0.771	5.90E+00	-7.592	2.6E-08
-7.5	3.16E-08	0	0.471	0.606	0.778	6.00E+00	-7.546	2.8E-08
-7.461	3.46E-08	0	0.478	0.612	0.782	6.06E+00	-7.523	3E-08
-7.416	3.83E-08	0	0.486	0.618	0.786	6.11E+00	-7.5	3.2E-08
-7.362	4.34E-08	0	0.504	0.633	0.796	6.25E+00	-7.445	3.6E-08
-7.293	5.09E-08	0	0.526	0.651	0.807	6.41E+00	-7.38	4.2E-08
-7.249	5.63E-08	0	0.541	0.664	0.815	6.53E+00	-7.338	4.6E-08
-7.18	6.60E-08	0	0.572	0.689	0.83	6.76E+00	-7.258	5.5E-08
-7.141	7.23E-08	0	0.58	0.696	0.834	6.82E+00	-7.238	5.8E-08
-7.116	7.65E-08	0	0.6	0.712	0.844	6.98E+00	-7.19	6.5E-08
-7.077	8.37E-08	0	0.609	0.718	0.847	7.04E+00	-7.172	6.7E-08
-7.043	9.07E-08	0	0.642	0.745	0.863	7.29E+00	-7.1	8E-08
-7.013	9.70E-08	0	0.66	0.758	0.871	7.42E+00	-7.065	8.6E-08
-6.974	1.06E-07	0	0.686	0.778	0.882	7.62E+00	-7.016	9.6E-08
-6.925	1.19E-07	0	0.714	0.799	0.894	7.83E+00	-6.97	1.1E-07
-6.9	1.26E-07	0	0.746	0.823	0.907	8.07E+00	-6.919	1.2E-07
-6.866	1.36E-07	0	0.775	0.844	0.919	8.29E+00	-6.879	1.3E-07
-6.826	1.49E-07	0	0.82	0.876	0.936	8.63E+00	-6.824	1.5E-07
-6.787	1.63E-07	0	0.871	0.912	0.955	9.02E+00	-6.771	1.7E-07
-6.757	1.75E-07	0	0.919	0.946	0.972	9.38E+00	-6.732	1.9E-07
-6.718	1.91E-07	0	0.975	0.983	0.992	9.81E+00	-6.697	2E-07
-6.674	2.12E-07	0	0.998	0.999	0.999	9.98E+00	-6.686	2.1E-07
-6.639	2.29E-07	0	1.027	1.018	1.009	1.02E+01	-6.674	2.1E-07
-6.6	2.51E-07	0	1.087	1.057	1.028	1.07E+01	-6.659	2.2E-07
-6.561	2.75E-07	0	1.143	1.093	1.045	1.11E+01	-6.654	2.2E-07
-8.346	4.51E-09	0.1	0.281	0.429	0.655	4.52E+00	-8.358	4.4E-09
-8.321	4.77E-09	0.1	0.286	0.434	0.659	4.56E+00	-8.33	4.7E-09
-8.287	5.17E-09	0.1	0.298	0.446	0.668	4.66E+00	-8.261	5.5E-09
-8.257	5.53E-09	0.1	0.306	0.454	0.674	4.72E+00	-8.22	6E-09
-8.218	6.05E-09	0.1	0.314	0.462	0.68	4.78E+00	-8.179	6.6E-09
-8.189	6.48E-09	0.1	0.322	0.47	0.685	4.85E+00	-8.138	7.3E-09
-8.149	7.09E-09	0.1	0.33	0.478	0.691	4.91E+00	-8.098	8E-09
-8.1	7.94E-09	0.1	0.344	0.491	0.701	5.02E+00	-8.032	9.3E-09
-8.026	9.41E-09	0.1	0.359	0.505	0.71	5.13E+00	-7.966	1.1E-08
-7.977	1.05E-08	0.1	0.373	0.518	0.72	5.25E+00	-7.901	1.3E-08
-7.918	1.21E-08	0.1	0.382	0.527	0.726	5.32E+00	-7.863	1.4E-08
-7.893	1.28E-08	0.1	0.398	0.541	0.735	5.44E+00	-7.8	1.6E-08
-7.79	1.62E-08	0.1	0.413	0.555	0.745	5.56E+00	-7.738	1.8E-08

Table 8-continued								
Log (da/dN)	da/dN	R	Log (K*)^3	Log (K*)^2	Log K*	K*	Reg eq	Antilog (reg eq)
-7.593	2.55E-08	0.1	0.456	0.593	0.77	5.89E+00	-7.583	2.6E-08
-7.539	2.89E-08	0.1	0.474	0.608	0.78	6.02E+00	-7.525	3E-08
-7.466	3.42E-08	0.1	0.492	0.623	0.789	6.15E+00	-7.469	3.4E-08
-7.377	4.20E-08	0.1	0.513	0.641	0.801	6.32E+00	-7.403	4E-08
-7.323	4.75E-08	0.1	0.532	0.657	0.81	6.46E+00	-7.35	4.5E-08
-7.284	5.20E-08	0.1	0.544	0.666	0.816	6.55E+00	-7.318	4.8E-08
-7.21	6.17E-08	0.1	0.571	0.688	0.83	6.75E+00	-7.248	5.7E-08
-7.161	6.91E-08	0.1	0.595	0.707	0.841	6.94E+00	-7.19	6.5E-08
-7.121	7.56E-08	0.1	0.611	0.72	0.849	7.06E+00	-7.152	7E-08
-7.082	8.28E-08	0.1	0.632	0.737	0.858	7.22E+00	-7.107	7.8E-08
-7.057	8.76E-08	0.1	0.658	0.757	0.87	7.41E+00	-7.055	8.8E-08
-7.023	9.49E-08	0.1	0.685	0.777	0.881	7.61E+00	-7.006	9.9E-08
-6.984	1.04E-07	0.1	0.712	0.797	0.893	7.82E+00	-6.959	1.1E-07
-6.949	1.12E-07	0.1	0.74	0.818	0.904	8.03E+00	-6.915	1.2E-07
-6.93	1.18E-07	0.1	0.769	0.839	0.916	8.24E+00	-6.874	1.3E-07
-6.895	1.27E-07	0.1	0.808	0.867	0.931	8.54E+00	-6.824	1.5E-07
-6.856	1.39E-07	0.1	0.838	0.889	0.943	8.77E+00	-6.79	1.6E-07
-6.821	1.51E-07	0.1	0.88	0.918	0.958	9.08E+00	-6.75	1.8E-07
-6.787	1.63E-07	0.1	0.923	0.948	0.974	9.41E+00	-6.716	1.9E-07
-6.777	1.67E-07	0.1	0.956	0.971	0.985	9.67E+00	-6.694	2E-07
-6.752	1.77E-07	0.1	1.002	1.001	1.001	1.00E+01	-6.671	2.1E-07
-6.718	1.91E-07	0.1	1.037	1.024	1.012	1.03E+01	-6.658	2.2E-07
-6.693	2.03E-07	0.1	1.085	1.056	1.027	1.07E+01	-6.646	2.3E-07
-6.669	2.14E-07	0.1	1.115	1.076	1.037	1.09E+01	-6.642	2.3E-07
-6.649	2.24E-07	0.1	1.153	1.1	1.049	1.12E+01	-6.641	2.3E-07
-6.61	2.46E-07	0.1	1.211	1.136	1.066	1.16E+01	-6.647	2.3E-07
-6.575	2.66E-07	0.1	1.285	1.182	1.087	1.22E+01	-6.667	2.2E-07
-8.459	3.48E-09	0.3	0.245	0.391	0.625	4.22E+00	-8.546	2.8E-09
-8.42	3.80E-09	0.3	0.249	0.396	0.629	4.26E+00	-8.518	3E-09
-8.38	4.17E-09	0.3	0.261	0.408	0.639	4.35E+00	-8.447	3.6E-09
-8.351	4.46E-09	0.3	0.268	0.415	0.645	4.41E+00	-8.405	3.9E-09
-8.311	4.88E-09	0.3	0.278	0.425	0.652	4.49E+00	-8.349	4.5E-09
-8.282	5.22E-09	0.3	0.282	0.43	0.656	4.53E+00	-8.321	4.8E-09
-8.243	5.72E-09	0.3	0.295	0.443	0.666	4.63E+00	-8.252	5.6E-09
-8.193	6.41E-09	0.3	0.298	0.446	0.668	4.65E+00	-8.238	5.8E-09
-8.154	7.01E-09	0.3	0.308	0.456	0.675	4.74E+00	-8.183	6.6E-09
-8.12	7.59E-09	0.3	0.316	0.464	0.681	4.80E+00	-8.142	7.2E-09
-8.056	8.80E-09	0.3	0.332	0.48	0.693	4.93E+00	-8.062	8.7E-09
-8.016	9.63E-09	0.3	0.346	0.493	0.702	5.04E+00	-7.995	1E-08
-7.972	1.07E-08	0.3	0.349	0.496	0.704	5.06E+00	-7.982	1E-08
-7.938	1.15E-08	0.3	0.37	0.515	0.718	5.22E+00	-7.891	1.3E-08
-7.884	1.31E-08	0.3	0.37	0.515	0.718	5.22E+00	-7.891	1.3E-08
-7.83	1.48E-08	0.3	0.376	0.521	0.721	5.27E+00	-7.865	1.4E-08

Table 8-continued								
Log (da/dN)	da/dN	R	Log (K*)^3	Log (K*)^2	Log K*	K*	Reg eq	Antilog (reg eq)
-7.687	2.06E-08	0.3	0.419	0.56	0.748	5.60E+00	-7.69	2E-08
-7.643	2.28E-08	0.3	0.432	0.572	0.756	5.70E+00	-7.642	2.3E-08
-7.608	2.46E-08	0.3	0.445	0.583	0.764	5.80E+00	-7.594	2.5E-08
-7.534	2.92E-08	0.3	0.476	0.61	0.781	6.04E+00	-7.49	3.2E-08
-7.495	3.20E-08	0.3	0.48	0.613	0.783	6.07E+00	-7.479	3.3E-08
-7.461	3.46E-08	0.3	0.484	0.616	0.785	6.09E+00	-7.467	3.4E-08
-7.411	3.88E-08	0.3	0.505	0.634	0.796	6.26E+00	-7.401	4E-08
-7.21	6.17E-08	0.3	0.57	0.687	0.829	6.75E+00	-7.224	6E-08
-7.131	7.39E-08	0.3	0.598	0.71	0.843	6.96E+00	-7.156	7E-08
-7.087	8.19E-08	0.3	0.623	0.729	0.854	7.15E+00	-7.101	7.9E-08
-7.043	9.07E-08	0.3	0.653	0.753	0.868	7.37E+00	-7.039	9.1E-08
-6.811	1.54E-07	0.3	0.832	0.885	0.941	8.72E+00	-6.771	1.7E-07
-6.782	1.65E-07	0.3	0.873	0.914	0.956	9.03E+00	-6.73	1.9E-07

Table 9. ANOVA table with the coefficients for the regression equation to determine the best fit line for the correlated data

Regression Analysis			
Regression Statistics			
Multiple R	0.996		
R Square	0.993		
Adjusted R Square	0.993		
Standard Error	0.049		
Observations	117		
ANOVA			
	df	*SS*	*MS*
Regression	4	36.463	9.116
Residual	112	0.2636	0.002
Total	116	36.726	
	Coefficients	*Standard Error*	*t Stat*
Intercept	-11.79	1.6417	-7.18
r	0.132	0.0381	3.467
k3	-9.953	2.8059	-3.55
k2	16.13	7.1182	2.266
k1	-1.068	5.953	-0.18

Using the coefficients from the ANOVA table a regression equation is developed for da/dN, which is represented by last column in Table 8. The best fit line is plotted in Fig.25 for K* and da/dN(antilog reg eq) for the smallest R-ratio in this case it is R=0 .

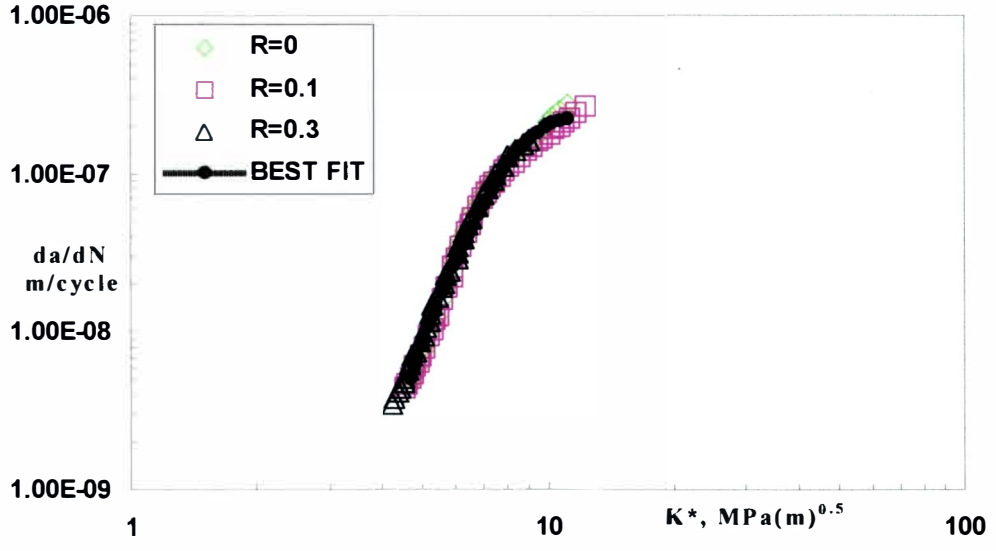

Figure 25. Fatigue crack growth data [20] of 7075-T651 as a function of K*(first method) with the best fit line.

Once the best-fit line is obtained for the correlated data in terms of the fatigue crack driving force K* we can predict for other R-ratios. The K* values of the best-fit line are used for prediction of other R ratio, using the formula $\Delta K = K^*(1-R)$ as shown in the previous examples (where R is the "predicted" R ratio).

The above stated method works very well for either linear or non-linear data and therefore it can be taken as a general for finding out the best-fit line to correlate and to predict for R-ratios effects.

Further analysis is done for other materials and the results are listed in Appendix D.

6. COMPARISON OF FATIGUE CRACK DRIVING FORCE K* WITH ΔK_{eff} METHODOLOGY

The previous chapter shows how fatigue crack driving force K* is effective in correlating the various R-ratios into a single trend and also in predicting the fatigue crack growth rate for other R-ratios.
Therefore, it is needed to compare how good the fatigue crack driving force K* approach is in comparison to the commonly used closure methodology or ΔK_{eff} parameter.
In this chapter a comparison between the fatigue crack driving force K* with the existing crack closure parameter ΔK_{eff} is perform to demonstrate their effectiveness in correlating the data for different materials.
Figure.26 shows the experimental data for 7075-T7451 aluminum alloy in terms of da/dN vs. ΔK. These data are correlated using K* and ΔK_{eff} as shown in Fig 27.

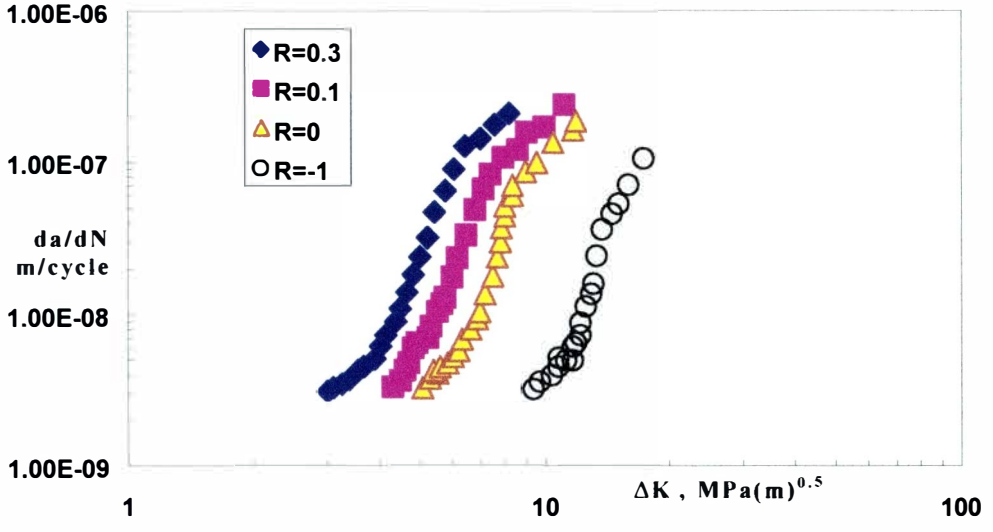

Figure 26. Fatigue crack growth data [21] of 7075-T7451 as a function of ΔK.

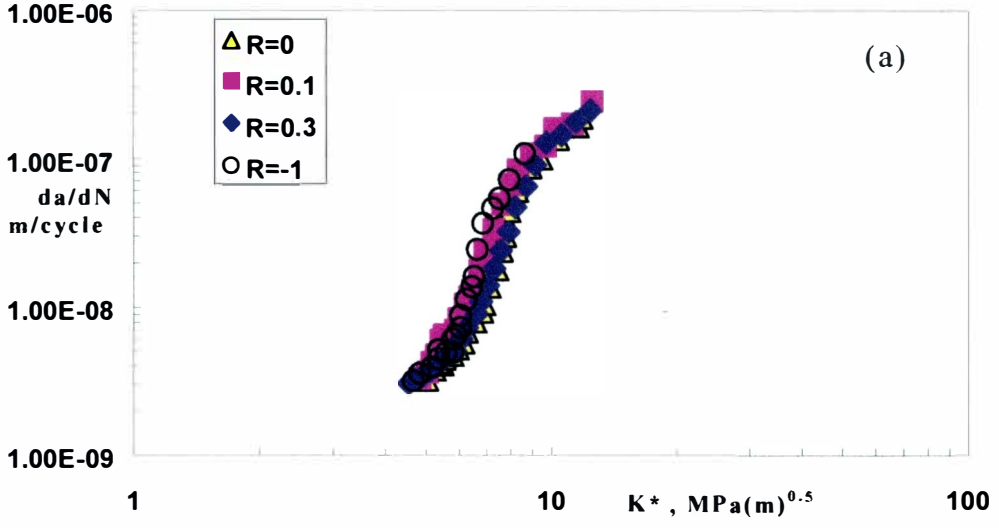

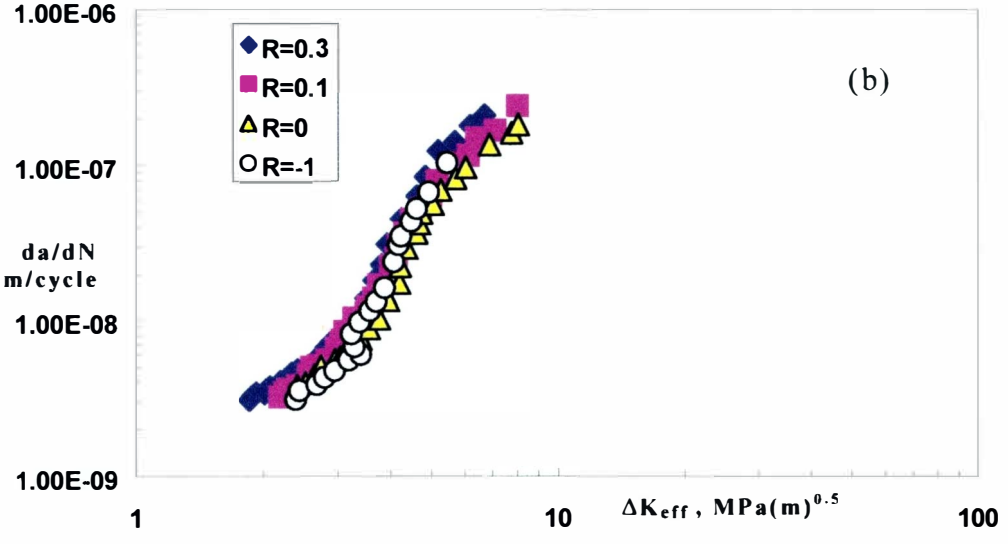

Figure 27. Fatigue crack growth data [21] of 7075-T7451 as a function of (a) K*; (b) ΔK_{eff}.

Table 10 summarizes the relative comparison between crack closure data and fatigue crack driving force in terms of the amount of scatter that each method results when it tries to correlate the data.

The amount of scatter is calculated in terms of the correlation co-efficient value R^2.

MATERIAL	R^2 VALUE FOR ΔK_{eff}	R^2 VALUE FOR K*
Medium carbon steel [16]	0.92	0.99
Grey cast iron [22]	0.74	0.82
Ti-6Al-4V [23]	0.96	0.92
Ti-10V-2Fe-3Al [24]	0.97	0.98
Steel, JIS SM50B [25]	0.92	0.96
Austempered ductile iron [22]	0.93	0.94
300M steel [26]	0.98	0.99
7075-T651 [20]	0.98	0.99
7075-T7451[21]	0.97	0.98

Table 10. Comparison between K* and ΔK_{eff} in correlating the fatigue crack growth data (when measured by correlation coefficient R^2)

Table 10, demonstrate the effectiveness of the fatigue crack driving force parameter K* in correlating the data when compared with crack closure, ΔK_{eff} parameter.

The graphical comparison of both these methods is listed in Appendix E.

7. CORRELATION OF FATIGUE CRACK GROWTH DATA USING g-FUNCTION

Sometimes the data obtained for fatigue crack growth rate da/dN vs ΔK can be of the form shown in Fig.28.

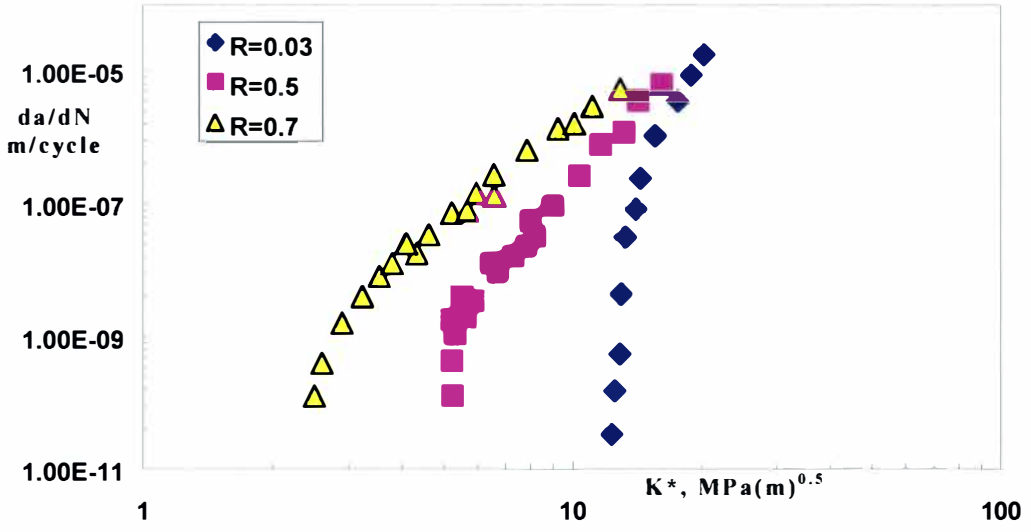

Figure 28. Fatigue crack growth data [27] of spheroidal cast iron microstructure as a function of ΔK.

Figure 28 indicates that the R-ratio effect is well pronounced in the threshold region and it decreases in the Paris region.

If the conventional K* approach is used to correlate the R ratios, then the data correlate in the way shown in Fig.29. This is because the effect of R-ratio is diminishing with increasing ΔK values. Therefore, the conventional K* approach, which is very successful in correlating the fatigue crack growth data as shown in the previous chapters, fails to correlate the data in this case. The average value of α, correlate the data reasonably well in the threshold region, but in the Paris region it will overshoot the results due to less pronounced R-ratio effect in this region, as it is depicted in Fig 29.

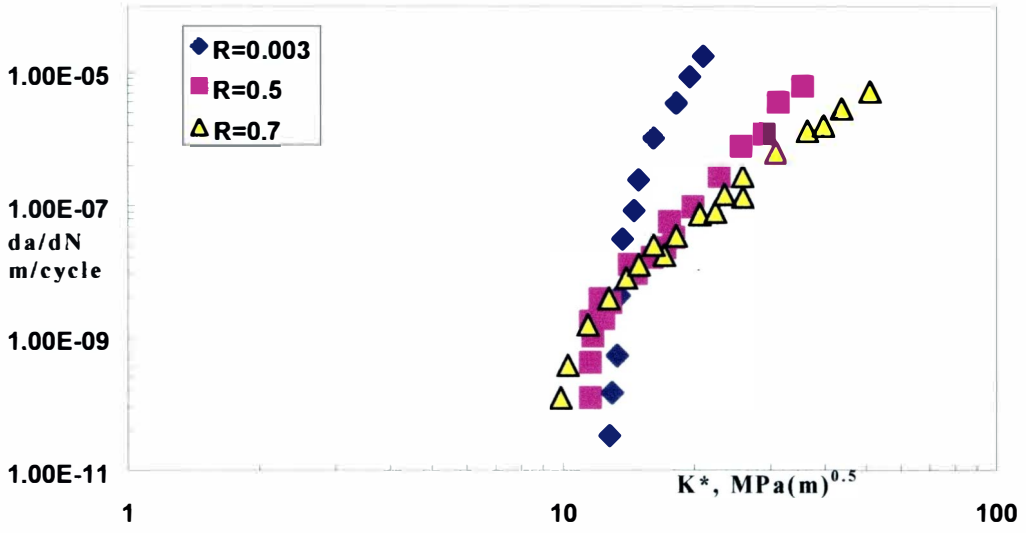

Figure 29. Fatigue crack growth data [27] of spheroidal cast iron microstructure as a function of K*.

In order to account for this decreasing R-ratio effect in the Paris region, a special g-function is introduced, which decreases the value of material parameter α exponentially from the value of the threshold region to the static failure region. The exponential function g [12] can be written as

$$g=\exp-(K_{max}/K_{maxth}-1), \qquad (6\text{-}1)$$

where K_{maxth} is the maximum stress intensity factor at the threshold for a given R-ratio, and K_{max} is the maximum stress intensity factor for a given da/dn. It is seen that at the threshold $K_{max}=K_{maxth}$ therefore g=1.

As one proceeds from the threshold region towards the Paris region it is seen that K_{max} is greater than K_{maxth} and the value of g decreases from 1 to a much lower value. Therefore, when the material parameter α is multiplied with the g function for a constant da/dN, the value of modified α also diminishes from that at the threshold region to much smaller value at the Paris region. This signifies that the R- ratio effect on crack growth rate diminishes when ΔK approaches the Paris region.

The data depicted in Fig.30 are used to demonstarte how the g function works.

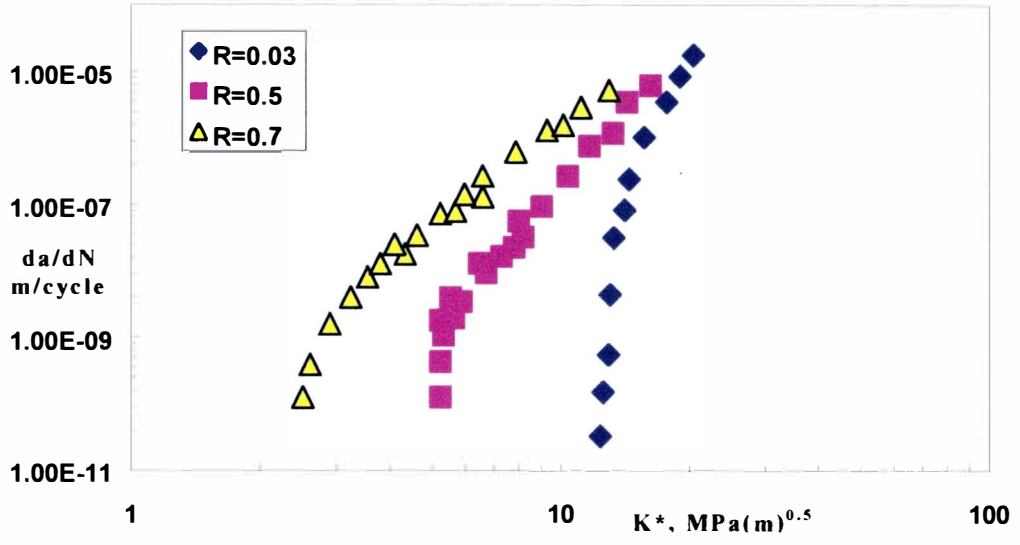

Figure 30. Fatigue crack growth data [27] of spheroidal cast iron microstructure as a function of ΔK.

Table 11. Calculation of the value of modified α using g function

R	da/dN	ΔK	K_{max}	m	α	g	modified alpha	K*
0.7	2.01E-10	2.566	8.553	0.259	1.349	1	1.35	13.035
0.5	2.01E-10	5.202	10.4			1	1.35	13.26
0.03	2.01E-10	12.51	12.9			1	1.35	13.036
0.7	4.02E-10	2.614	8.712	0.263	1.358	0.982	1.325	12.884
0.5	4.02E-10	5.25	10.5			0.991	1.325	13.153
0.03	4.02E-10	12.86	13.26			0.972	1.325	13.392
0.7	7.00E-10	2.7	8.999	0.256	1.344	0.949	1.306	13.007
0.5	7.00E-10	5.226	10.45			0.995	1.306	12.921
0.03	7.00E-10	13.04	13.45			0.958	1.306	13.571
0.7	9.97E-10	2.84	9.468	0.23	1.299	0.899	1.279	13.247
0.5	9.97E-10	5.299	10.6			0.982	1.279	12.858
0.03	9.97E-10	12.98	13.38			0.963	1.279	13.498

Table 11-continued								
R	da/dN	ΔK	K_{max}	m	α	g	modified alpha	K*
0.7	3.98E-09	3.218	10.73	0.162	1.193	0.776	1.176	13.256
0.5	3.98E-09	5.865	11.73			0.88	1.176	13.253
0.03	3.98E-09	13.04	13.45			0.958	1.176	13.518
0.7	7.04E-09	3.529	11.76	0.104	1.116	0.687	1.1	13.268
0.5	7.04E-09	6.463	12.93			0.785	1.1	13.854
0.03	7.04E-09	13.1	13.51			0.954	1.1	13.549
0.7	1.00E-08	3.713	12.38	0.065	1.069	0.64	1.066	13.4
0.5	1.00E-08	6.553	13.11			0.771	1.066	13.72
0.03	1.00E-08	13.04	13.45			0.958	1.066	13.472
0.7	2.01E-08	4.167	13.89	-0.013	0.987	0.536	0.948	13.048
0.5	2.01E-08	7.632	15.26			0.627	0.948	14.724
0.03	2.01E-08	13.22	13.63			0.945	0.948	13.611
0.7	4.01E-08	4.854	16.18	0.135	1.156	0.41	0.8544	13.577
0.5	4.01E-08	8.067	16.13			0.576	0.8544	14.585
0.03	4.01E-08	13.66	14.08			0.912	0.8544	14.019
0.7	7.08E-08	5.226	17.42	0.197	1.245	0.355	0.7939	13.592
0.5	7.08E-08	8.646	17.29			0.516	0.7939	14.99
0.03	7.08E-08	13.91	14.34			0.894	0.7939	14.254
0.7	1.01E-07	5.865	19.55	-0.331	0.751	0.276	0.7346	14.204
0.5	1.01E-07	9.013	18.03			0.481	0.7346	14.997
0.03	1.01E-07	14.17	14.61			0.876	0.7346	14.493
0.7	1.99E-07	6.404	21.35	-0.428	0.7	0.224	0.6589	14.156
0.5	1.99E-07	10.26	20.51			0.378	0.6589	16.195
0.03	1.99E-07	14.37	14.81			0.862	0.6589	14.662
0.7	4.07E-07	7.361	24.54	-0.647	0.607	0.154	0.5908	14.992
0.5	4.07E-07	10.92	21.84			0.333	0.5908	16.45
0.03	4.07E-07	14.91	15.37			0.826	0.5908	15.178
0.7	6.83E-07	8.19	27.3	-0.849	0.541	0.112	0.5383	15.659
0.5	6.83E-07	11.71	23.42			0.286	0.5383	17.006
0.03	6.83E-07	15.33	15.8			0.798	0.5383	15.581
0.7	1.01E-06	9.071	30.24	-1.06	0.485	0.079	0.487	16.304
0.5	1.01E-06	12.97	25.94			0.225	0.487	18.176
0.03	1.01E-06	15.62	16.1			0.78	0.487	15.849

Table 11-continued								
R	da/dN	ΔK	K_{max}	m	α	g	modified alpha	K*
0.7	3.83E-06	12.67	42.24	-2.36	0.298	0.019	0.3735	19.866
0.5	3.83E-06	14.63	29.27			0.163	0.3735	18.956
0.03	3.83E-06	17.95	18.5			0.648	0.3735	18.154
0.7	6.91E-06	13.21	44.04	-2.24	0.309	0.016	0.3316	19.695
0.5	6.91E-06	16.21	32.41			0.121	0.3316	20.394
0.03	6.91E-06	18.89	19.47			0.601	0.3316	19.081

In this case the α value is first calculated using K*(first method) approach as explained in Chapter 3.

Since R-ratio effect changes from the threshold region to the Paris region drastically, therefore the α value for each da/dN=constant is modified using the g- function. The values of g- functions are given in the 7^{th} column in Table 11.

The g values are different for each R-ratio for a given da/dN, therefore the average value of g is taken for a given da/dN and it is multiplied with the α to get the modified α value.

One can see from the modified α values, that they decrease from the threshold region to the Paris region. The modified α value for each da/dN is used to calculate K* , which is represented by the last column in Table 11.

Next da/dN vs K* is plotted for each R-ratio and the results are shown in Fig 31.

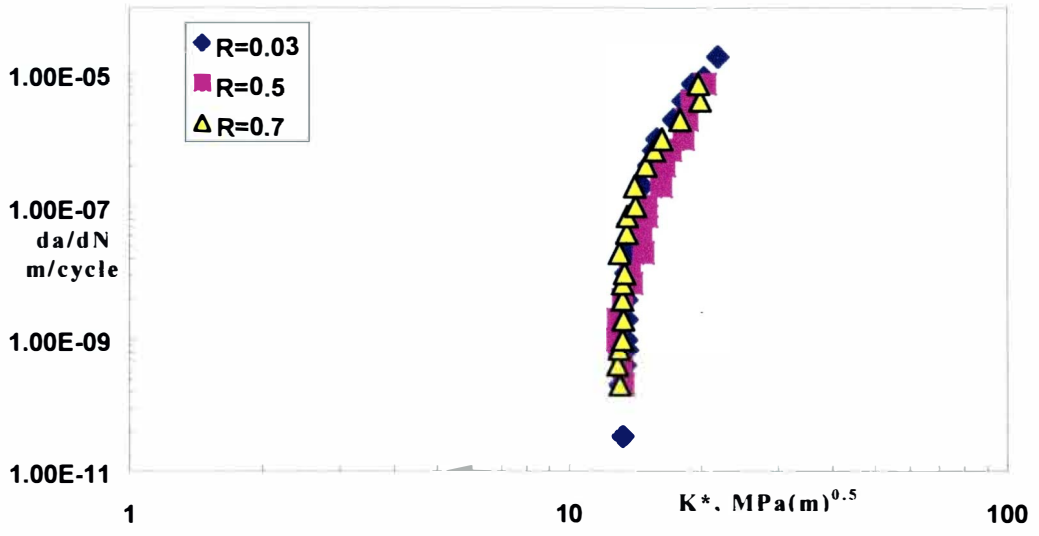

Figure 31. Fatigue crack growth data [27] of spheroidal cast iron microstructure as a function of K* using the g function.

Once the R ratios are correlated then the best-fit line for the correlated data can be used to predict for other R-ratios as explained in Chapter 3. Additional materials exhibiting diminishing R-ratio effects with increasing ΔK have been analyzed using g function and the results can be seen in the Appendix F.

8. MASTER CURVE ANALYSIS

During the service life of most engineering components, they experience an alternating stress σ_a and a mean stress σ_m. Mean stress may be introduced in the component by residual stresses due to the manufacturing processes.

For a metal a tensile mean stress usually has a detrimental effect while a compressive mean stress has a beneficial effect.

Kujawski and Ellyin [28] showed the effect of mean stress on fatigue limit (threshold) could be accounted through an appropriate mean stress function $f(\sigma_m/\sigma_a)$. They formulated an equation to emphasis the effect of mean stress on fatigue limit (threshold)

$$\sigma_a/\sigma_{-1} = 1/(f)^{0.5} \qquad (7\text{-}1)$$

where $1/(f)^{0.5}$ describes the threshold condition in terms of σ_a/σ_{-1} for different $\sigma m/\sigma a$ values, and

σ_m : mean stress corresponding to a given R-ratio,

σ_a : stress amplitude corresponding to a given R-ratio,

σ_{-1}: stress amplitude for R=-1(fully-reversed loading),

f : Mean stress function; $f^2-(\sigma_m/\sigma_a)f-1=0$.

A graphical representation of the above equation is shown in Fig.32, along with the experimental data, which indicates the effectiveness of this

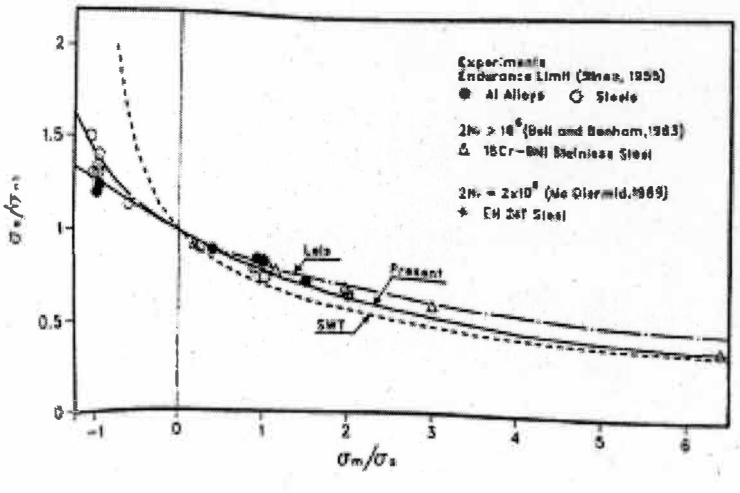

Figure 32. Mean stress effect on fatigue limit [28].

mean stress function in predicting the threshold condition.
On the other hand for a member with a crack like flaw or defect, the fatigue life may be estimated by crack growth rate analysis, e.g. SIF range ΔK.
However there is important difference between smooth and cracked specimen. In a smooth uniaxial specimen with no crack or notch the stress distribution is uniform and the load ratio applied at the end's remain the same throughout the specimen. That is for a load ratio of R=-1 apply at the end the stress ratio at the middle of the specimen also remain the same. This is illustrated by the sketch in Fig.33.

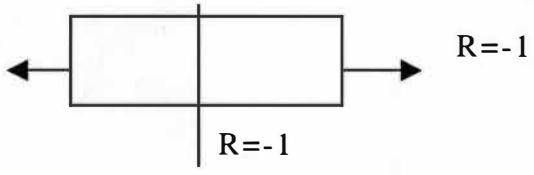

Figure 33. Load ratio effect on an unnotched specimen.

But in case of a specimen with a crack the situation is different. Usually the applied gross stress is elastic, i.e. below the yield stress. Since there is a crack induces a high stress concentration at the crack tip and plastic deformation will occur. Therefore during unloading it experience a compressive cyclic stress thus we have a negative R=-1 ratio in the tip for an applied load ratio of R=0.

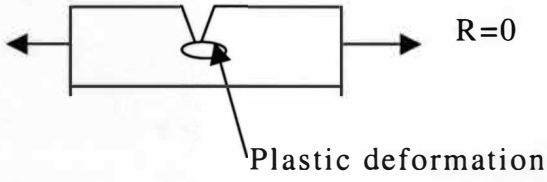

Figure 34. Load ratio effect on a notched specimen.

In general the crack growth driving force is describe in terms of stress intensity factor range ΔK.

The following relationship exists between amplitudes and ranges of the applied stresses,

$\sigma_a/\sigma_{-1} = \Delta\sigma/\Delta\sigma_{-1}$. (7-2)

Also the relation between ΔK and gross stress $\Delta\sigma$ is given by

$\Delta K = \Delta\sigma F(\pi l)^{0.5}$ (7-3)

where F is the function depending on geometry of the crack (e.g. for an infinite plate with a central crack of length 2l, F=1).

Thus σ_a/σ_{-1} can be written as

$\sigma_a/\sigma_{-1} = \Delta\sigma/\Delta\sigma_{-1} = \Delta K/\Delta K_0$

where $\Delta\sigma = 2\sigma_a$ and $\Delta\sigma_{-1} = 2\sigma_{-1}$.

In master curve approach the SIF data is normalized in terms of ΔK at R=0 i.e., ΔK_0. Since gross loading with R=0 induces R~ -1 at the crack tip.

Therefore, to predict the fatigue crack growth rate for a R-ratio, one needs to normalize the SIF data available for various R-ratio and plot them in terms of $\Delta K/K_0$ vs. K_m/K_a, from which the crack growth rate for a given R-ratio can be predicted.

This is illustrated by an example given below.

Consider the following set of crack growth data in Fig.35.

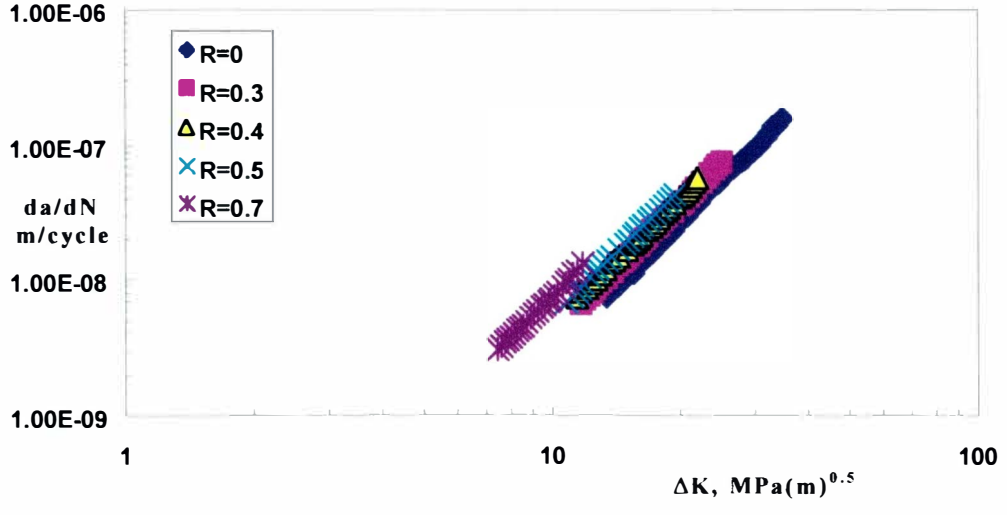

Figure 35. Fatigue crack growth data [16] of medium carbon structural steel as a function of ΔK.

From the above graph the value of ΔK for corresponding R ratio at a constant da/dn can be determined, and then the corresponding K_{max} is calculated using the formula

$K_{max}=\Delta K/(1-R)$. (7-4)

Then K_m/K_a is calculated as

$K_m/K_a=(1+R)/(1-R)$ (7-5)

where:

Km: mean value of stress intensity factor,

Ka: amplitude of stress intensity factor.

Next the ΔK value is normalized using the ΔK_0 value of the particular da/dN. This is given by the last column in Table 12.

Table 12. Calculation of K_m/K_a and $\Delta K/\Delta K_0$.

R	da/dN	ΔK	K_{max}	K_m/K_a	$\Delta K/\Delta K_0$
0.7	7.E-09	9.8845	32.948	5.667	0.739
0.5	7.E-09	10.847	21.694	3	0.811
0.4	7.E-09	11.469	19.115	2.333	0.858
0.3	7.E-09	11.794	16.848	1.857	0.882
0	7.E-09	13.37	13.37	1	1
0.7	1.E-08	11.102	37.007	5.667	0.743
0.5	1.E-08	12.015	24.03	3	0.804
0.4	1.E-08	12.763	21.272	2.333	0.854
0.3	1.E-08	13.37	19.1	1.857	0.894
0	1.E-08	14.948	14.948	1	1
0.5	2.E-08	15.228	30.456	3	0.834
0.4	2.E-08	15.952	26.587	2.333	0.874
0.3	2.E-08	16.48	23.543	1.857	0.903
0	2.E-08	18.254	18.254	1	1
0.5	3.E-08	17.184	34.367	3	0.834
0.4	3.E-08	17.918	29.863	2.333	0.87
0.3	3.E-08	18.857	26.939	1.857	0.915
0	3.E-08	20.598	20.598	1	1
0.5	4.E-08	19.033	38.067	3	0.85
0.4	4.E-08	19.846	33.077	2.333	0.886
0.3	4.E-08	20.598	29.426	1.857	0.92
0	4.E-08	22.395	22.395	1	1
0.4	6.E-08	21.881	36.468	2.333	0.858
0.3	6.E-08	23.243	33.205	1.857	0.911
0	6.E-08	25.507	25.507	1	1

The data are arranged with respect to the R-ratio as given in Table13.

Table 13. Data of K_m/K_a and $\Delta K/\Delta K_0$ for the given R-ratios

R	K_m/K_a	$\Delta K/\Delta K_0$
0.7	5.666667	0.739298
0.7	5.666667	0.742741
0.5	3	0.811302
0.5	3	0.803797
0.5	3	0.834241
0.5	3	0.834241
0.5	3	0.849893
0.4	2.333333	0.857829
0.4	2.333333	0.853852
0.4	2.333333	0.873923
0.4	2.333333	0.869871
0.4	2.333333	0.886192
0.4	2.333333	0.857829
0.3	1.857143	0.882083
0.3	1.857143	0.894466
0.3	1.857143	0.902818
0.3	1.857143	0.915493
0.3	1.857143	0.919757
0.3	1.857143	0.911248
0.3	1.857143	0.89032
0	1	1
0	1	1
0	1	1
0	1	1
0	1	1
0	1	1
0	1	1

Using the above table one can observe that for the same R-ratio the K_m/K_a value remains constant while the $\Delta K/\Delta K_0$ varies. If $\Delta K/\Delta K_0$ is plotted versus K_m/K_a it will be difficult to obtain a single curve, which will take into account of all the R-ratios.

Therefore, the average value of K_m/K_a and $\Delta K/\Delta K_0$ for a given R-ratio is calculated (this is given in Table 14.) and the resulting curve is plotted in terms of K_m/K_a vs. $\Delta K/\Delta K_0$ in Fig.36.

Table 14. Calculation of average K_m/K_a and average $\Delta K/\Delta K_0$ for the given R-ratios

		K_m/K_a	$\Delta K/\Delta K_0$
R=0.7	Ave =	5.666667	0.741019
R=0.5	Ave =	3	0.826695
R=0.4	Ave =	2.333333	0.866583
R=0.3	Ave =	1.857143	0.902312
R=0.0	Ave =	1	1

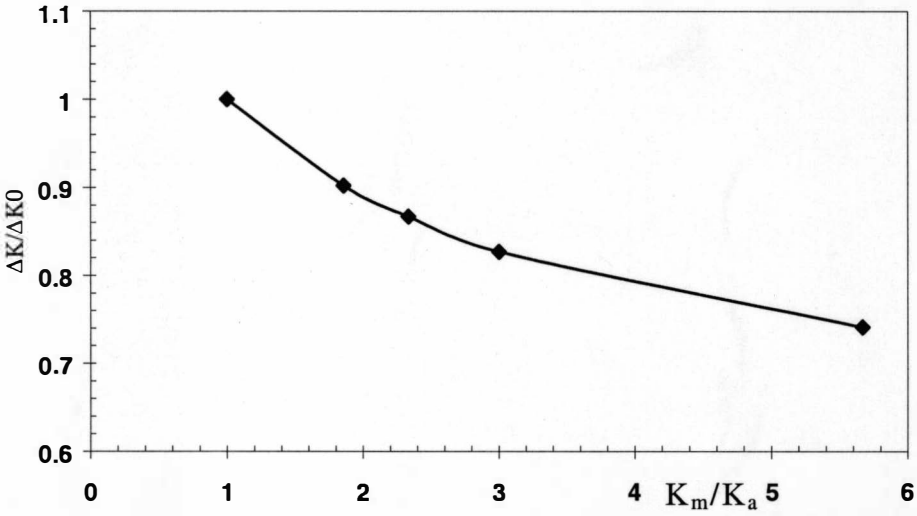

Figure 36. Master curve for medium carbon structural steel[16].

In order to predict the crack growth rate for a given R-ratio, one needs to first calculate the K_m/K_a for that R-ratio and then the corresponding $\Delta K/\Delta K_0$ can be determined from Fig.36.

Knowing the value of $\Delta K/\Delta K_0$ one can calculate ΔK for a fixed da/dN. This ΔK value is the stress intensity factor range for the given R-ratio at the particular da/dN value which is the crack growth rate corresponding to ΔK_0 that is taken to calculate ΔK.

The value of $\Delta K/\Delta K_0$ obtained from master curve is the average value and it is assumed to be constant for a given K_m/K_a value. Therefore one can

calculate ΔK value for all the da/dN values simply by multiplying $\Delta K/\Delta K_0$ with the value of ΔK_0 for a given da/dN.

The above approach can be illustrated by taking an example.

In order to predict the crack growth rate for R=0.1 for the material in Fig.35, the following steps are performed.

First K_m/K_a is calculated,

$K_m/K_a=(1+R)/(1-R)$

$=1.1/0.9$

$=1.22$

For K_m/K_a =1.22, from Fig.36, the value of $\Delta K/\Delta K_0$ = 0.97 is determined Using this value of $\Delta K/\Delta K_0$, one can calculate the value of ΔK for R=0.1 for all the da/dN value from Table 14. These da/dN values are shown in the last column in Table 14.

Table 15. Calculation of ΔK for the given R-ratio

R	da/dN	ΔK_0	K_m/K_a	$\Delta K/\Delta K_0$	ΔK for R=0.1
0	7.02E-09	13.37012	1.22	0.97	12.96901376
0	1.02E-08	14.94759	1.22	0.97	14.49916107
0	1.99E-08	18.25375	1.22	0.97	17.7061404
0	3.02E-08	20.59797	1.22	0.97	19.98003082
0	4.01E-08	22.39502	1.22	0.97	21.72316477
0	6.08E-08	25.50703	1.22	0.97	24.74182175
0	7.99E-08	28.25267	1.22	0.97	27.40509235

Thus, the resulting crack growth data for R=0.1 are given in Table 16.

Table 16. Crack growth data for R=0.1 in terms of ΔK and da/dN

da/dN	ΔK
7.02E-09	12.96901
1.02E-08	14.49916
1.99E-08	17.70614
3.02E-08	19.98003
4.01E-08	21.72316
6.08E-08	24.74182
7.99E-08	27.40509

The above set of crack growth rate data for R=0.1 when plotted along with the original set of data are depicted in Fig.37.

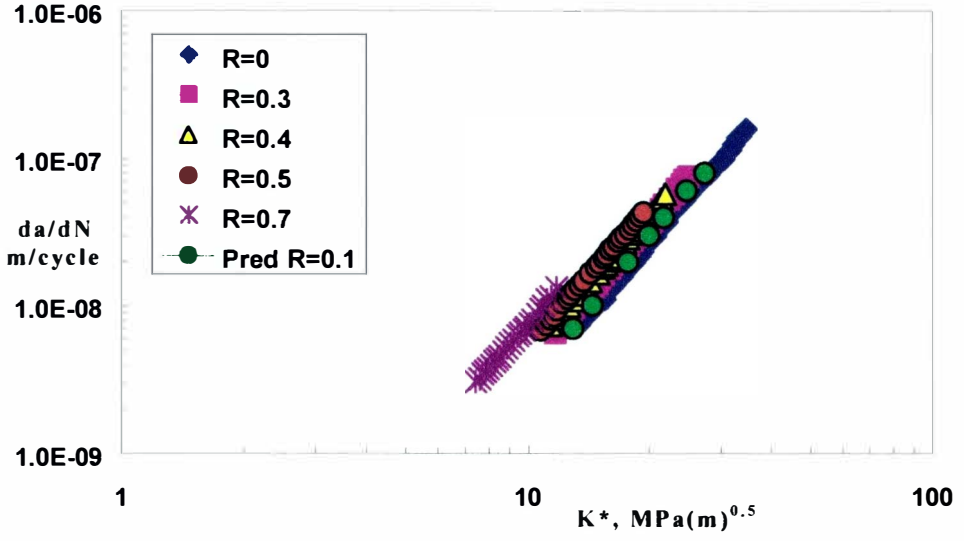

Figure 37. Fatigue crack growth data [16] of medium carbon structural steel as a function of K* by master curve approach.

Appendix G contains more results obtained using the "master curve" approach.

Sometimes the data that are available from the literature might not contain the crack growth rate data for R=0. In this case either the crack growth rate data for R=0 is predicted using the K* approach from the existing data or the value of ΔK is extrapolated from a plot of ΔK vs R for a constant da/dN.

9. PREDICTION ACCURACY OF MASTER CURVE APPROACH

This chapter deals with the accuracy of the master curve method. The following steps are performed to check the accuracy of the master curve approach using the data in Fig.38.

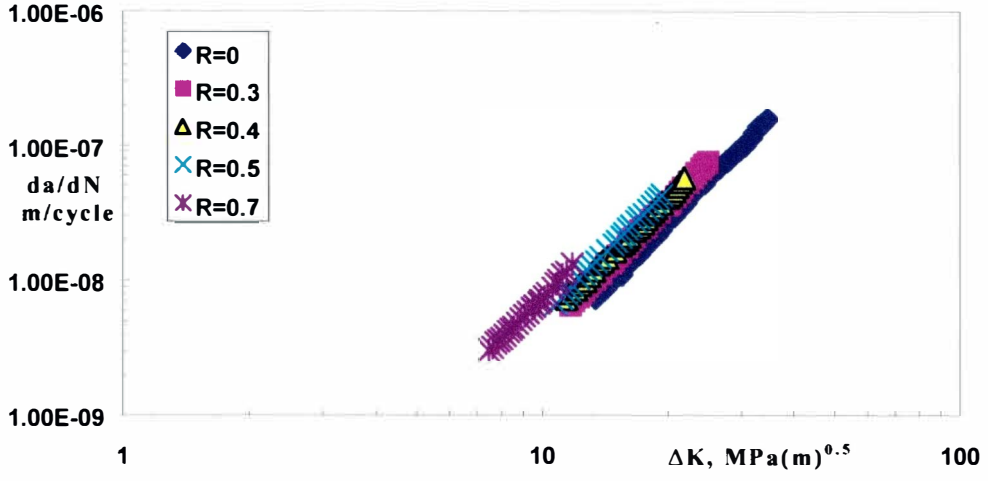

Figure 38. Fatigue crack growth data [16] of medium carbon structural steel as a function of ΔK.

Instead of using all the five R ratio in Fig.38 for the master curve determination, only four R-ratios that are R=0, 0.4, 0.5 and 0.7 are used. R=0.3 data are predicted and compared with experimental results. Table 17 represents the analysis performed with the above four R-ratios.

Table 17. Calculation of K_m/K_a and $\Delta K \Delta K_0$ for four R-ratios

R	da/dN	ΔK	K_{max}	K_m/K_a	$\Delta K/\Delta K_0$
0.7	7.E-09	9.884	32.948	5.667	0.739
0.5	7.E-09	10.85	21.694	3	0.811
0.4	7.E-09	11.47	19.115	2.333	0.858
0	7.E-09	13.37	13.37	1	1
0.7	1.E-08	11.1	37.007	5.667	0.743
0.5	1.E-08	12.01	24.03	3	0.804
0.4	1.E-08	12.76	21.272	2.333	0.854
0	1.E-08	14.95	14.948	1	1
0.5	2.E-08	15.23	30.456	3	0.834
0.4	2.E-08	15.95	26.587	2.333	0.874

Table 17-continued					
R	da/dN	ΔK	K_{max}	K_m/K_a	$\Delta K/\Delta K_0$
0	2.E-08	18.25	18.254	1	1
0.5	3.E-08	17.18	34.367	3	0.834
0.4	3.E-08	17.92	29.863	2.333	0.87
0	3.E-08	20.6	20.598	1	1
0.5	4.E-08	19.03	38.067	3	0.85
0.4	4.E-08	19.85	33.077	2.333	0.886
0	4.E-08	22.4	22.395	1	1
0.4	6.E-08	21.88	36.468	2.333	0.858
0	6.E-08	25.51	25.507	1	1

The obtained results are arranged with respect to the R-ratio as given in Table 18.

Table 18. Data of K_m/K_a and $\Delta K/\Delta K_0$ for the given R-ratios

R	K_m/K_a	$\Delta K/\Delta K_0$
0.7	5.666667	0.739298
0.7	5.666667	0.742741
0.5	3	0.811302
0.5	3	0.803797
0.5	3	0.834241
0.5	3	0.834241
0.5	3	0.849893
0.4	2.333333	0.857829
0.4	2.333333	0.853852
0.4	2.333333	0.873923
0.4	2.333333	0.869871
0.4	2.333333	0.886192
0.4	2.333333	0.857829
0	1	1
0	1	1
0	1	1
0	1	1
0	1	1
0	1	1
0	1	1

The average values of K_m/K_a and $\Delta K/\Delta K_0$ for a given R-ratio are depicted in Table 19.

Table 19. Calculation of average K_m/K_a and average $\Delta K/\Delta K_0$ for the given R-ratios

		K_m/K_a	$\Delta K/\Delta K_0$
R=0.7	Ave =	5.666667	0.741019
R=0.5	Ave =	3	0.826695
R=0.4	Ave =	2.333333	0.866583
R=0.0	Ave =	1	1

The corresponding master curve is shown in Fig.39.

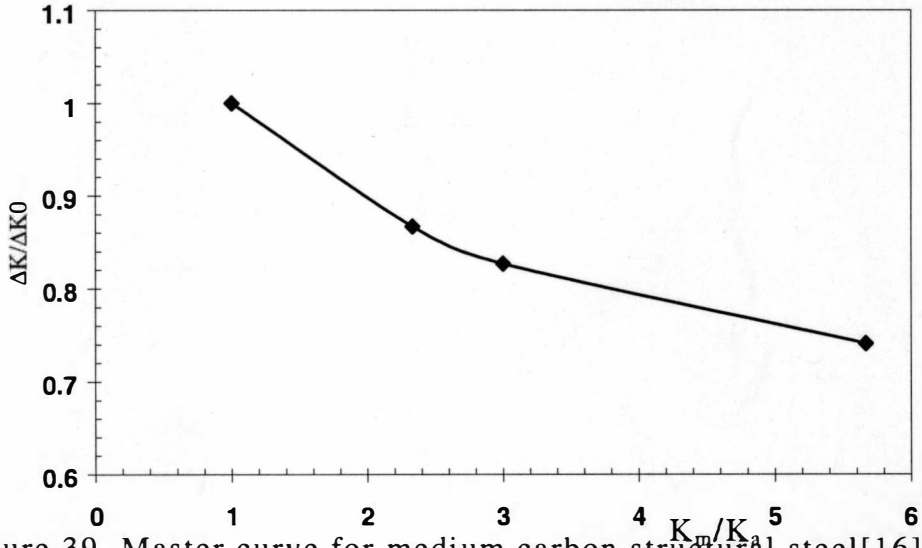

Figure 39. Master curve for medium carbon structural steel[16].

Now for R=0.3 the following conclusion are made:

$K_m/K_a=(1+R)/(1-R)$

$=1.3/0.7$

$=1.857$

For K_m/K_a =1.857, from Fig.39, the value of $\Delta K/\Delta K_0$ = 0.915 .

Using this value of $\Delta K/\Delta K_0$,one can calculate the value of ΔK for R=0.3.

The above step is repeated for all the da/dN value from Table 17.

Calculated values of ΔK are shown in the last column in Table 20.

Table 20. Calculation of ΔK for R=0.3

R	da/dN	ΔK_0	$\Delta K/\Delta K_0$	ΔK for R=0.3
0	7.02E-09	13.37012	0.915	12.233657
0	1.02E-08	14.94759	0.915	13.677044
0	1.99E-08	18.25375	0.915	16.702184
0	3.02E-08	20.59797	0.915	18.847142
0	4.01E-08	22.39502	0.915	20.491439
0	6.08E-08	25.50703	0.915	23.338935
0	7.99E-08	28.25267	0.915	25.851195

The above set of predicted crack growth rate data in Table 20, for R=0.3 are plotted along with the original set of data and are shown in Fig.40.

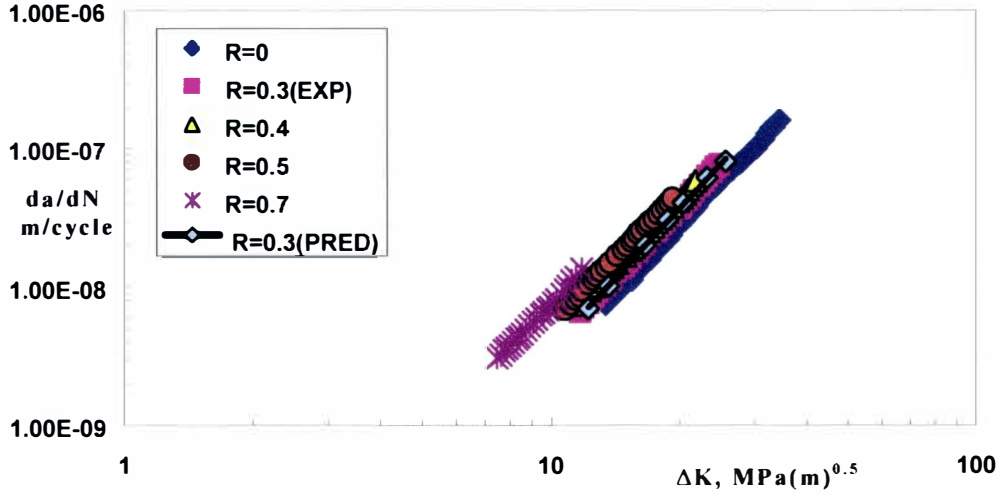

Figure 40. Fatigue crack growth data [16] of medium carbon structural steel as a function of ΔK showing the predicted data and the experimental data for R=0.3.

Similar type of analysis was performed for other materials and the results are shown in the Appendix H.

10. CONCLUSIONS

Experimental data for fatigue crack growth rate for 31 different materials, were analyzed using the fatigue crack driving force K* and the "master curve" approach. It was shown that both methods were very effective in predicting the R-ratio effects on fatigue crack growth rate.

The fatigue crack driving force parameter K* consolidates the data into a single scatter band. It also predicts accurately da/dN rate for a given R-ratio.

The fatigue crack driving force parameter K* was compared with the closure based ΔK_{eff} approach. It was seen that the K* approach was as effective as the closure methodology in consolidating the da/dN data for different R-ratios.

The "master curve" approach predicts the fatigue crack growth rate for different R-ratios with reasonable accuracy. But in case of fatigue crack growth data where the effects of R-ratios are diminishing with increasing ΔK values, the "master curve" approach fails to predict the actual behavior. Therefore further analyses of the "master curve" approach for this type of data are required.

REFERENCES

[1] Wohler A; Versuche uber die Festigkeit der Eisenbahnwagenachsen, Zeitschrift fur Bouwasen 1860, 10: English summary (1867), Engineering 4,160-161.

[2] Brockenbrough R L and Johnson B.G, 1981, USS Steel Design Manual, ADUSS 27-3400-04, United States Steel Corp, Monroville, PA.

[3] Wells, A.A; The Condition of Fast Fracture in Aluminum Alloys with Particular Reference to Comet Failures. British welding Research Association Report, April 1955.

[4] Winne D.H. and Wundt B.M.; Application of the Griffith-Irwin Theory of Crack Propagation to the Bursting Behavior of Disks, Including Analytical and Experimental Studies; Transactions of the American Society of Mechanical Engineers, Vol 80,1958, pp. 1643-1655.

[5] Wells, A.A; Unstable Crack Propagation in Metals; Cleavage and Fast fracture. Proceedings of the Crack Propagation Symposium, Vol 1, paper 84, Cranfiled, U.K, 1961.

[6] Rice J.R; A Path Independent Integral and the Approximate Analysis of Strain Concentration by Notches and Cracks, Journal of Applied Mechanics, Vol 35,1968,p 379-386.

[7] Mechanical Behavior of Materials; Norman E. Dowling, second edition, prentice Hall.1998.

[8] Fracture Mechanics, T.L Anderson, second edition,CRC Press, 1995.

[9] Dubey s, Soboyejo ABO, Soboyejo WO; An investigation of the effects of stress ratio and crack closure on the micro-mechanisms of fatigue crack growth in TI-6A1-4V; Acta Mater. Vol 45 No 7, 1997, pp 2777-2787.

[10] Elber V,(1971); The significance of fatigue crack closure. In : Damage Tolerance in Aircraft Structures, ASTM STP 486, Philadelphia, PA, American Society for Testing and Materials, pp 230-242.

[11] Donald K, Paris PC, An evaluation of ΔK_{eff} estimation procedure on 6061-T6 and 2024-T3 aluminum alloys, Int. J. of Fatigue,1999, Vol 21, pp.547-557.

[12] Kujawski D; Enhanced model of partial crack closure for correlation of R-ratio effects in aluminum alloys; Int. J. Fatigue 23 (2001) 95-102.

[13] McClung, R.C., The Influence of Applied Stress, Crack Length and Stress Intensity Factor on Crack Closure. Metallurgical Transactions, Vol 22A, 1991, pp. 1559-1571.

[14] Donald K, Gary H. Bray and Ralp W.Bush;Introducing the Kmax sensitivity concept for correlating fatigue crack growth data The Minerals , Metals & Materials Society,1997.

References-continued.

[15] Sadananda K and Vasudevan A.K.; Analysis of fatigue crack closure and thresholds; Fracture Mechanics 25,ASTM STP 1220.

[16] Tsukuda H, Ogiyama H, Shiraishi H; Fatigue crack growth and closure at high stress ratios; Fatigue Fract. Engng. Mater. Struct. Vol 18 No 4, 1995, pp 503-514 .

[17] Kujawski D; A fatigue crack driving force parameter with load ratio effects; Int. J. Fatigue (2001). Vol 23, Supplement, pp. S239-S246.

[18] Walker K, The effect of stress ratio during crack propagation and fatigue for 2024-T3 and 7075-T6 aluminum. In: Effects of Enviroment and Complete Loading History On Fatigue Life, ASTM STP 462, Philadelphia, PA. American Society for Testing and Materials, 1970, pp 1-14.

[19] Zhen J, Powell B.E, Effect of stress ratio and test methods on fatigue crack growth rate for nickel based superalloy Udimet 720, Int J of Fatigue, 1999, Vol 21, p 507-513.

[20] Oh SC, Song JH; Crack growth and closure behavior of surface cracks under pure bending loading; Int. J. Fatigue 23 (2001) 251-258.

[21] J.H. Kim, S.B. Lee; Behavior of plasticity-induced crack closure and roughness induced crack closure in aluminum alloy; Int. J. Fatigue 23(2001)S247-S251.

[22] James MN, Wenfong L; Fatigue crack growth in austempered ductile and grey cast irons – stress ratio effects in air and mine water; Mater. Sci. Engng. A265(1999) 129-139.

[23] Ritchie RO, Boyce BL, Campbell JP, Roder O, Thompson AW, Milligan WW; Thresholds for high-cycle fatigue in a turbine engine Ti-6A1-4V alloy; Int. J. Fatigue 21 (1999) 653-662.

[24] Jha SK, Ravichandran KS; Effect of mean stress (stress ratio) and aging on fatigue-crack growth in a metastable beta titanium alloy, Ti-10V-2Fe-3Al; Metallurgical Mater. Trans. Vol 31A March 2000-703.

[25] Tanaka T, Jono M, Komai K; Current research on fatigue cracks; Curr. Jap. Mater. Research-Vol 1.

[26] Chang T, Guo W; Effects of strain hardening and stress state on fatigue crack closure; Int. J. Fatigue 21 (1999) 881-888.

[27] Bulloch JH; Effect of temperature on the threshold fatigue crack growth behavior of spheroidal graphite cast iron; Int. J. Pres. Ves. & Piping 54 (1993) 497-522.

[28] D.Kujawski, F.Ellyin; A unified approach to mean stress effect on fatigue threshold conditions; Int J. Fatigue 17, No 2, pp101-106,1995.

[29] Zhuang WZ; Prediction of crack growth from bolt holes in a disc; Int. J. Fatigue 22 (2000) 241-250.

References-continued.

[30] K.R. Dennis. 1986. Fatigue crack growth of gun tube steel under spectrum loading. MS Thesis, Engineering science and mechanical dept. Virginia polytechnic institute and state University, Blacksburg,VA, may 1986.

[31] D.V. Ramsamooj, T.A. Shugar; Model prediction of fatigue crack propagation in metal alloys in laboratory air; Int. J. Fatigue 23(2001)S287-S300.

[32] Gross TS, Zhong L; Effect of load ratio on crack tip cyclic plastic work – evidence for fractional work; Scripta Metallurgia Vol 20 pp 1713-1713 1986.

[33] Bulloch JH; Near threshold fatigue behaviour of flake graphite cast irons microstructures; Theoretical Appl. Fract. Mech. 24 (1995) 65-78.

[34] Kamat SV, Srinivas M; Effect of load ratio on the fatigue crack growth behavior of Dispal 2 alloy; Int. J. Fatigue 21 (1999) 169-172.

[35] Chen DL, Weiss B, Stickler R; Effect of stress ratio and loading condition on the fatigue threshold; Int. J. Fatigue 14 No 5 (1992) pp 325-329.

[36] Zhang S, Marissen R, Schulte K, Trautmann KK, Nowack H, Schijve J; Crack propagation studies on A1 7475 on the basis of constant amplitude and selective variable amplitude loading histories; Fatigue Pract. Dngng. Mater. Struct. Vol 10 No 4 pp 315-332 1987.

[37] Onofrio G, Osinkolu GA, Marchionni M; Fatigue crack growth of UDIMET 720 Li superalloy at elevated temperature; Int. J. Fatigue 23 (2001) 887-895.

[38] Radhakrishnan VM; Endurance diagram; Int. J. Fatigue 12 No 6 (1990) pp 513-517.

[39] Bulloch JH; Fatigue threshold in steels-mean stress and microstructure influences; Int. J. Pres. Ves. & Piping 58 (1994) 103-127.

APPENDIX : A

COMPARISION OF FIRST METHOD AND SECOND METHOD IN CORRELATING CRACK GROWTH DATA

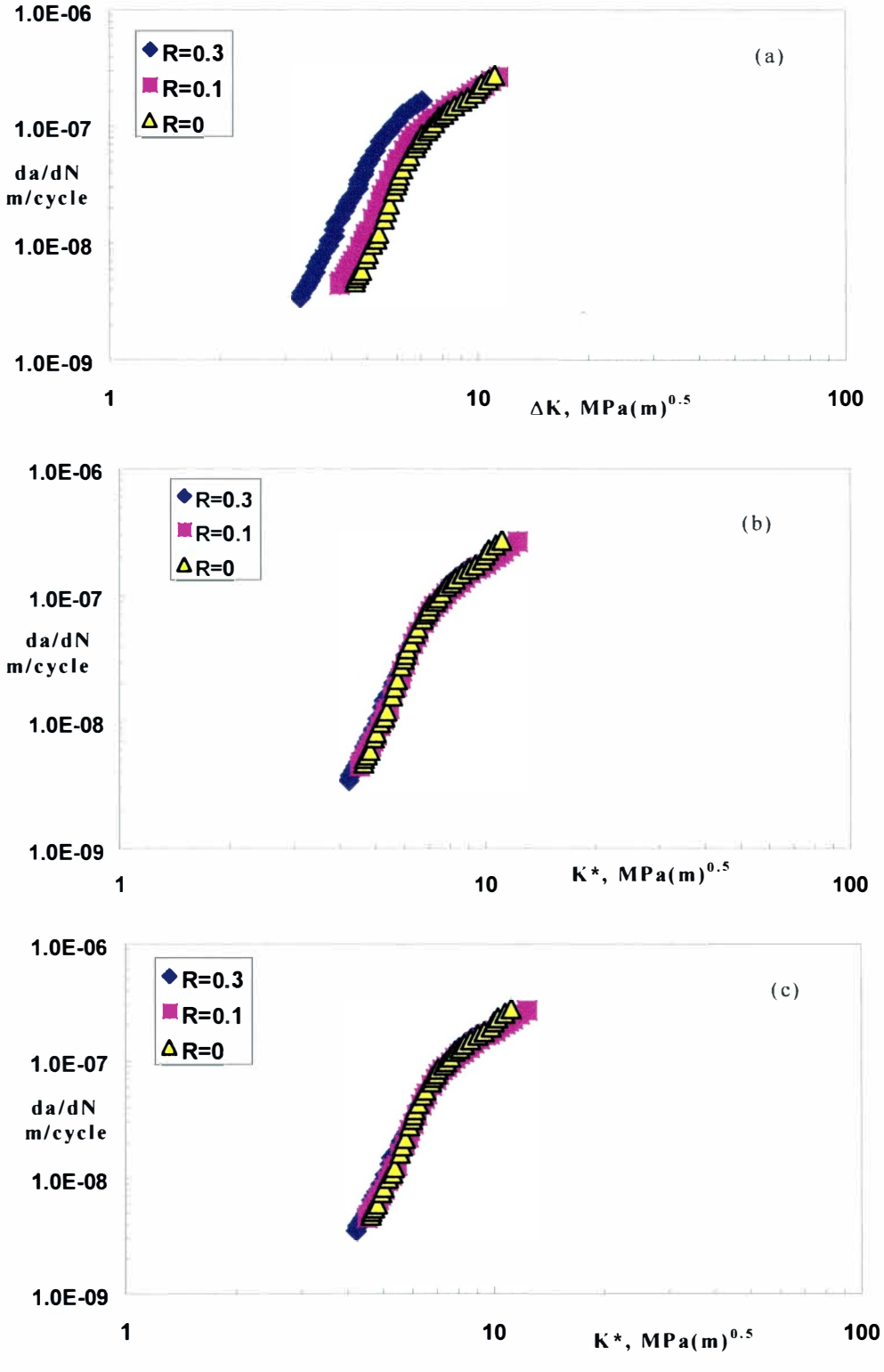

Figure 41. Fatigue crack growth data [20] of 7075-T651 as a function of (a) ΔK; (b) K*(first method); (c) K*(second method).

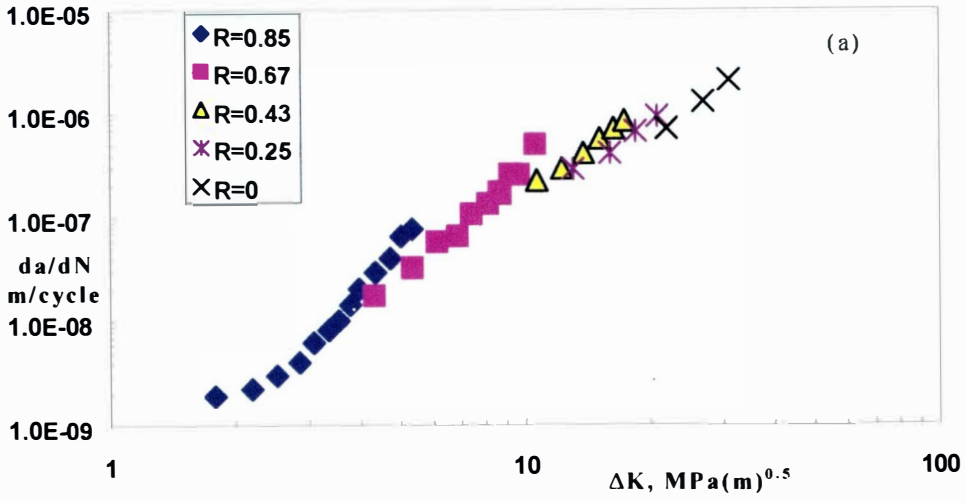

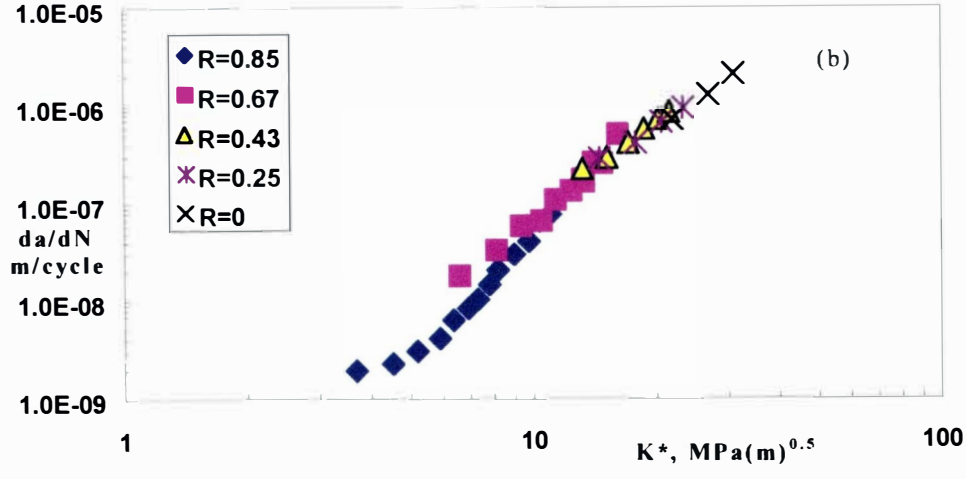

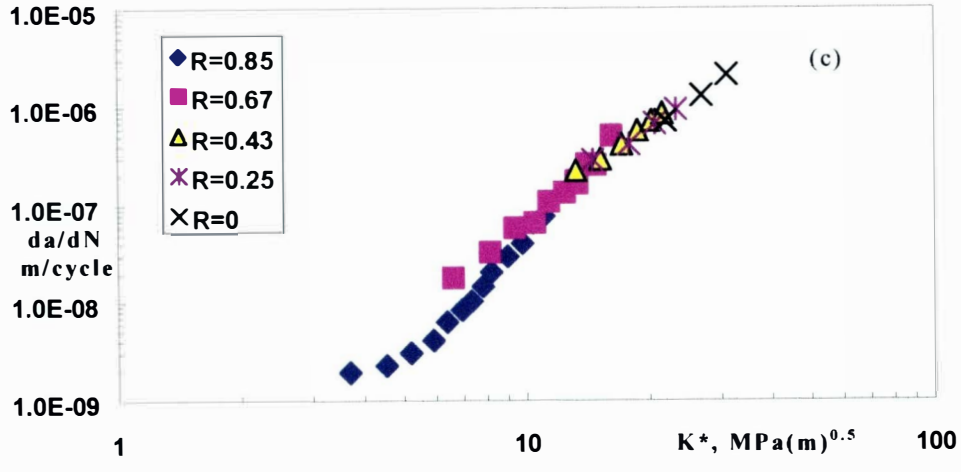

Figure 42. Fatigue crack growth data [29] of Ti 8-1-1 as a function of (a) ΔK; (b) K*(first method); (c) K*(second method).

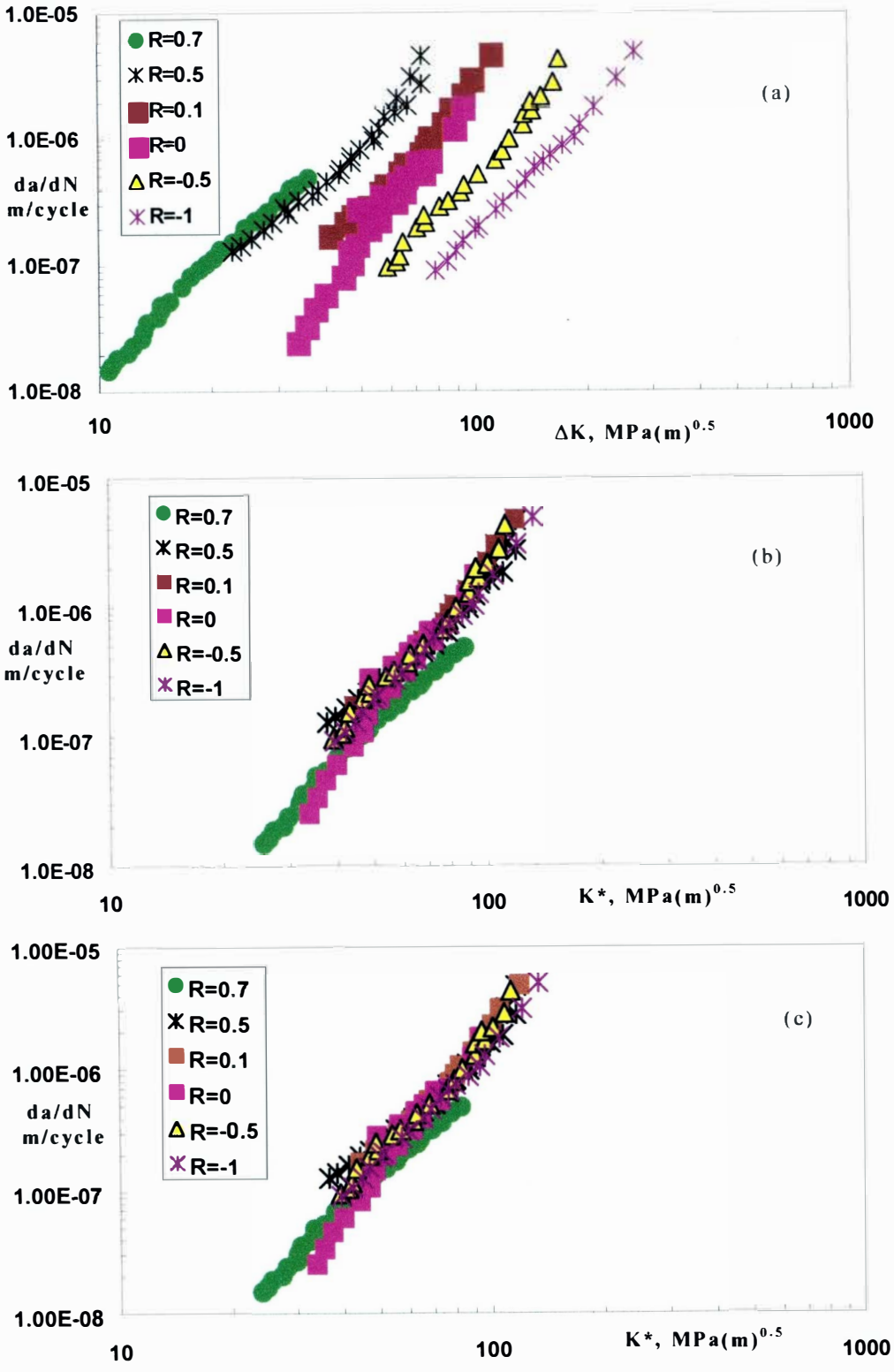

Figure 43. Fatigue crack growth data [30] of AISI 4340 steel as a function of (a) ΔK; (b) K*(first method); (c) K*(second method).

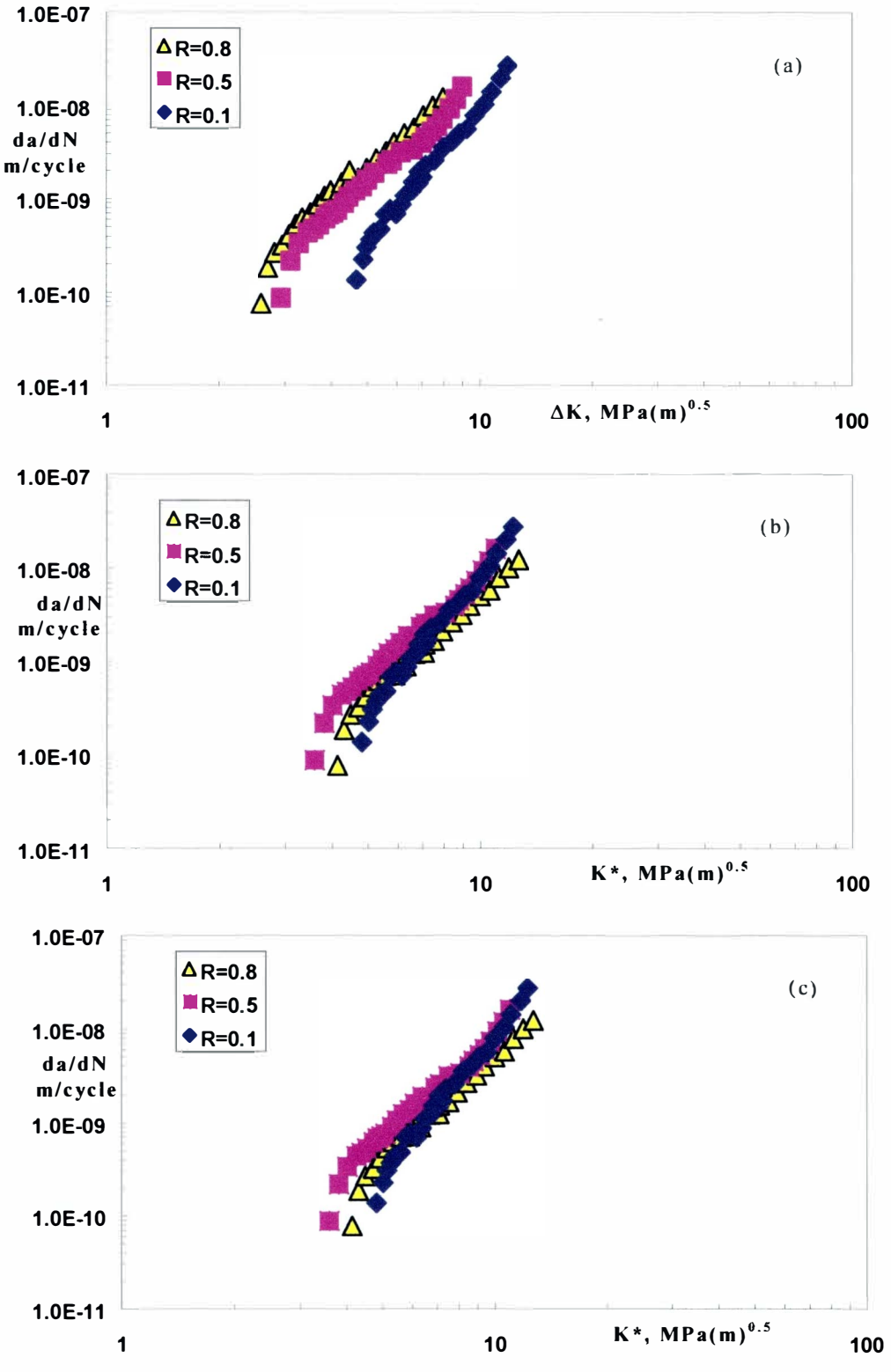

Figure 44. Fatigue crack growth data [23] of Ti-6Al-4V as a function of (a) ΔK; (b) K*(first method); (c) K*(second method).

APPENDIX : B

CORRELATION OF EXPERIMENTAL CRACK GROWTH DATA USING K*

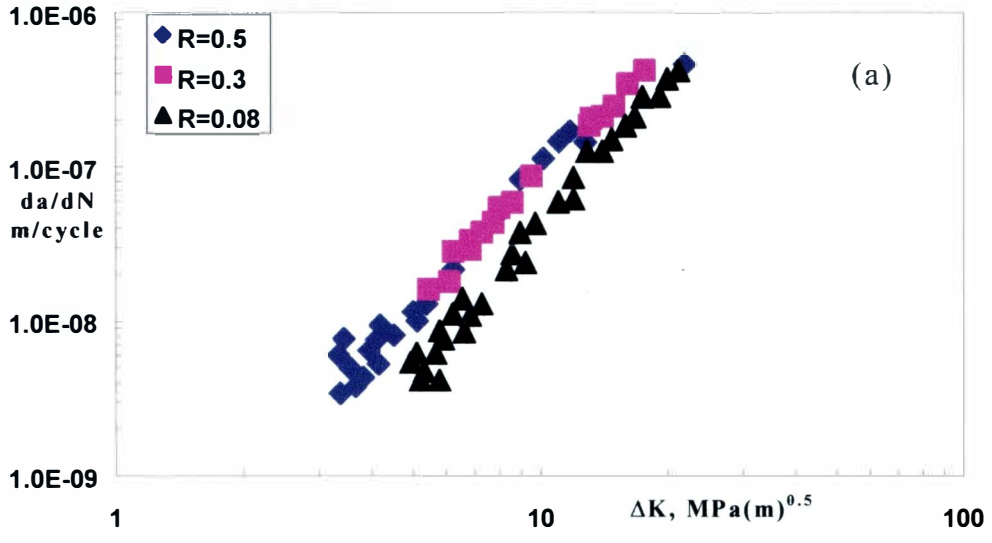

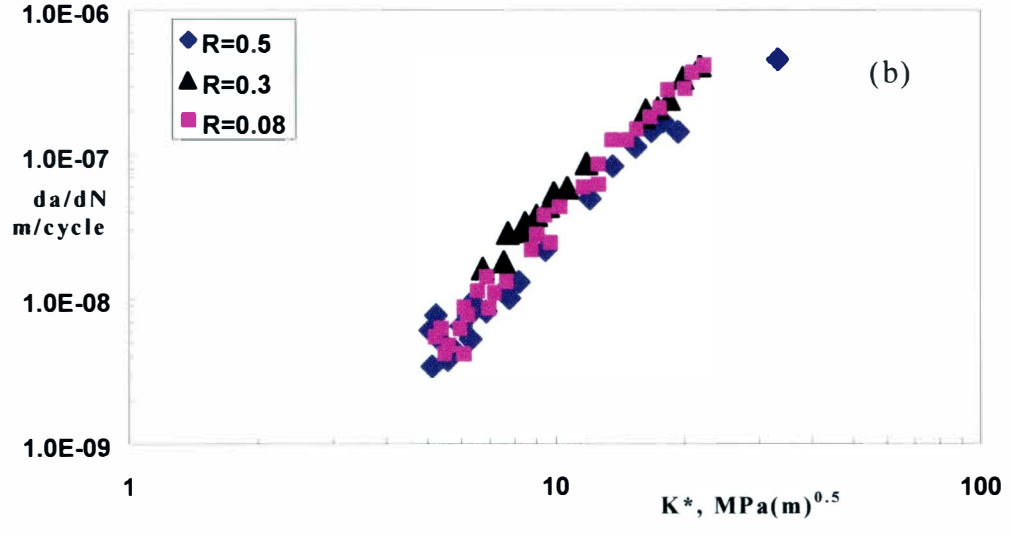

Figure 45. Fatigue crack growth data [31] of 7075-T651 as a function of (a) ΔK; (b) K*(first method).

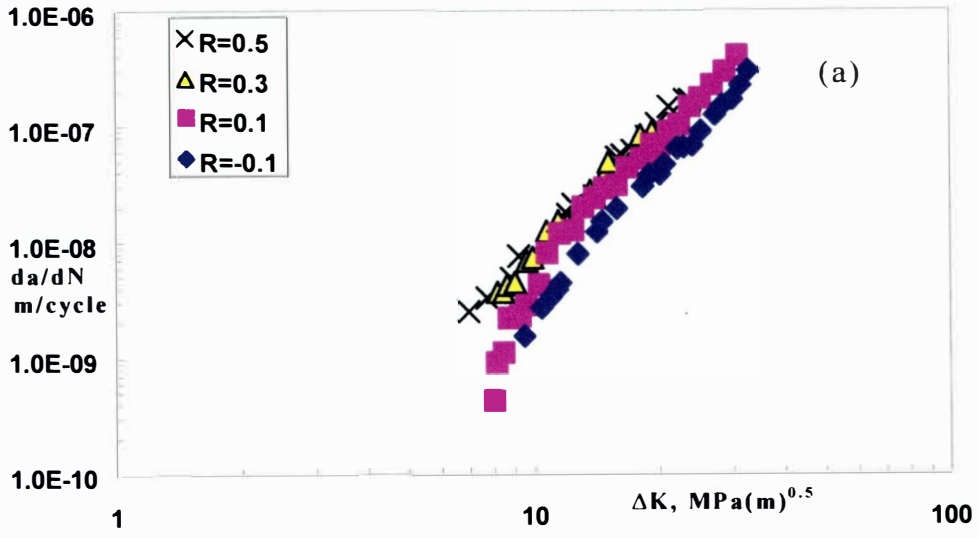

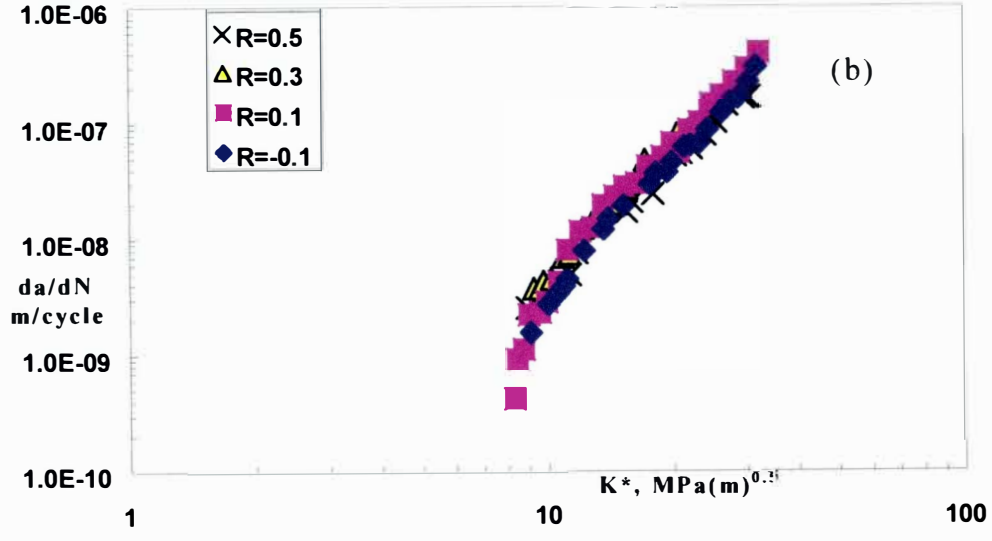

Figure 46. Fatigue crack growth data [32] of 304 stainless steel as a function of (a) ΔK; (b) K*(first method).

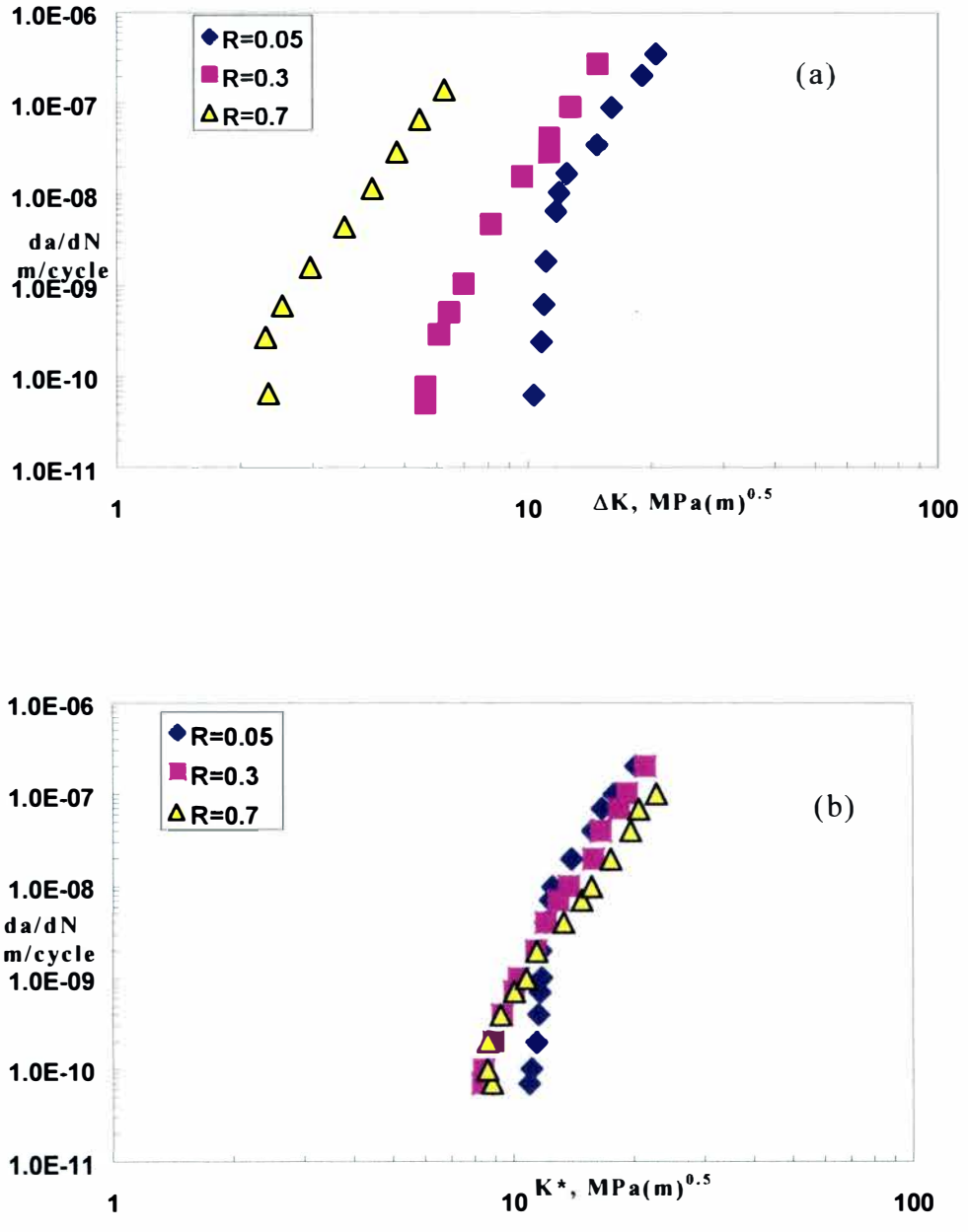

Figure 47. Fatigue crack growth data [33] of pearlitic microstructure as a function of (a) ΔK; (b) K*(first method).

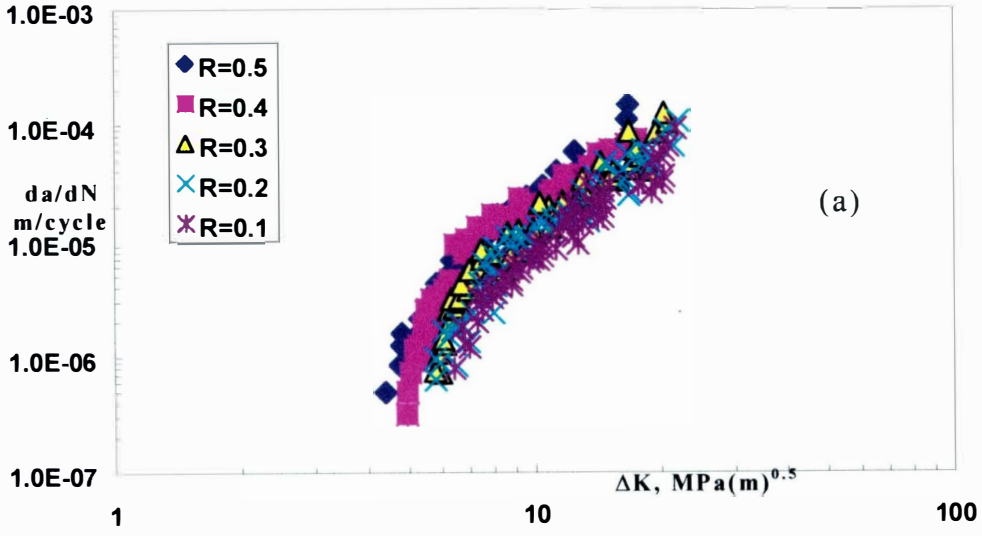

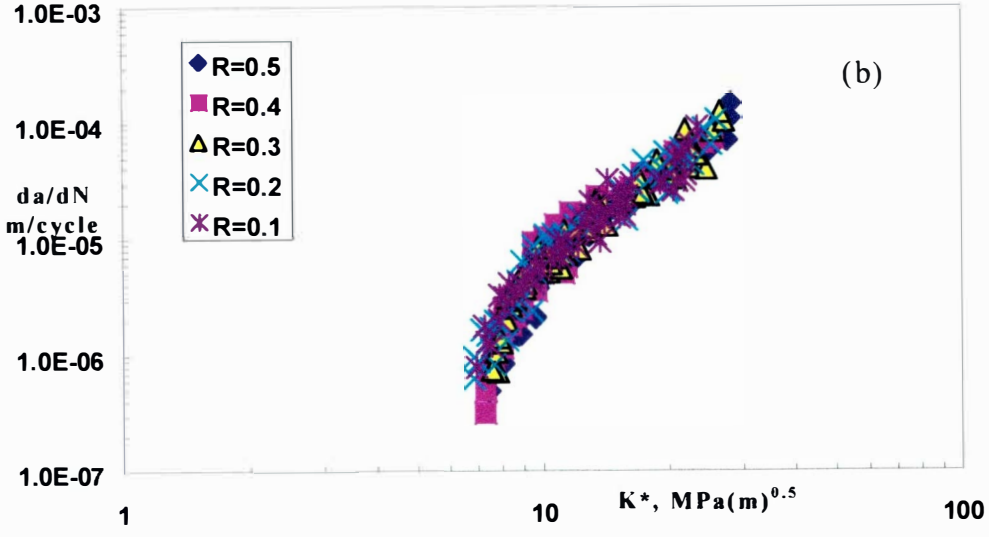

Figure 48. Fatigue crack growth data [22] of austempered ductile iron as a function of (a) ΔK; (b) K*(first method).

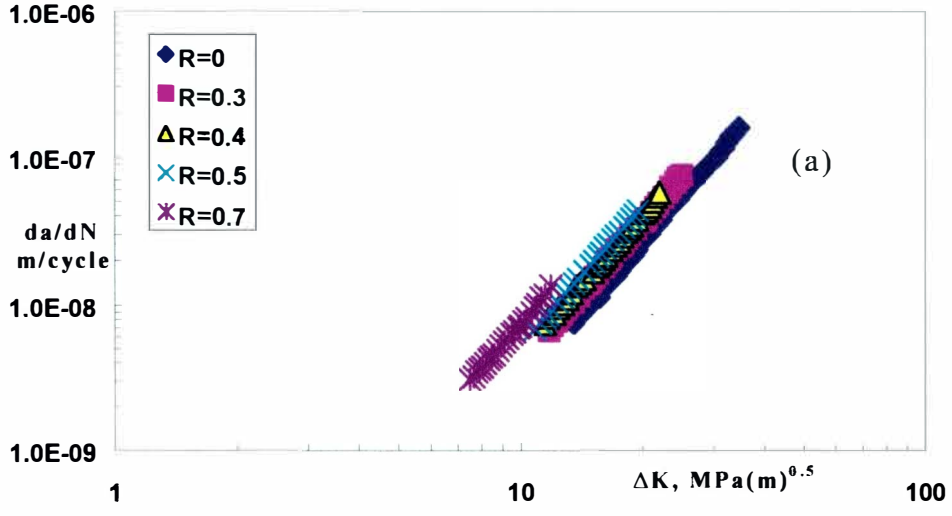

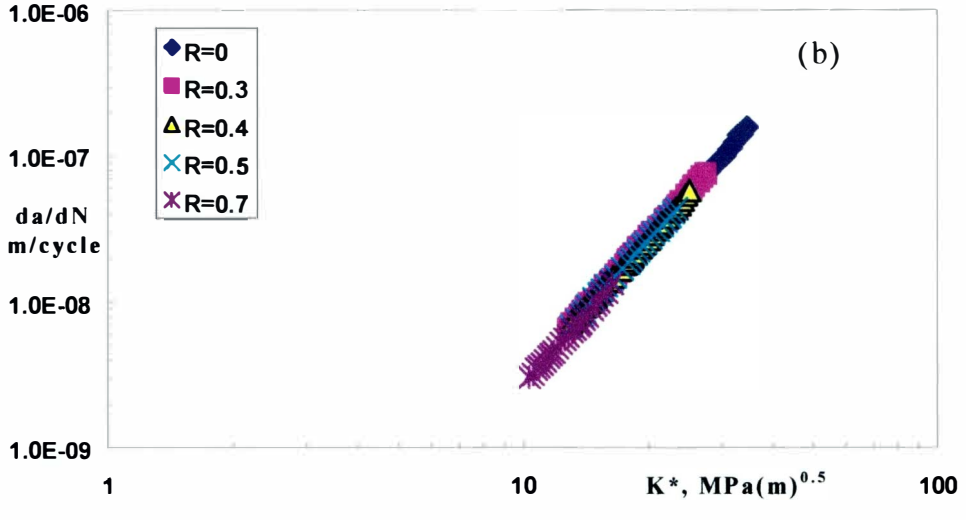

Figure 49. Fatigue crack growth data [16] of medium carbon structural steel as a function of (a) ΔK; (b) K*(first method).

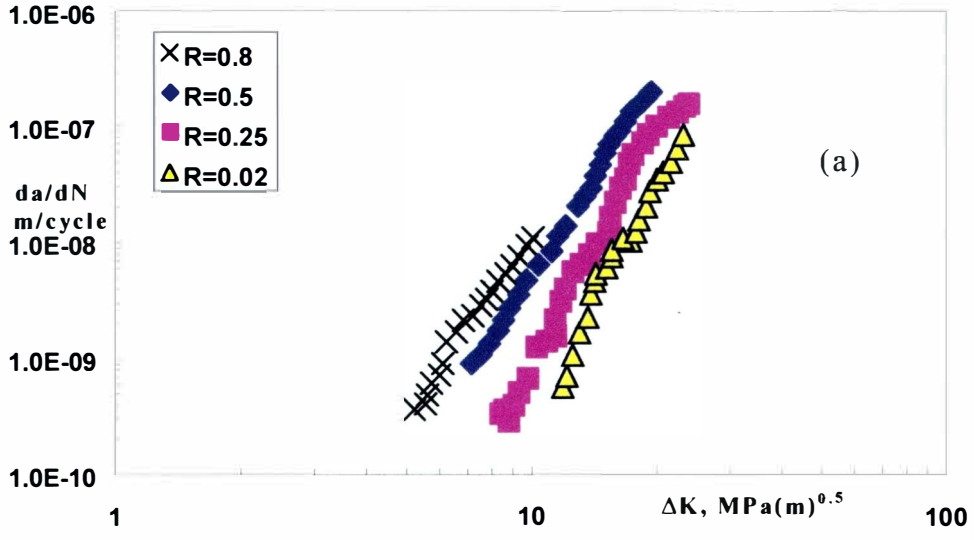

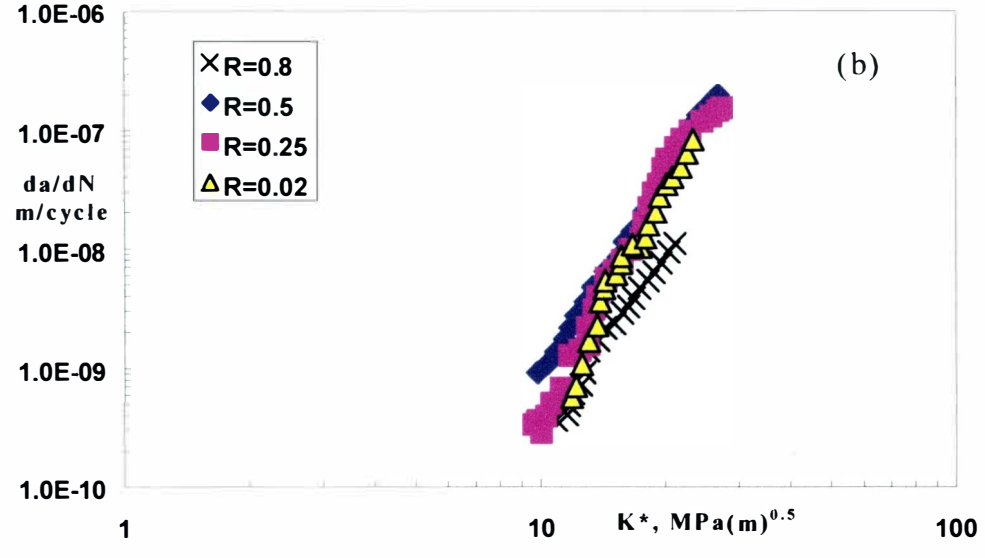

Figure 50. Fatigue crack growth data [9] of Ti-6Al-4V as a function of (a) ΔK; (b) K*(first method).

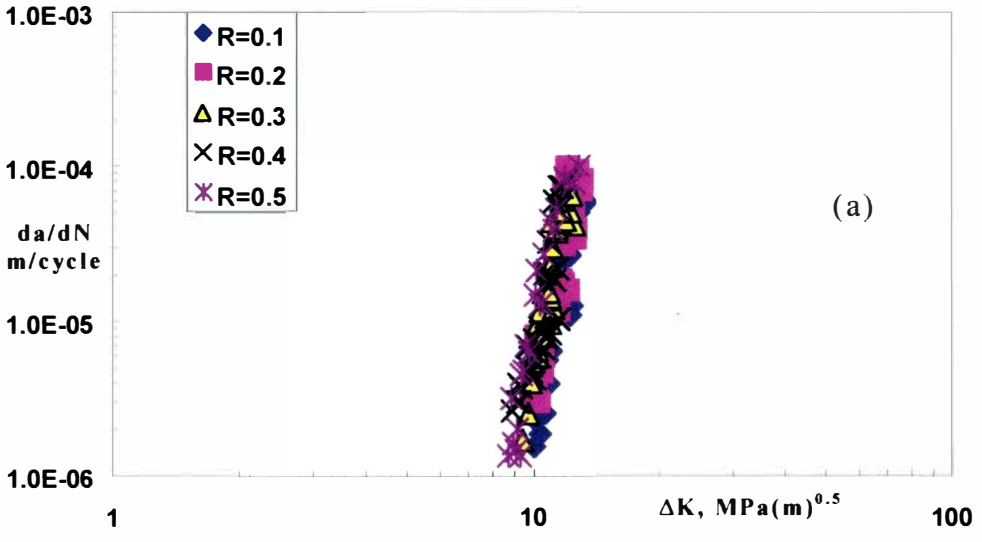

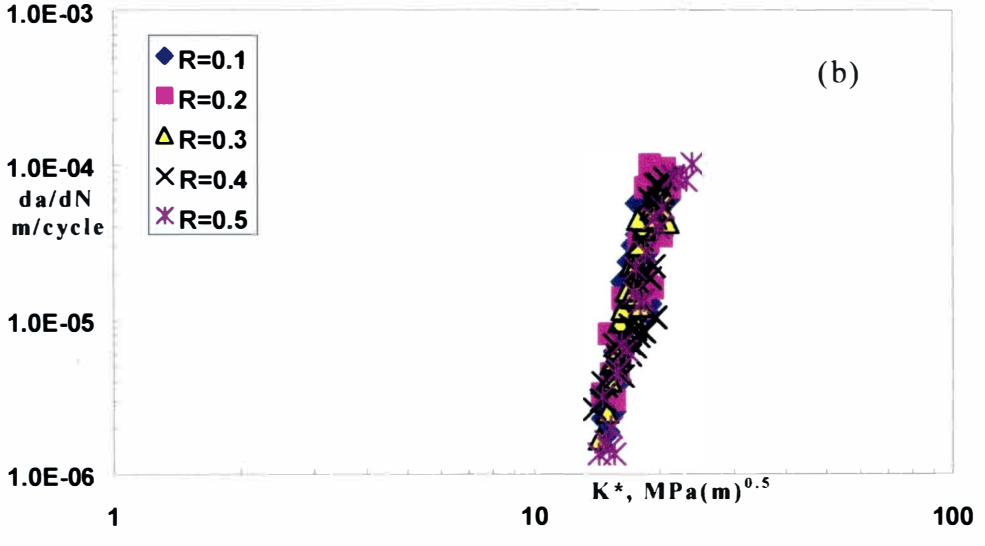

Figure 51. Fatigue crack growth data [22] of grey cast iron as a function of (a) ΔK; (b) K*(first method).

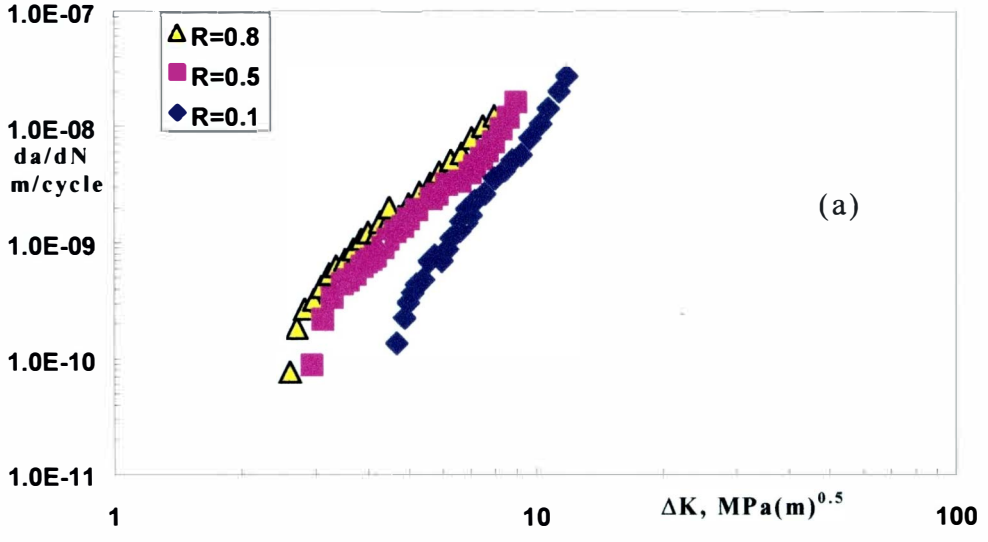

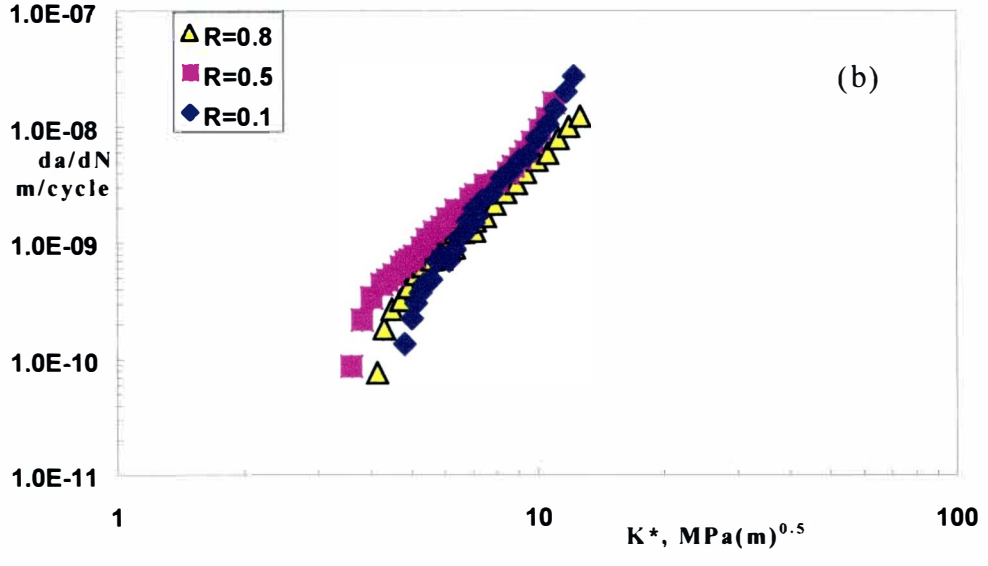

Figure 52. Fatigue crack growth data [23] of Ti-6Al-4V as a function of (a) ΔK; (b) K*(first method).

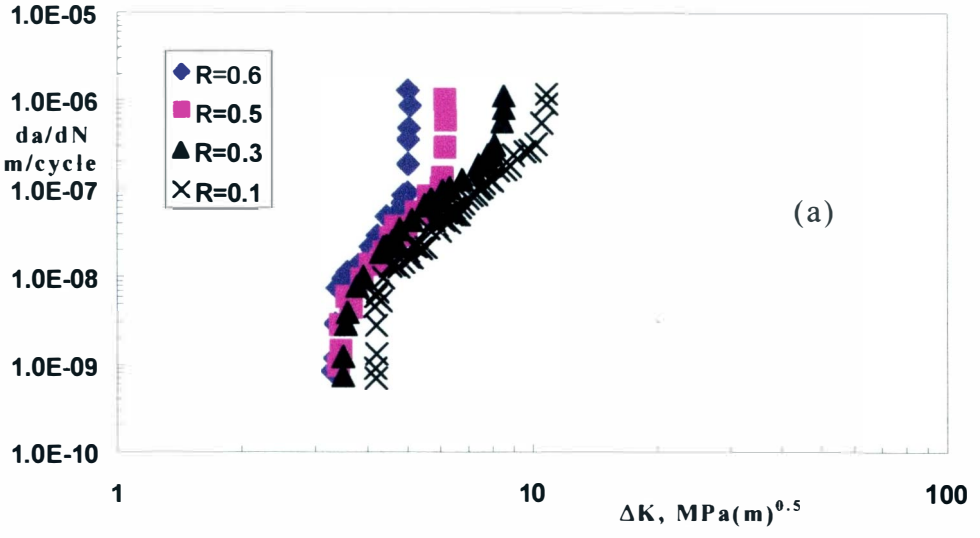

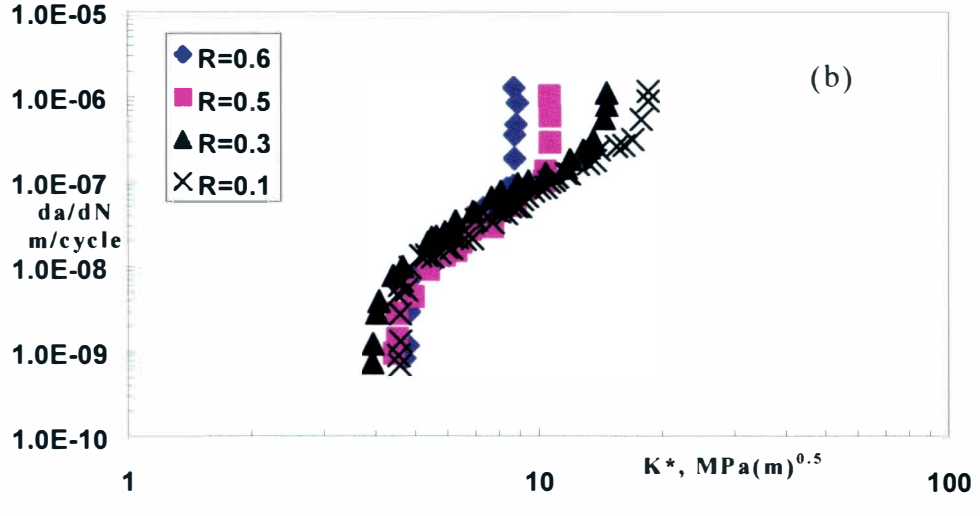

Figure 53. Fatigue crack growth data [34] of dispal 2 alloy as a function of (a) ΔK; (b) K*(first method).

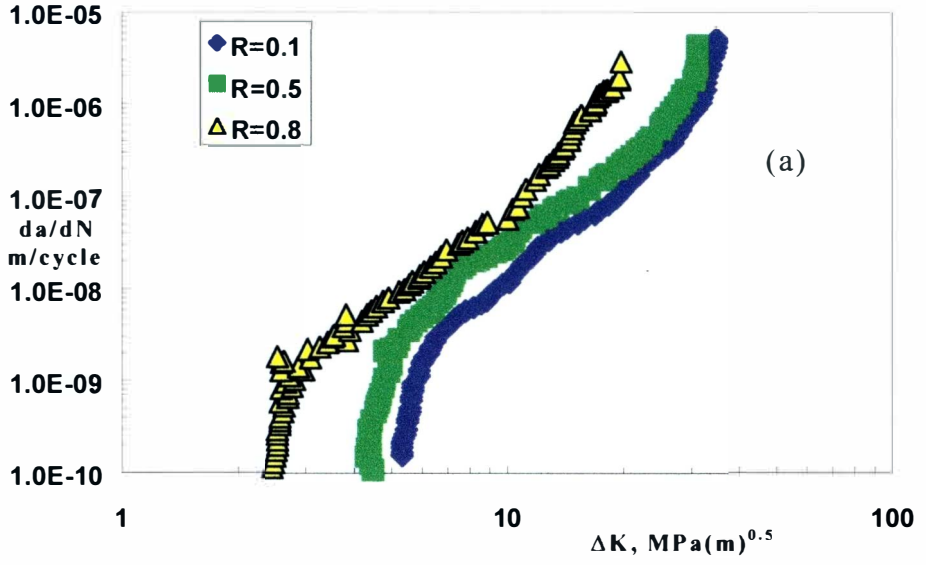

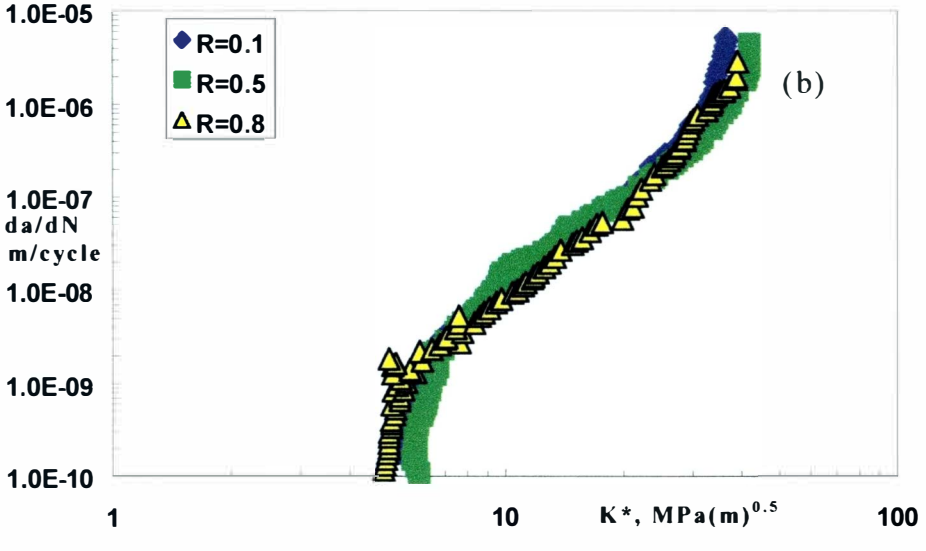

Figure 54. Fatigue crack growth data [24] of Ti-10V-2Fe-3Al as a function of (a) ΔK; (b) K*(first method).

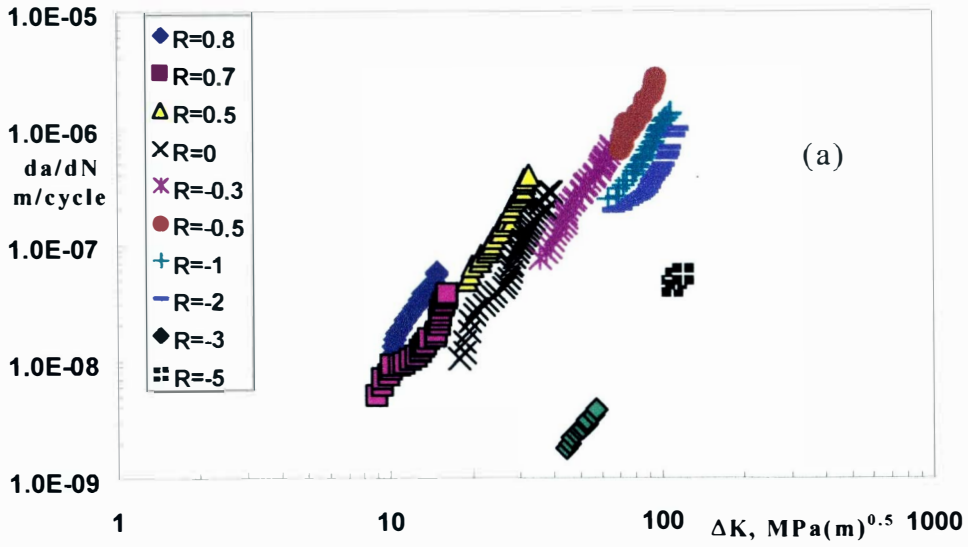

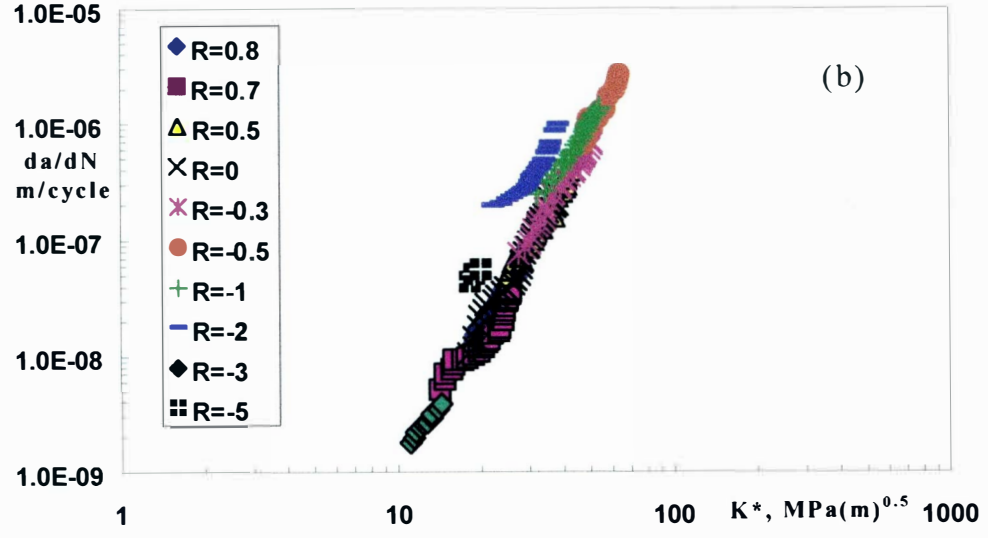

Figure 55. Fatigue crack growth data [25] of structural steel, JIS SM50B as a function of (a) ΔK; (b) K*(first method).

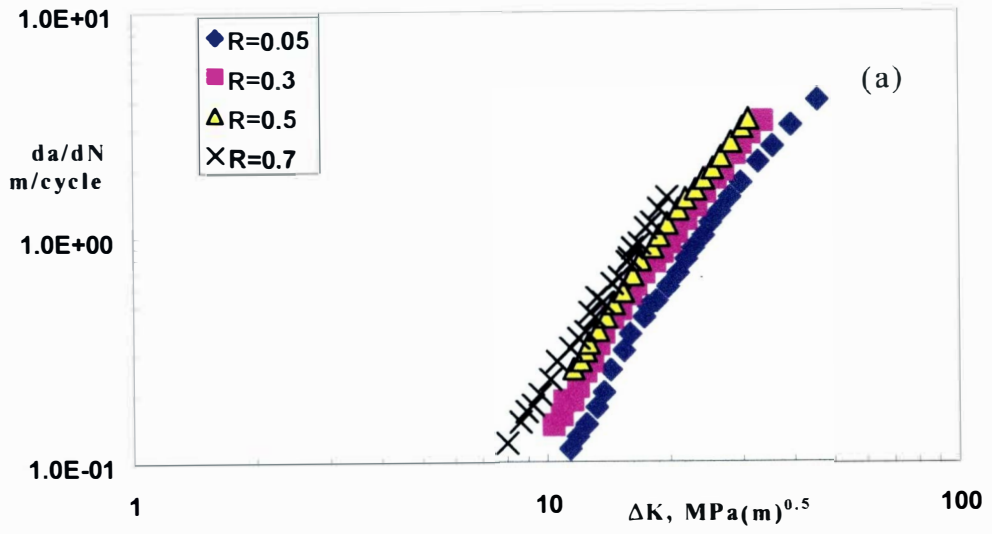

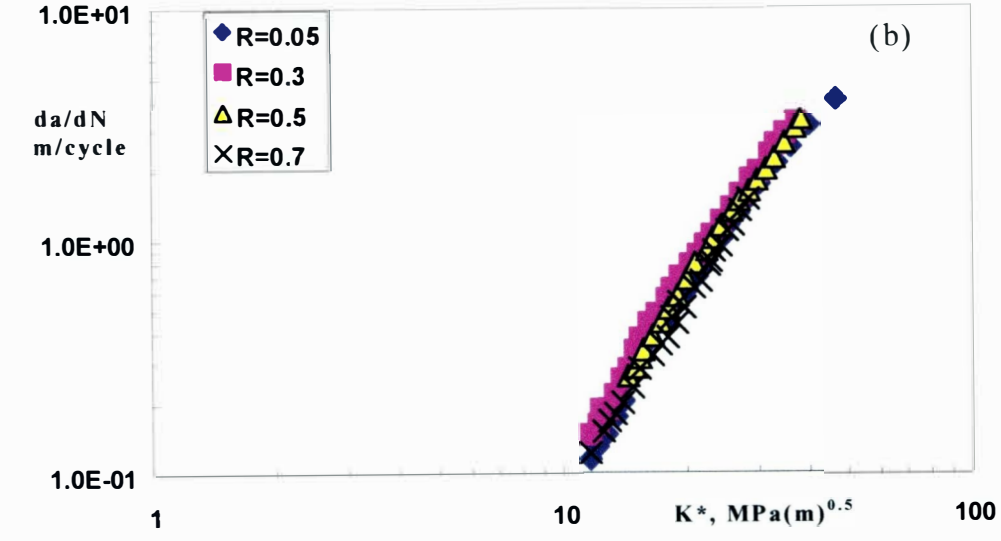

Figure 56. Fatigue crack growth data [26] of 300M steel as a function of (a) ΔK; (b) K*(first method).

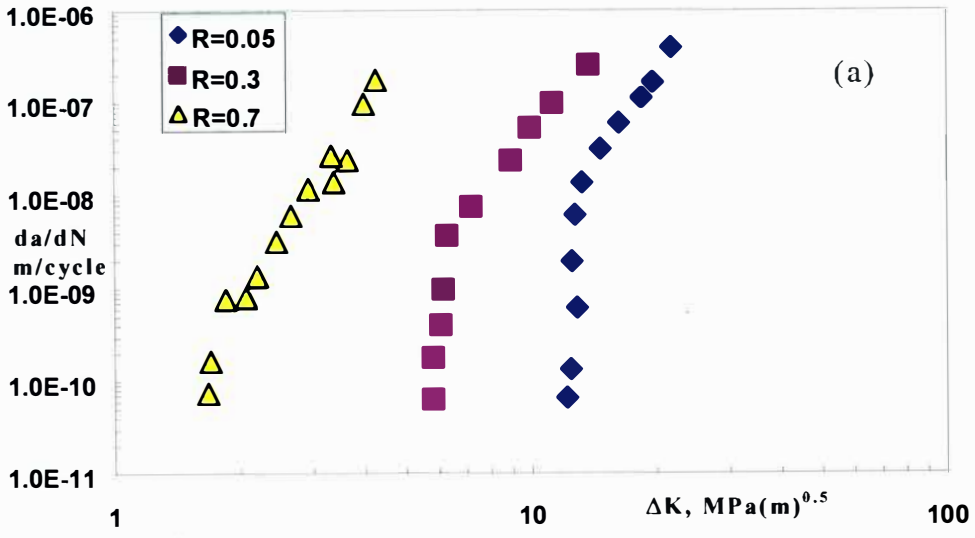

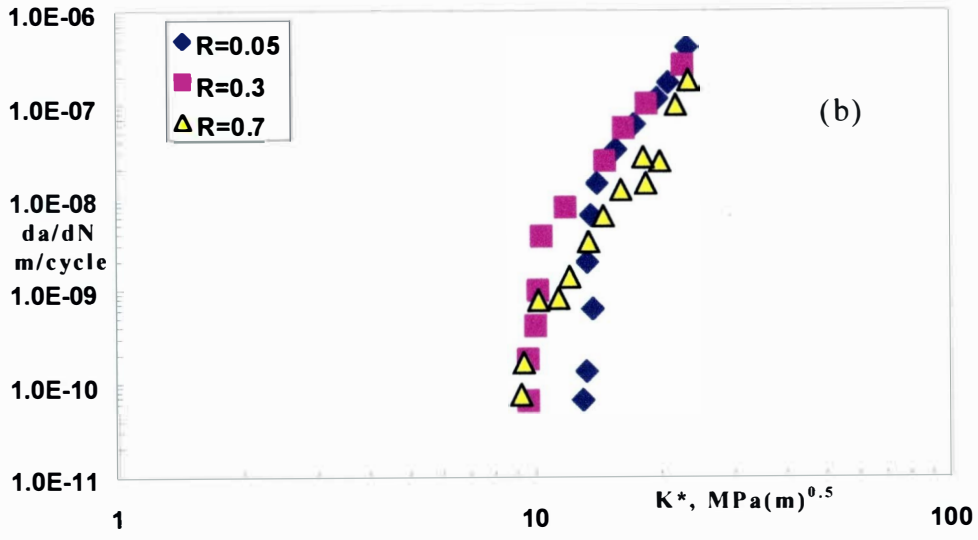

Figure 57. Fatigue crack growth data [33] of ferritic microstructure as a function of (a) ΔK; (b) K*(first method).

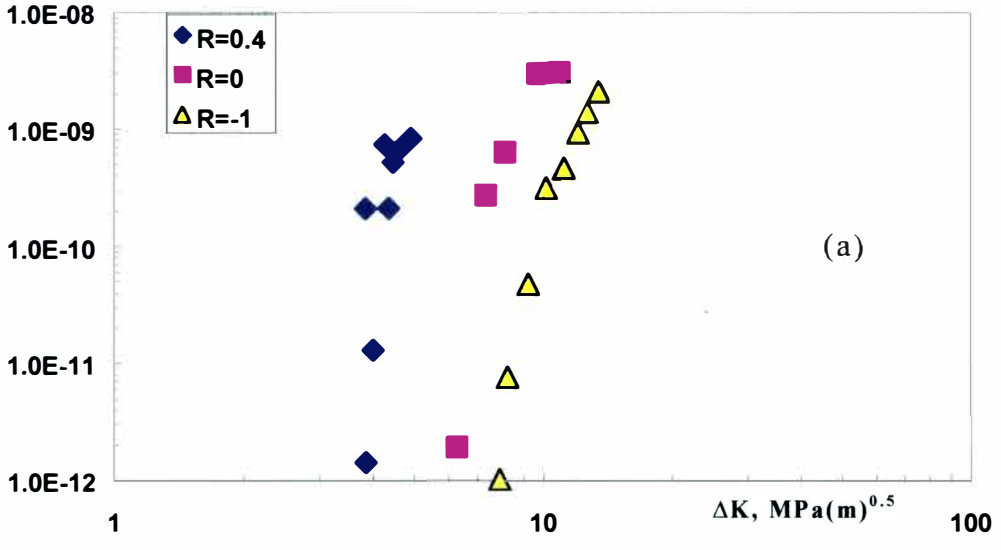

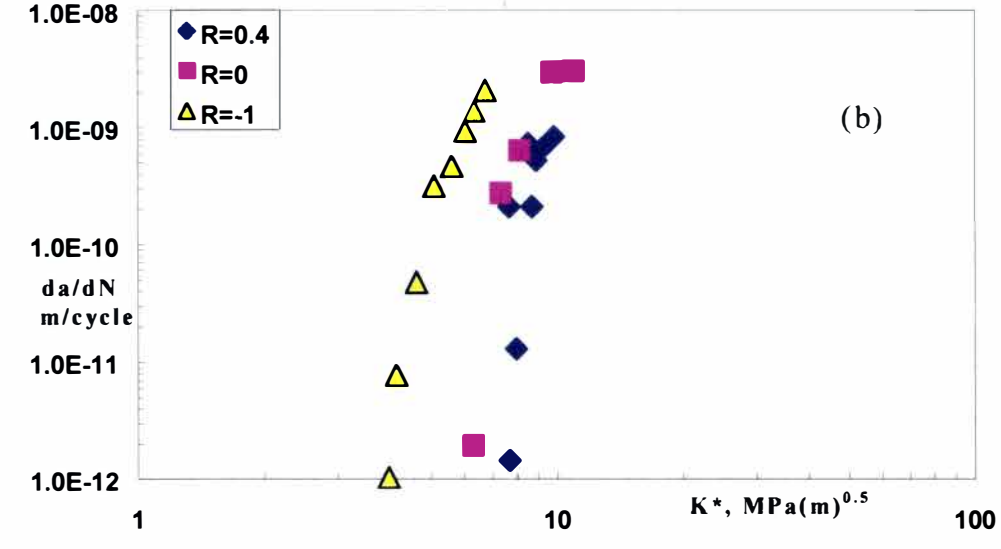

Figure 58. Fatigue crack growth data [35] of copper as a function of (a) ΔK; (b) K*(first method).

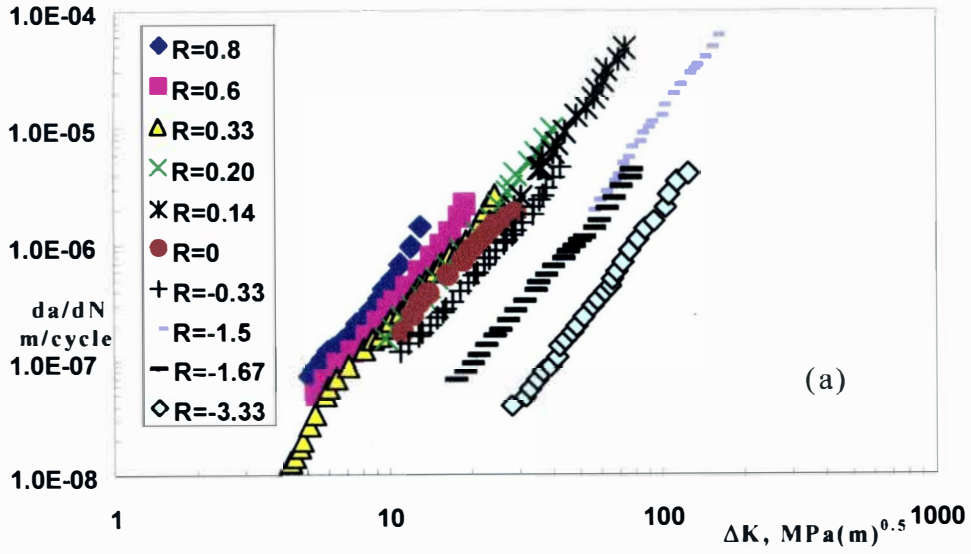

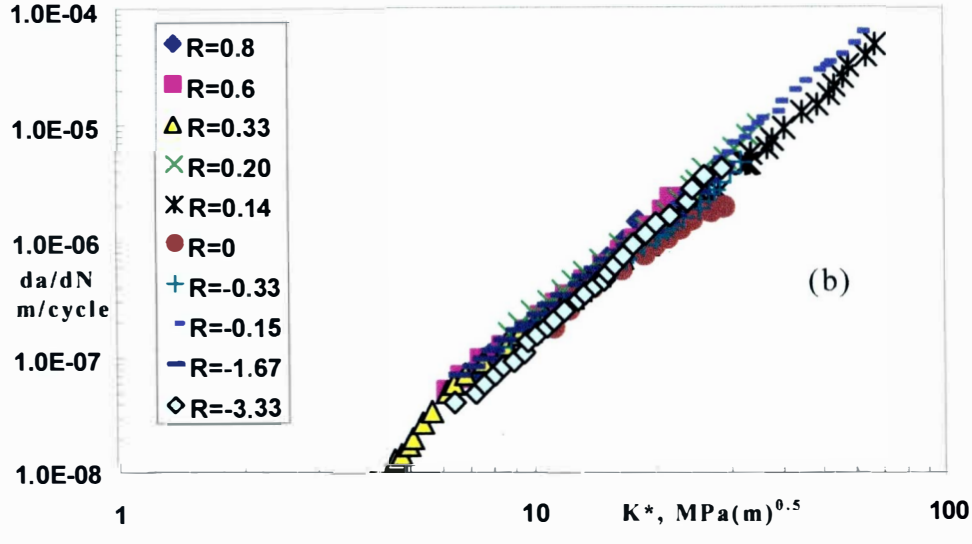

Figure 59. Fatigue crack growth data [36] of Al 7475-T7351 as a function of (a) ΔK; (b) K*(first method).

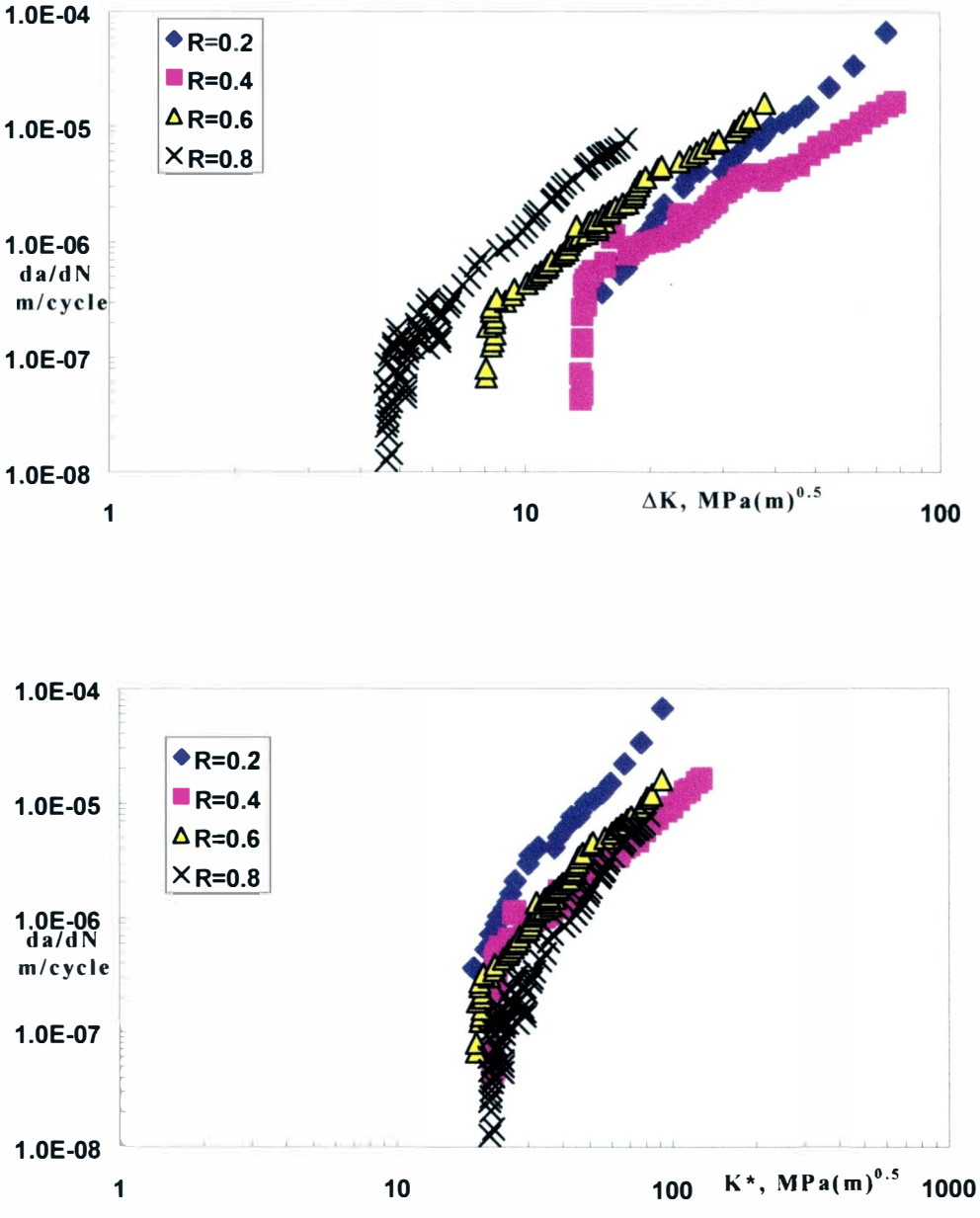

Figure 60. Fatigue crack growth data [37] of Udimet 720 Li superalloy as a function of (a) ΔK; (b) K*(first method).

APPENDIX : C

PREDICTION ACCURACY OF K*

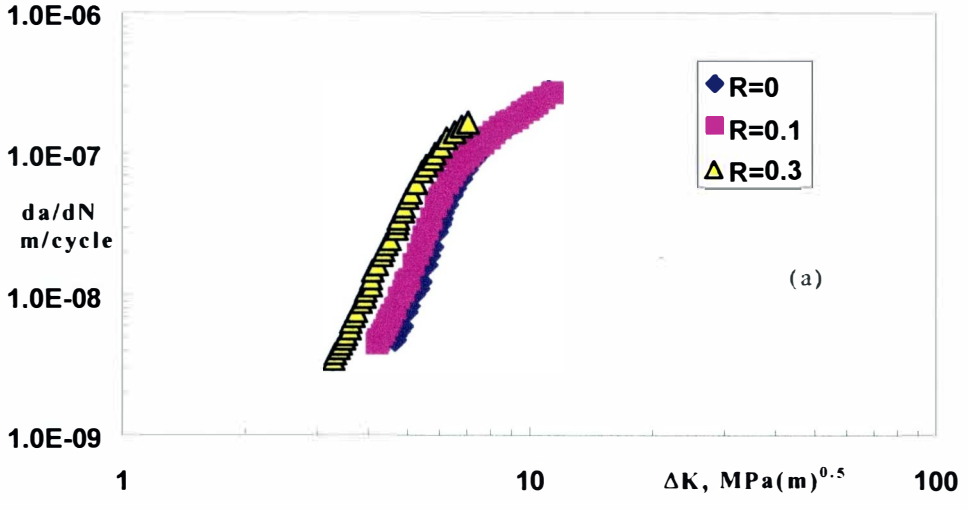

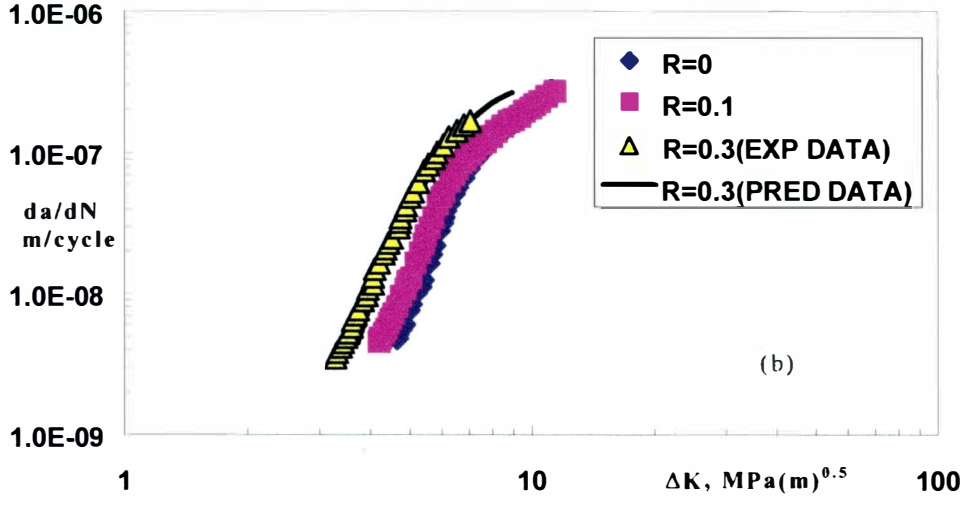

Figure 61. (a)Experimental fatigue crack growth data [20] of 7075-T651;(b)Predicted fatigue crack growth data for R=0.3 are compared with experimental data.

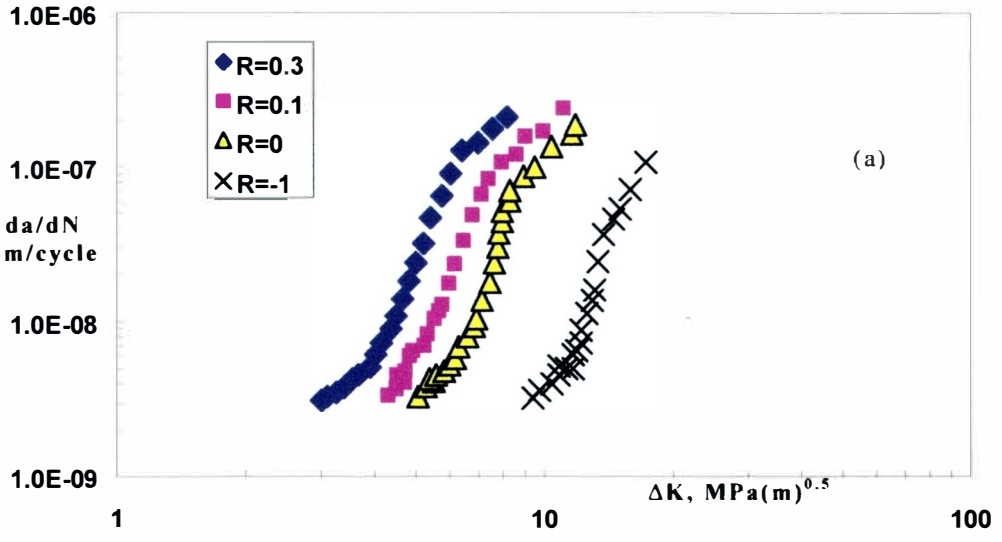

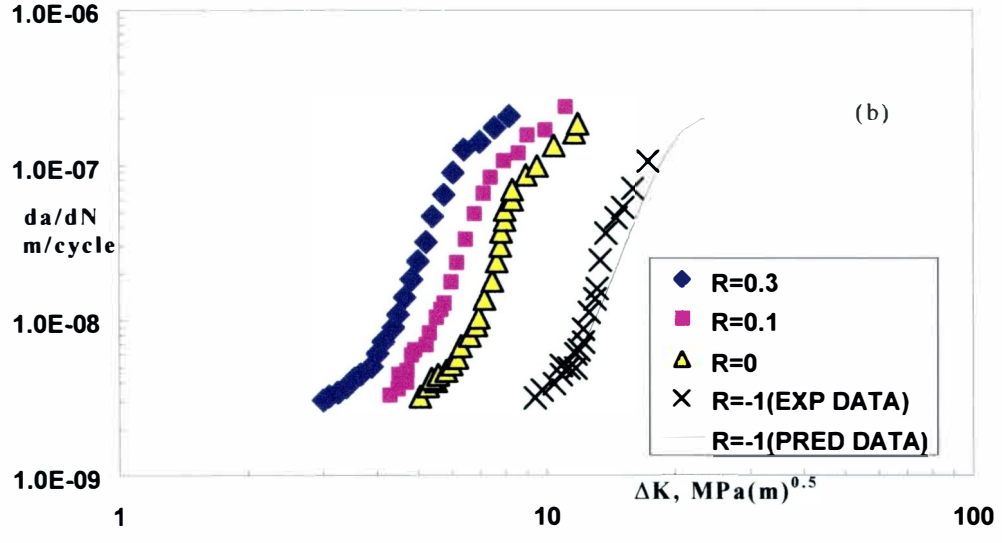

Figure 62 . (a)Experimental fatigue crack growth data [21] of 7075-T7451;(b)Predicted fatigue crack growth data for R=-1 are compared with experimental data.

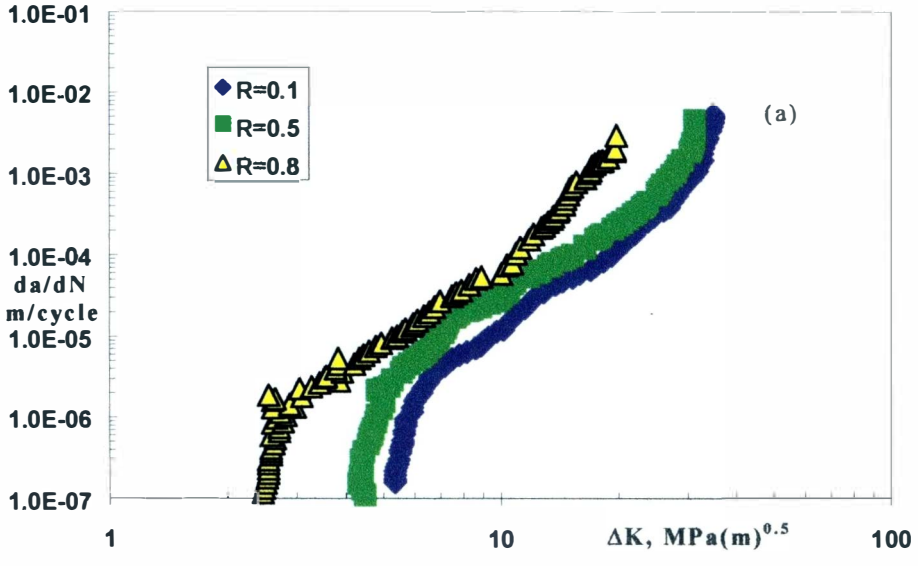

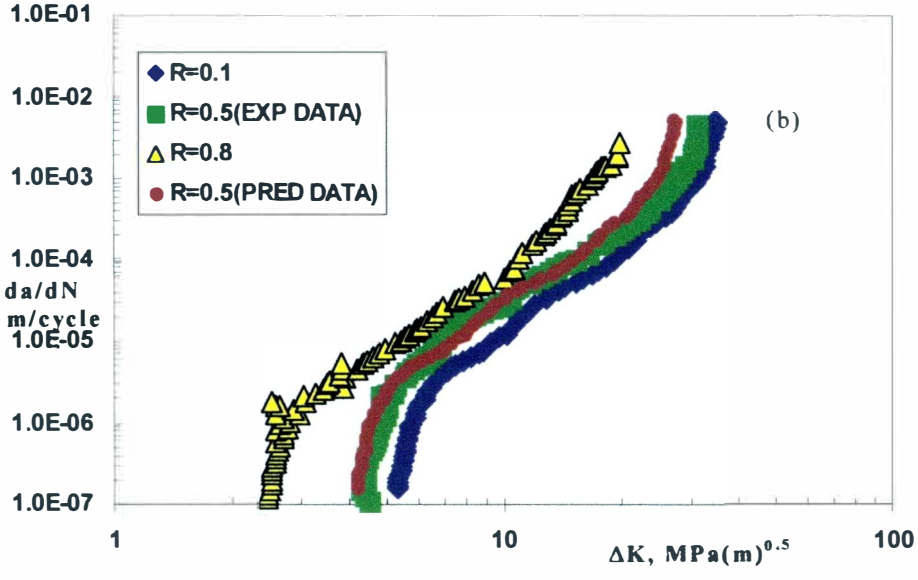

Figure 63 . (a)Experimental fatigue crack growth data [24] of Ti-10V-2Fe-3Al; (b)Predicted fatigue crack growth data for R=0.5 are compared with experimental data.

APPENDIX : D

BEST FIT LINE FOR THE CORRELATED DATA USING K*

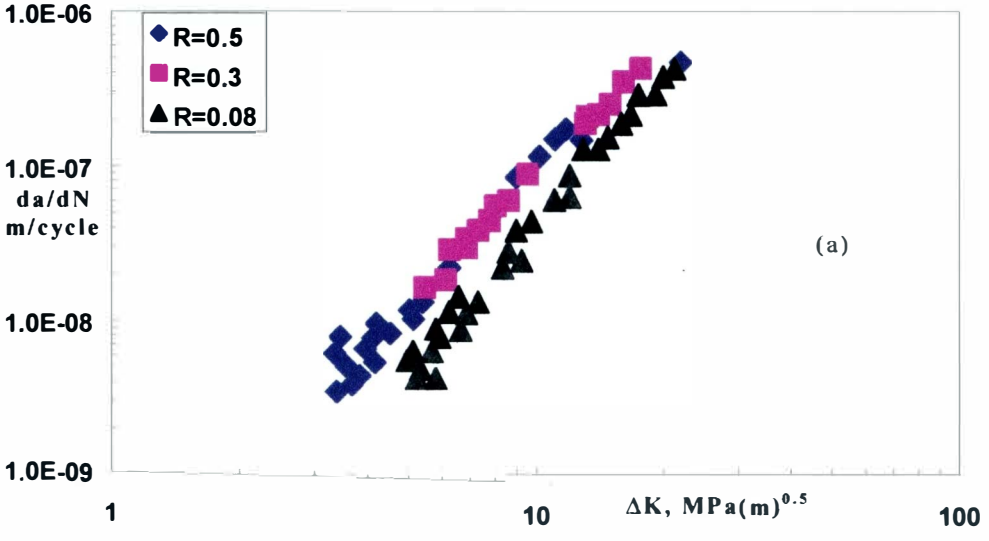

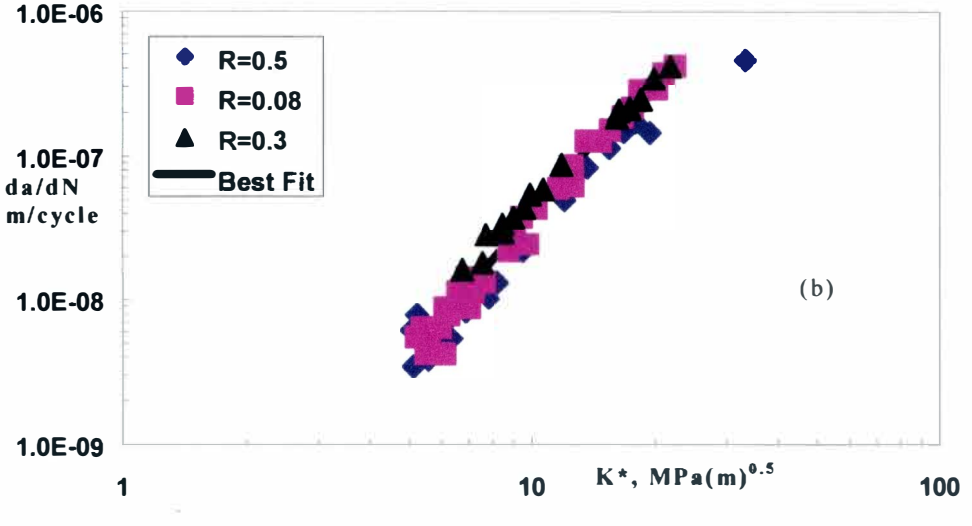

Figure 64. Fatigue crack growth data [31] of 7075-T651 as a function of (a) ΔK; (b) K*(first method) with the best fit line.

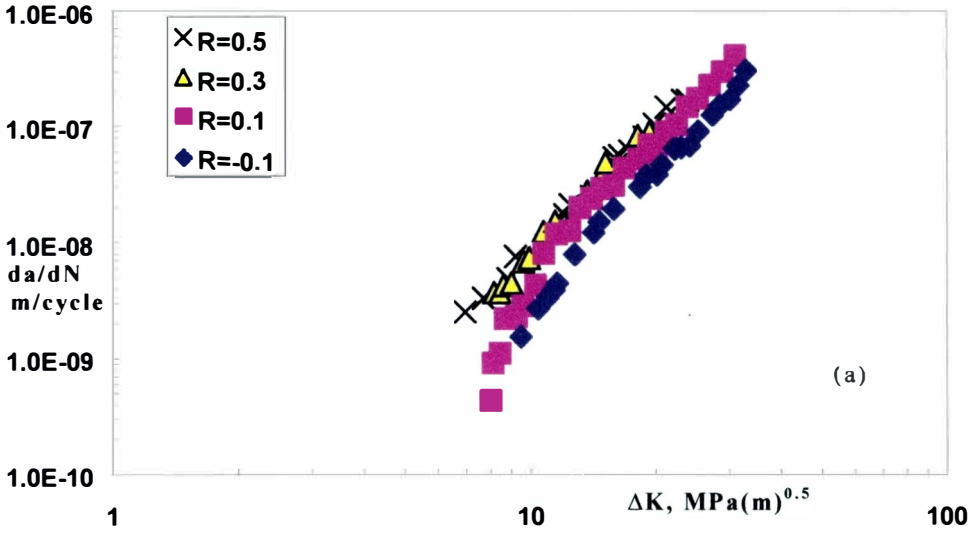

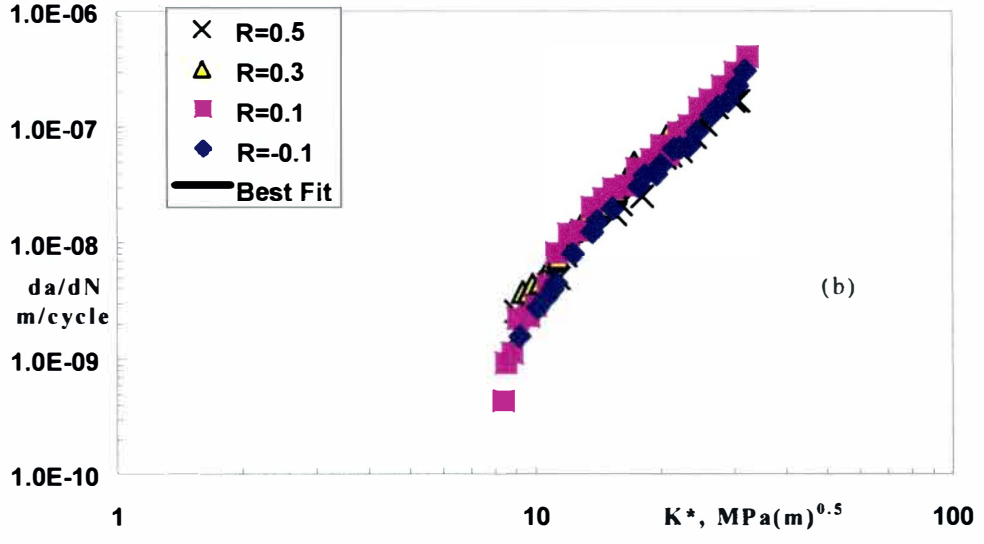

Figure 65. Fatigue crack growth data [32] of 304 stainless steel as a function of (a) ΔK; (b) K*(first method) with the best fit line.

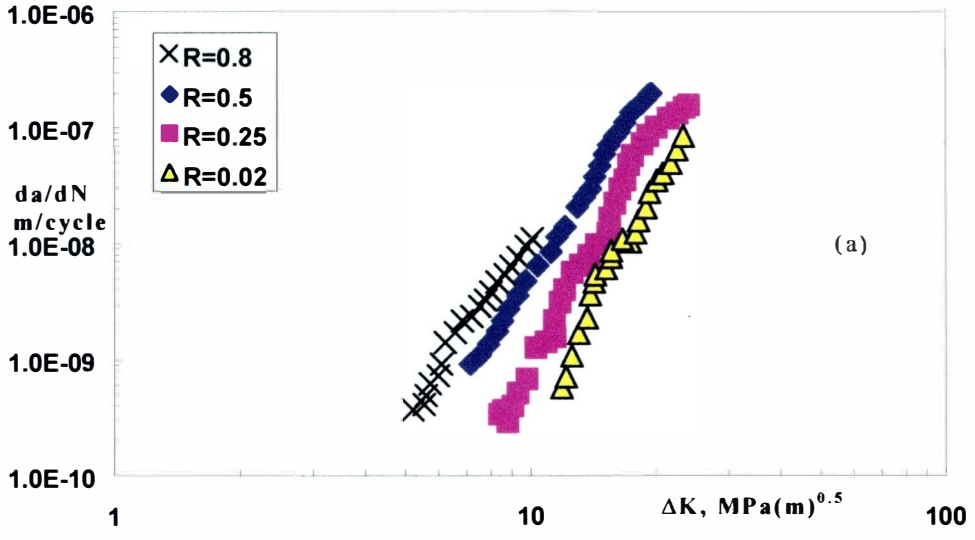

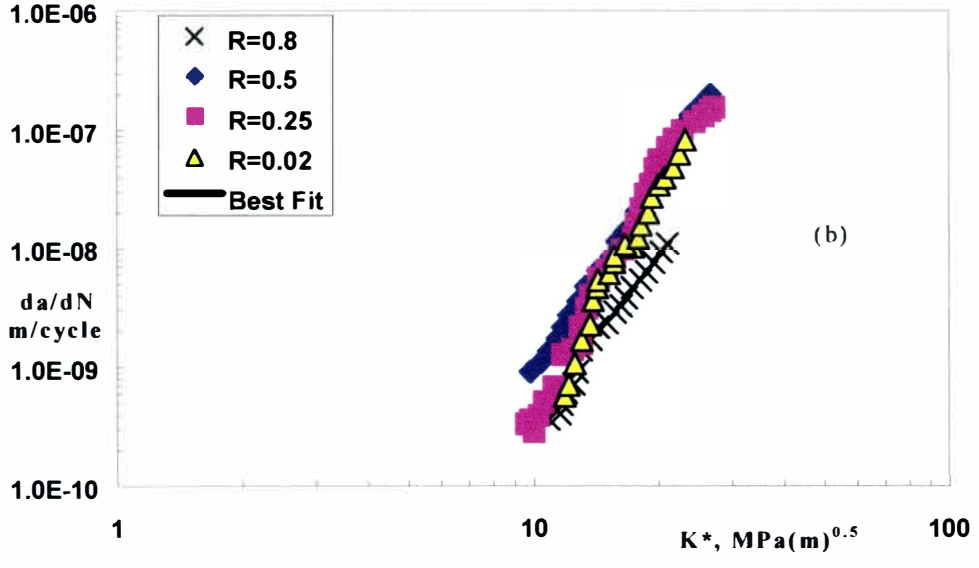

Figure 66. Fatigue crack growth data [9] of Ti-6Al-4V as a function of (a) ΔK; (b) K*(first method) with the best fit line.

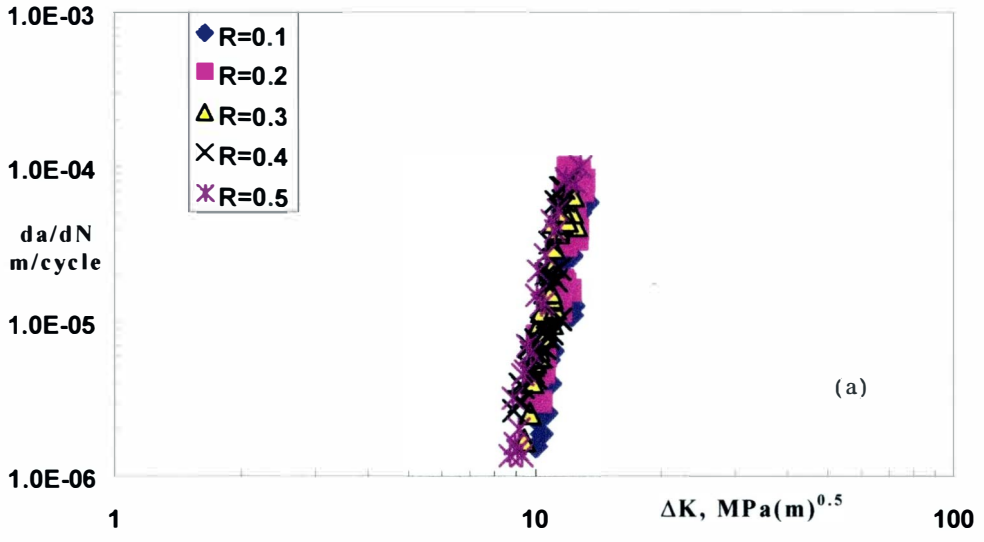

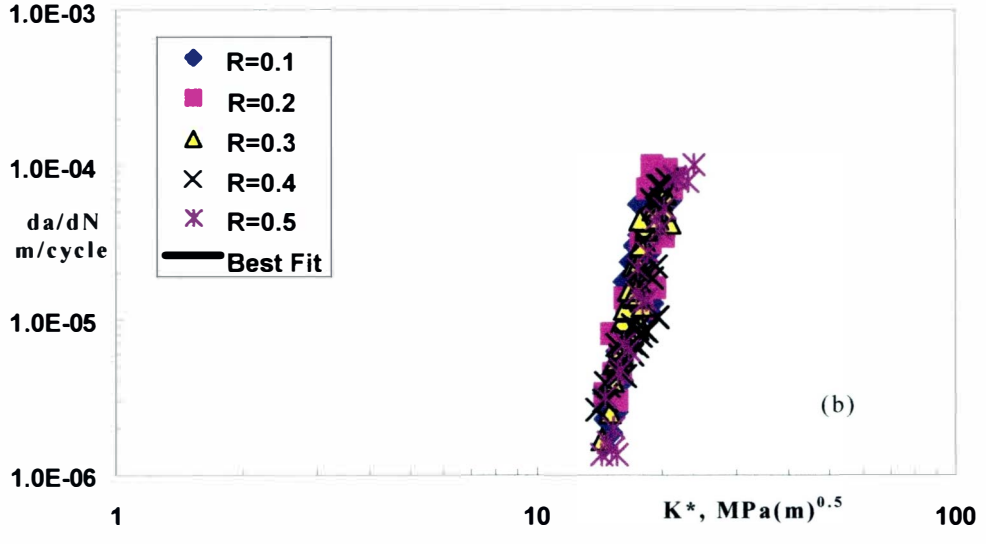

Figure 67. Fatigue crack growth data [22] of grey cast iron as a function of (a) ΔK; (b) K*(first method) with the best fit line.

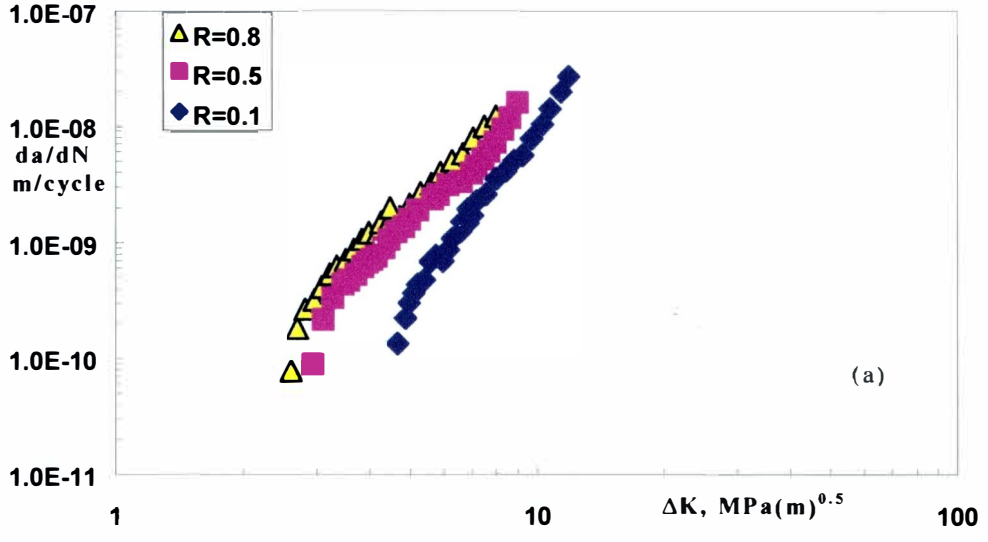

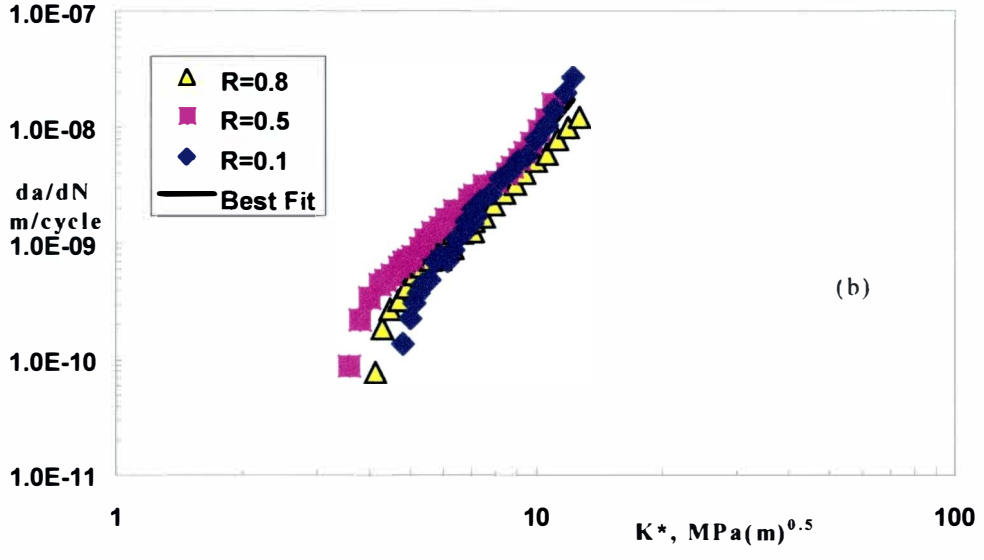

Figure 68. Fatigue crack growth data [23] of Ti-6Al-4V as a function of (a) ΔK; (b) K*(first method)with the best fit line.

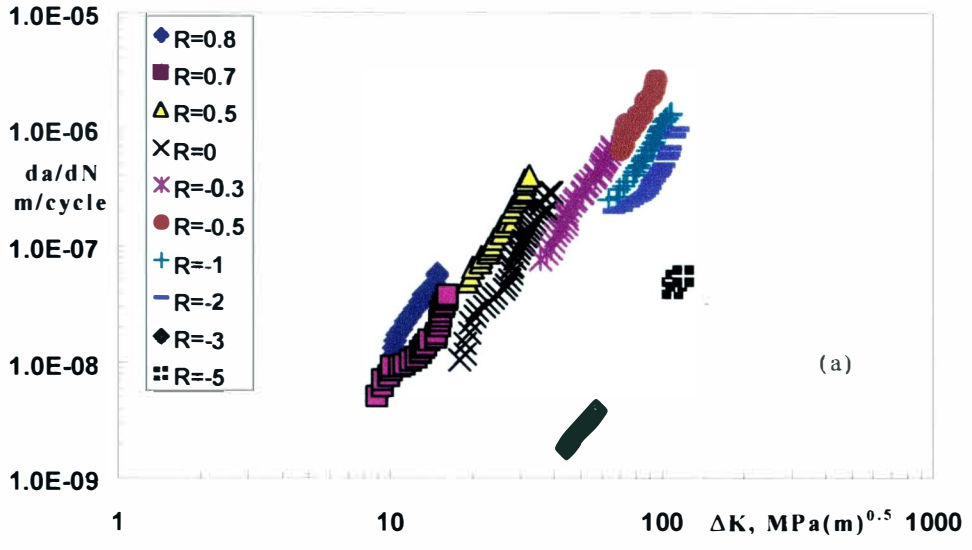

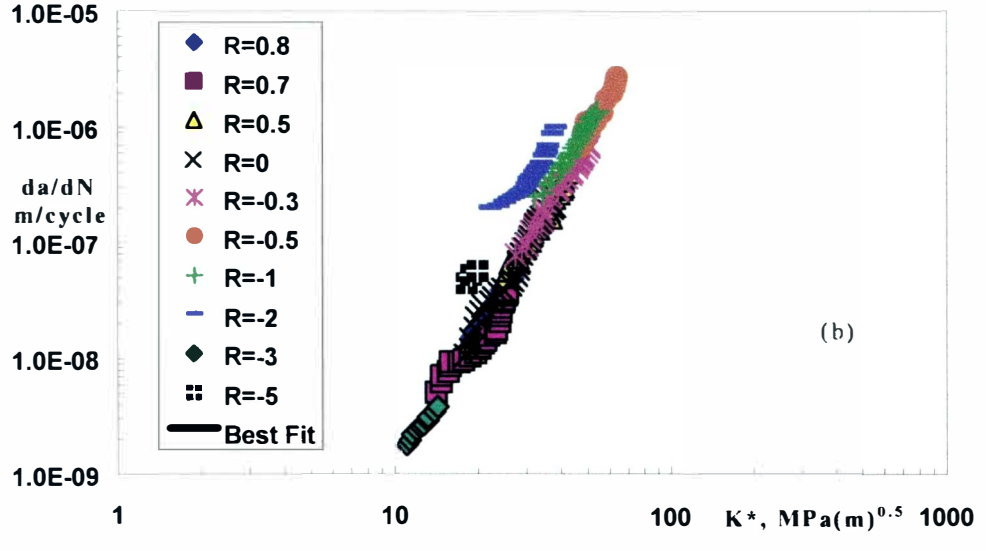

Figure 69. Fatigue crack growth data [25] of structural steel, JIS SM50B as a function of (a) ΔK; (b) K*(first method) with the best fit line.

APPENDIX : E

COMPARISON BETWEEN K* AND ΔK_{EFF}

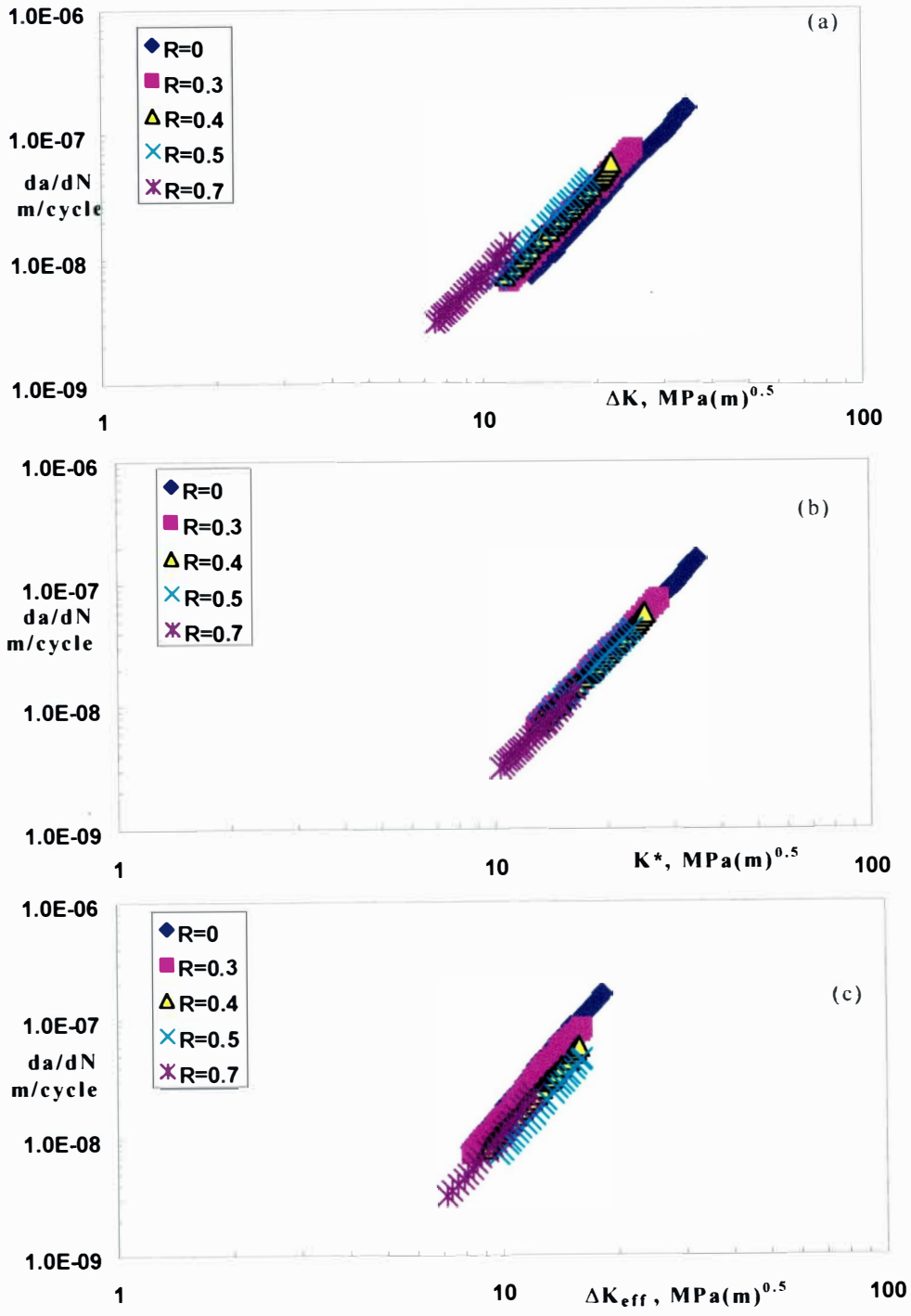

Figure 70. Fatigue crack growth data [16] of medium carbon structural steel as a function of (a) ΔK; (b) K^*(first method). (c) ΔK_{eff}.

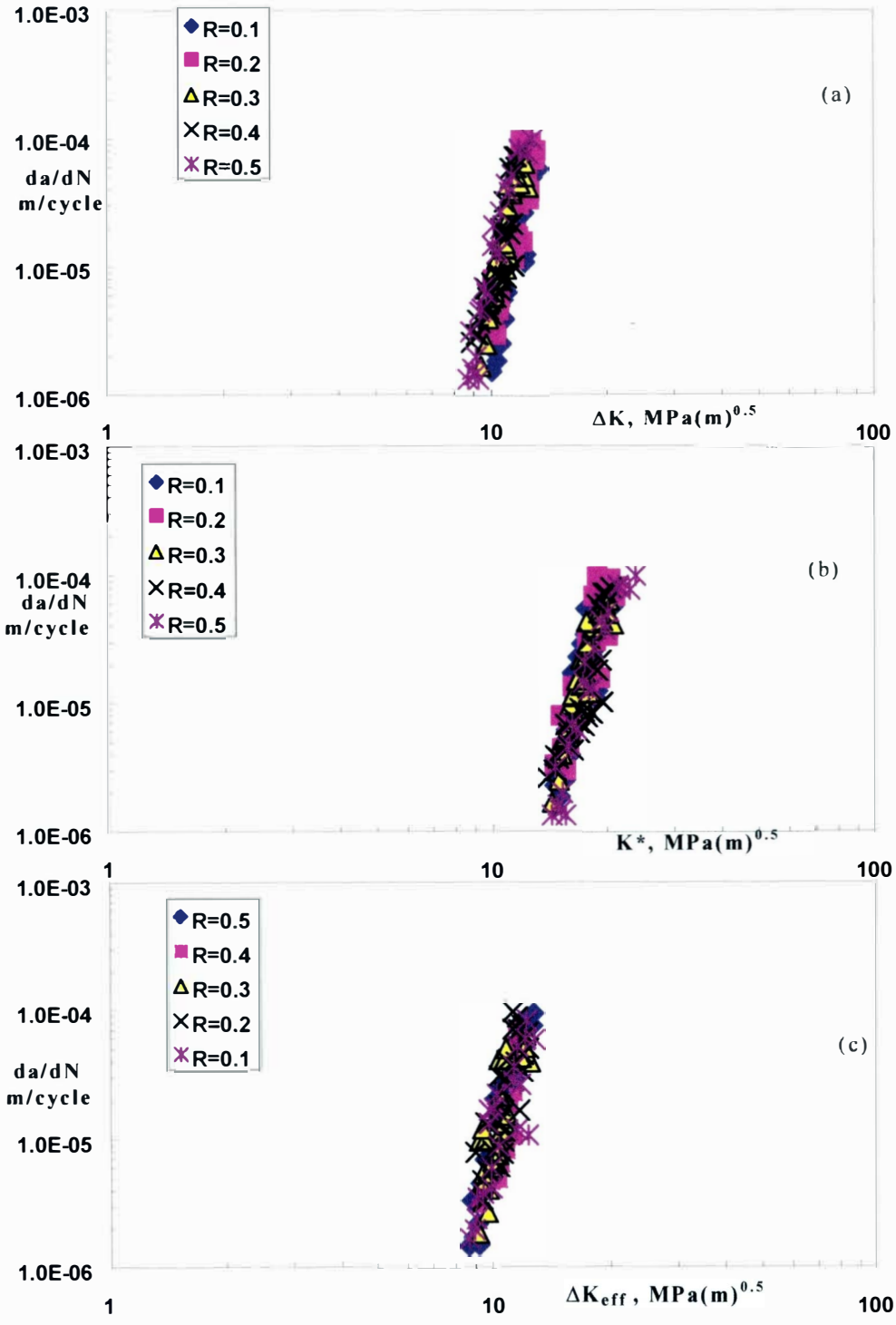

Figure 71. Fatigue crack growth data [22] of grey cast iron as a function of (a) ΔK; (b) K^*(first method). (c) ΔK_{eff}.

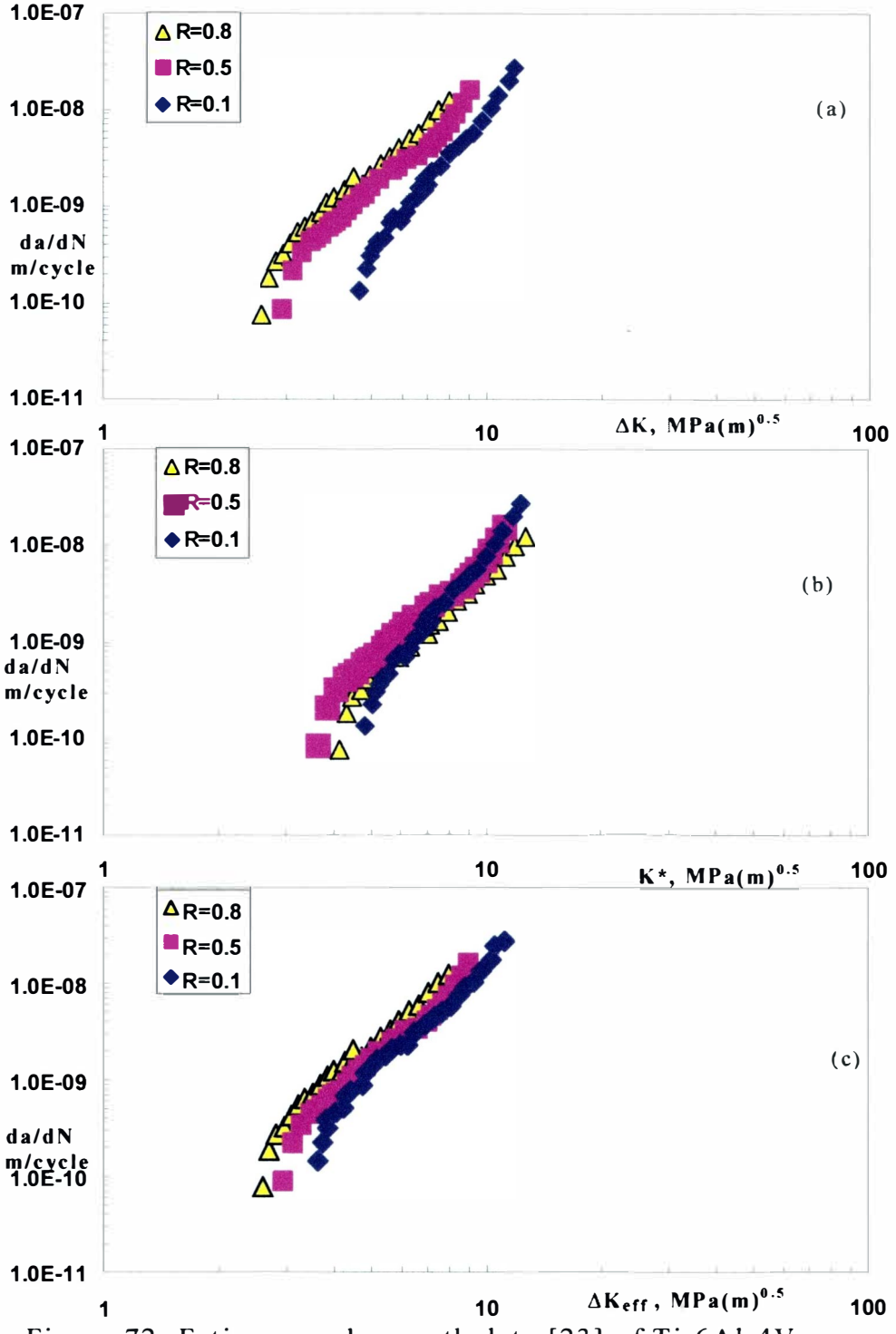

Figure 72. Fatigue crack growth data [23] of Ti-6Al-4V as a function of (a) ΔK; (b) K^*(first method). (c) ΔK_{eff}.

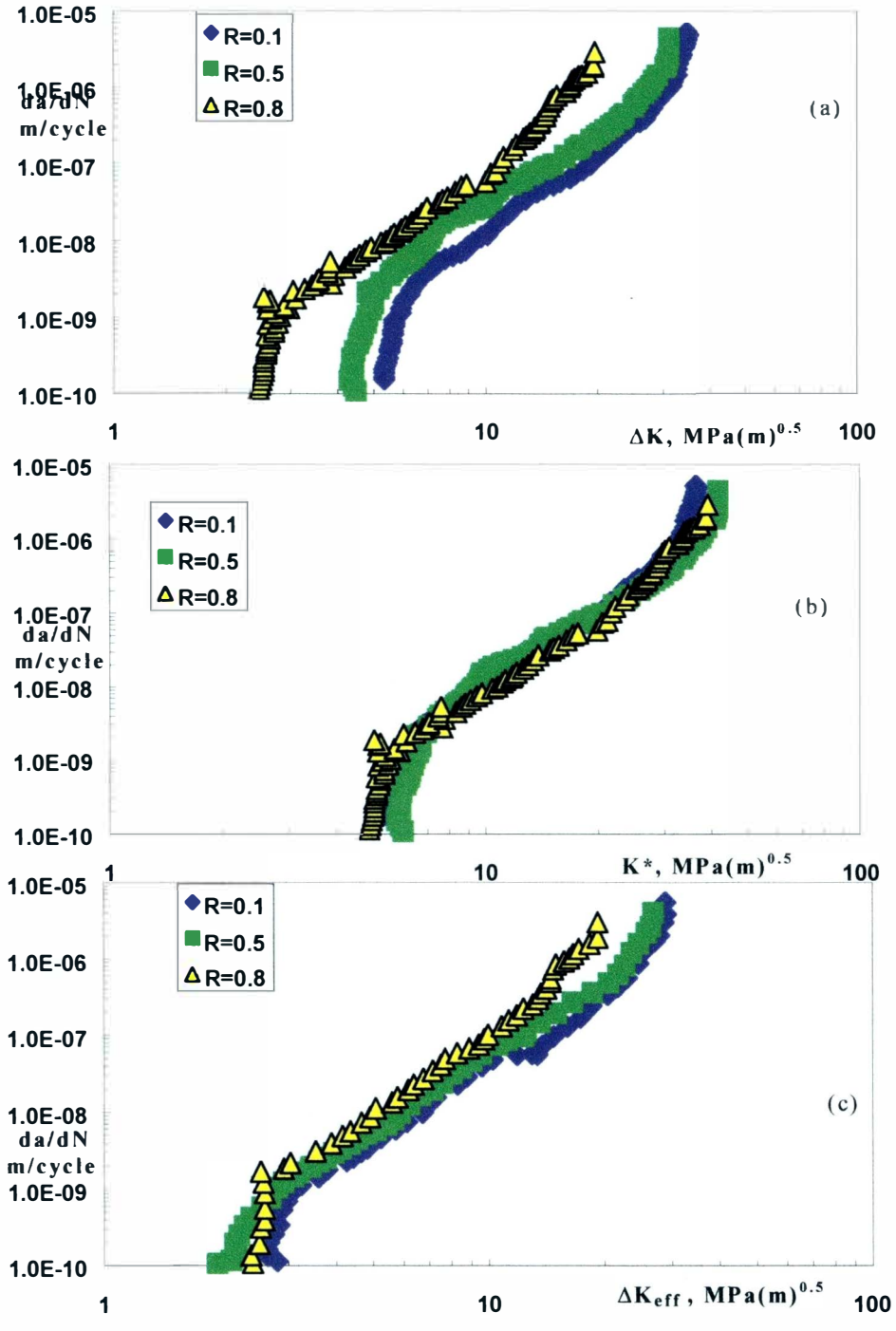

Figure 73. Fatigue crack growth data [24] of Ti-10V-2Fe-3Al as a function of (a) ΔK; (b) K^*(first method). (c) ΔK_{eff}.

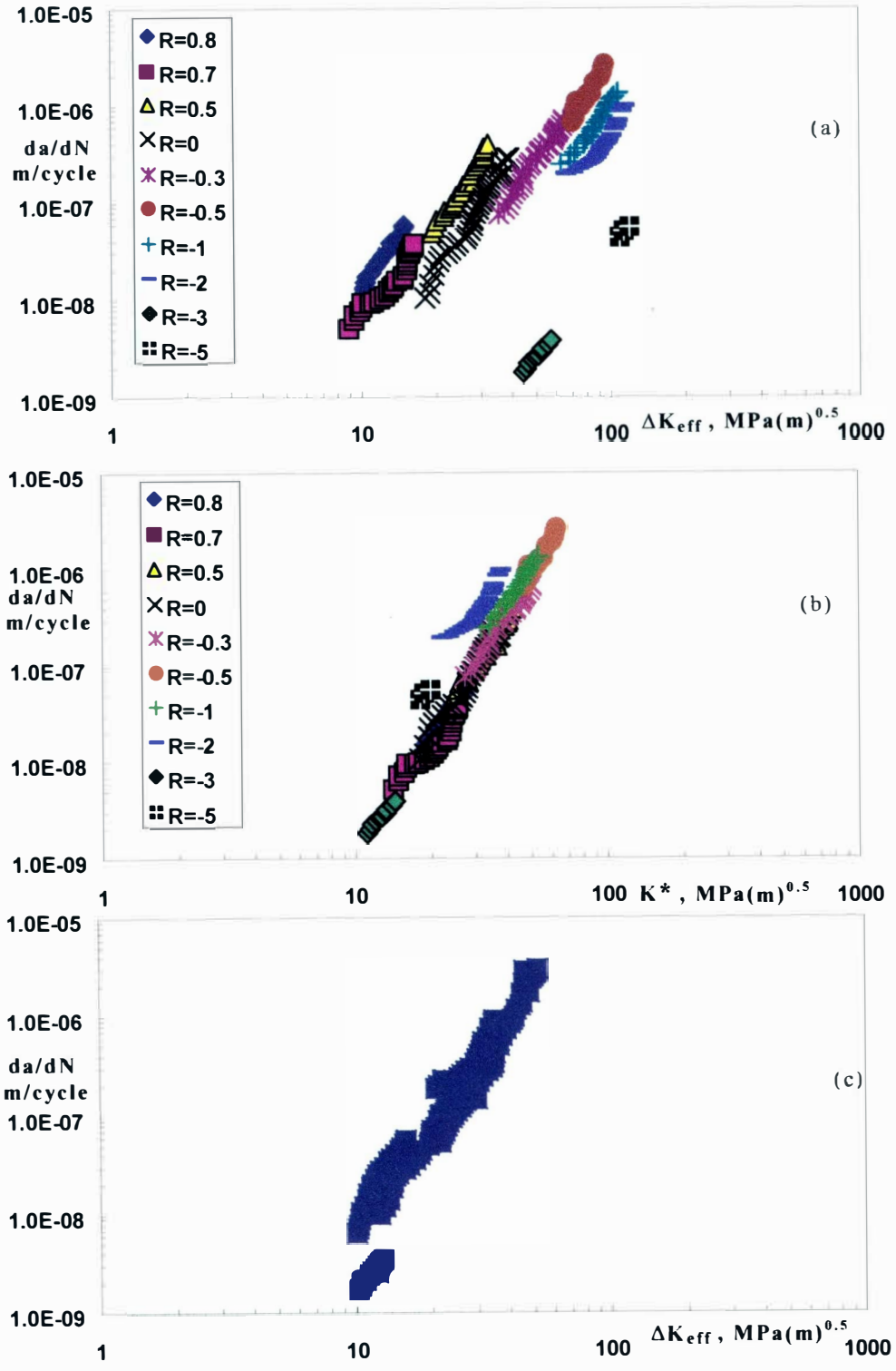

Figure 74. Fatigue crack growth data [25] of structural steel, JIS SM50B as a function of (a) ΔK; (b) K^*(first method); (c) ΔK_{eff}.

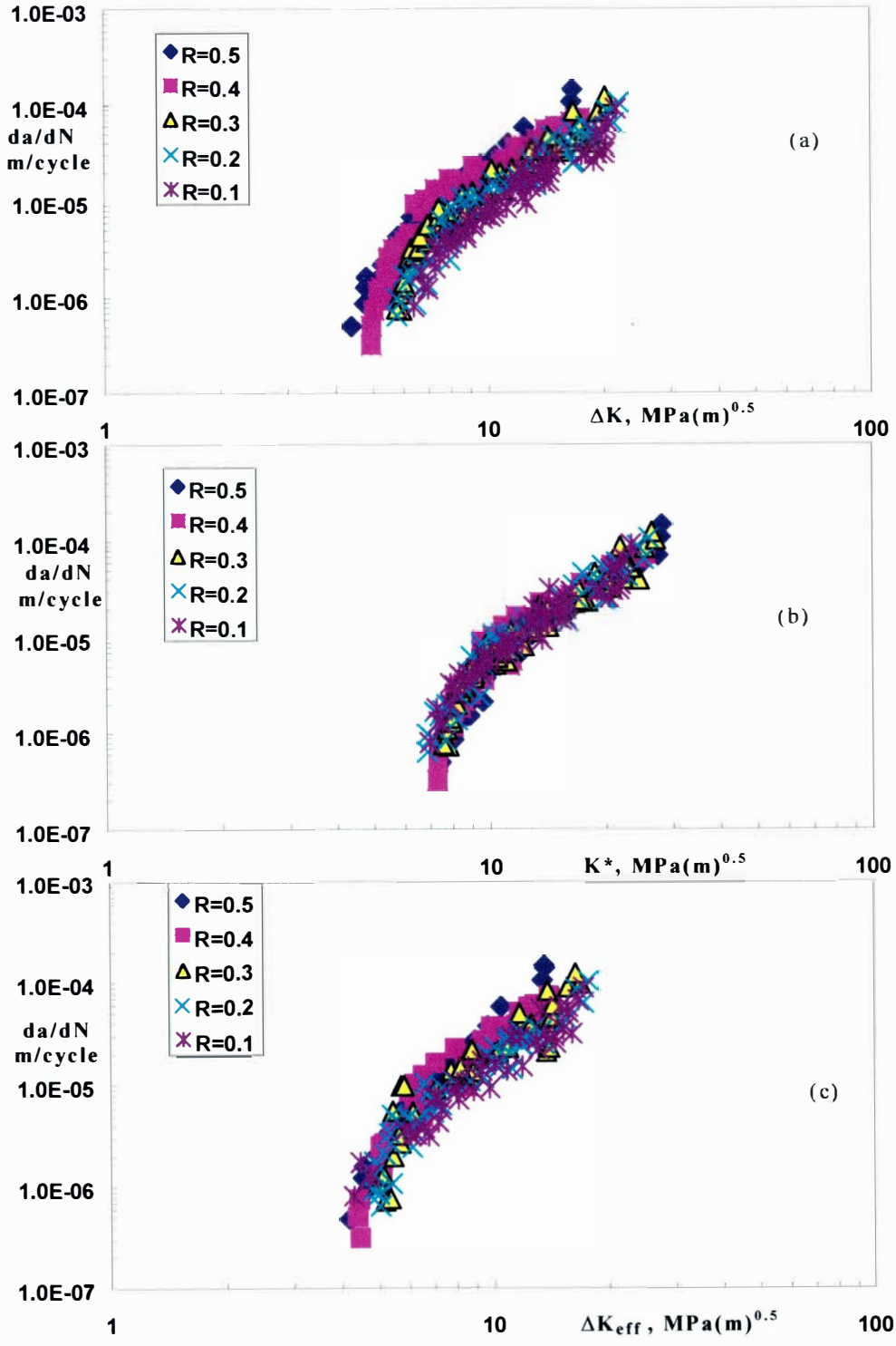

Figure 75. Fatigue crack growth data [22] of austempered ductile iron as a function of (a) ΔK; (b) K*(first method); (c) ΔK_{eff}.

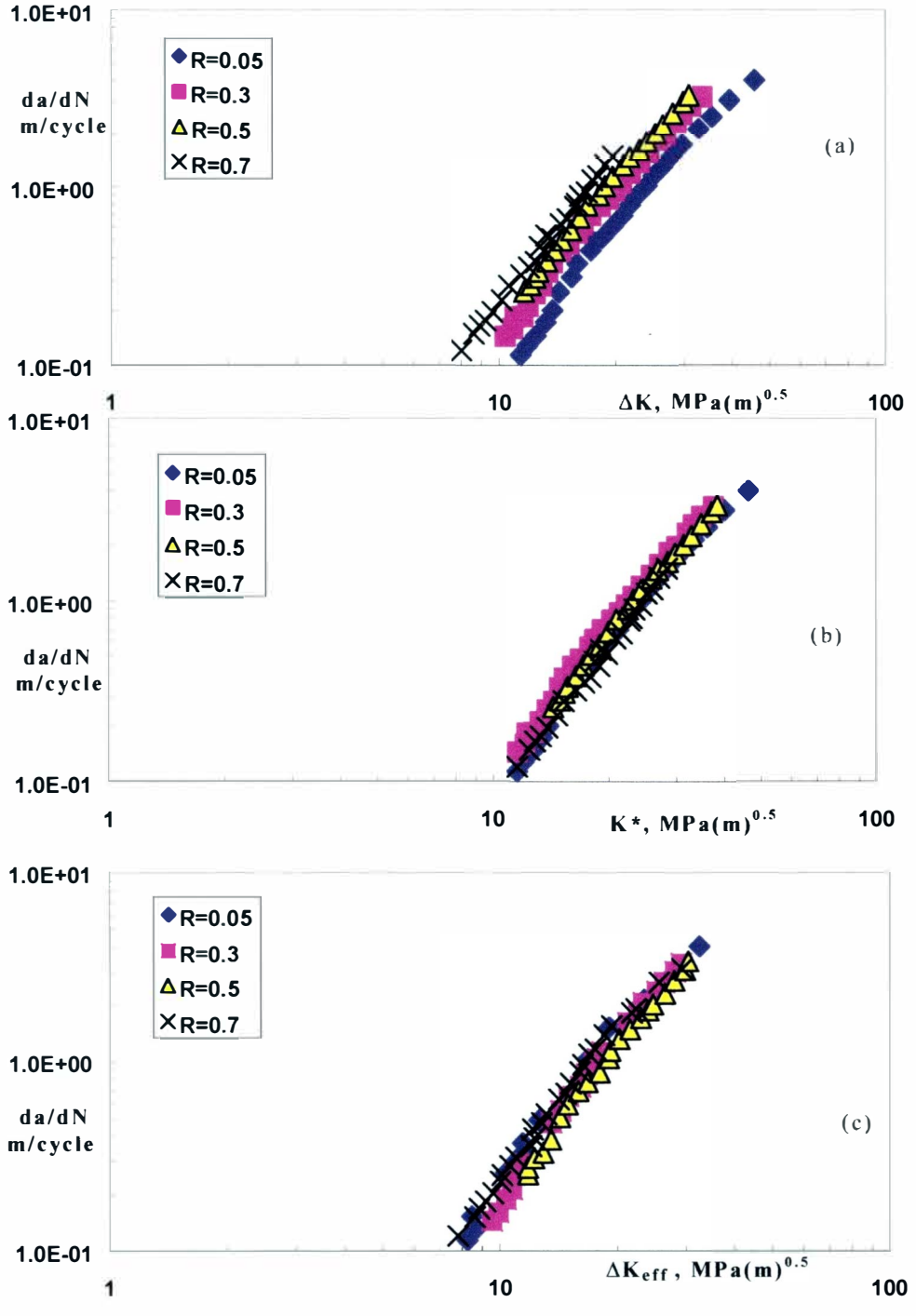

Figure 76. Fatigue crack growth data [26] of 300M steel as a function of (a) ΔK; (b) K^*(first method); (c) ΔK_{eff}.

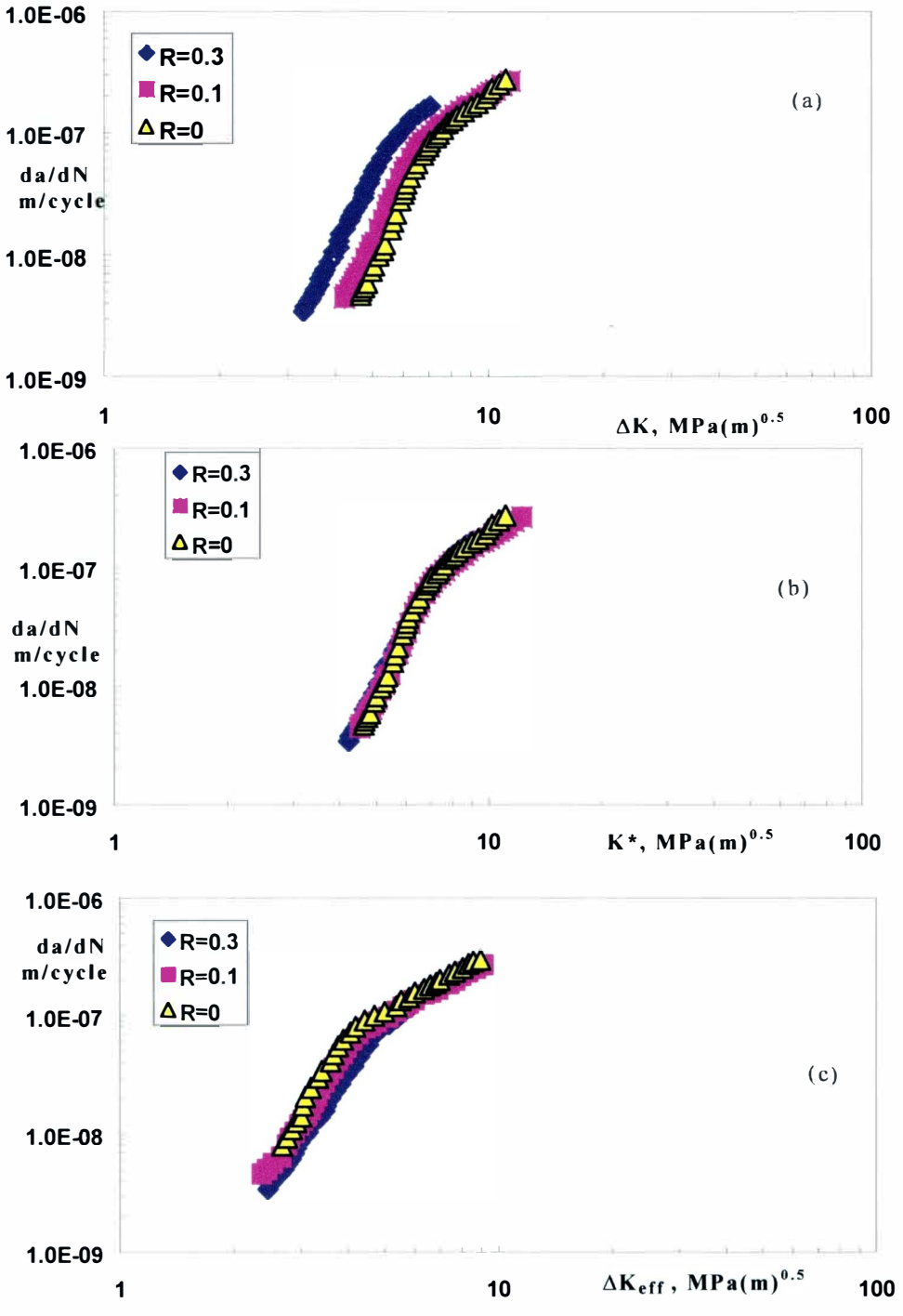

Figure 77. Fatigue crack growth data [20] of 7075-T651 as a function of (a) ΔK; (b) K^*(first method); (c) ΔK_{eff}.

APPENDIX : F

CORRELATION OF EXPERIMENTAL CRACK GROWTH DATA USING g FUNCTION

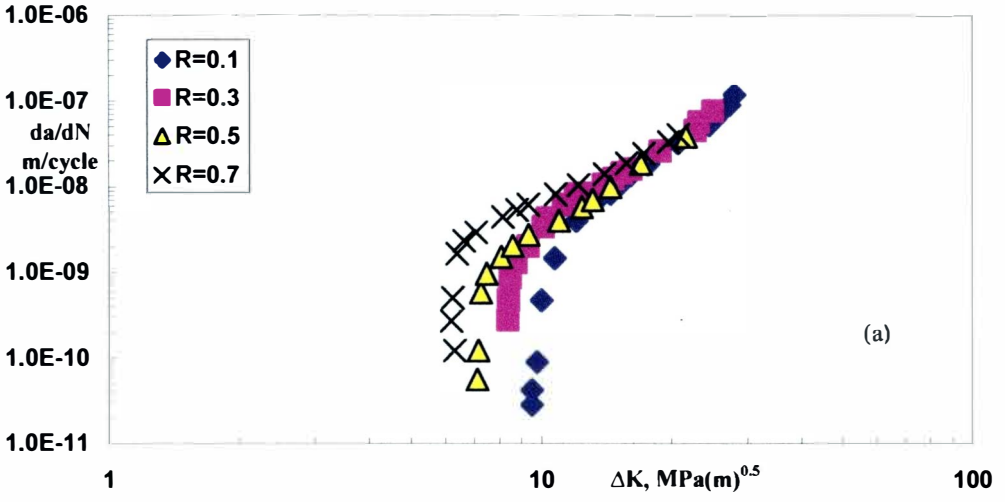

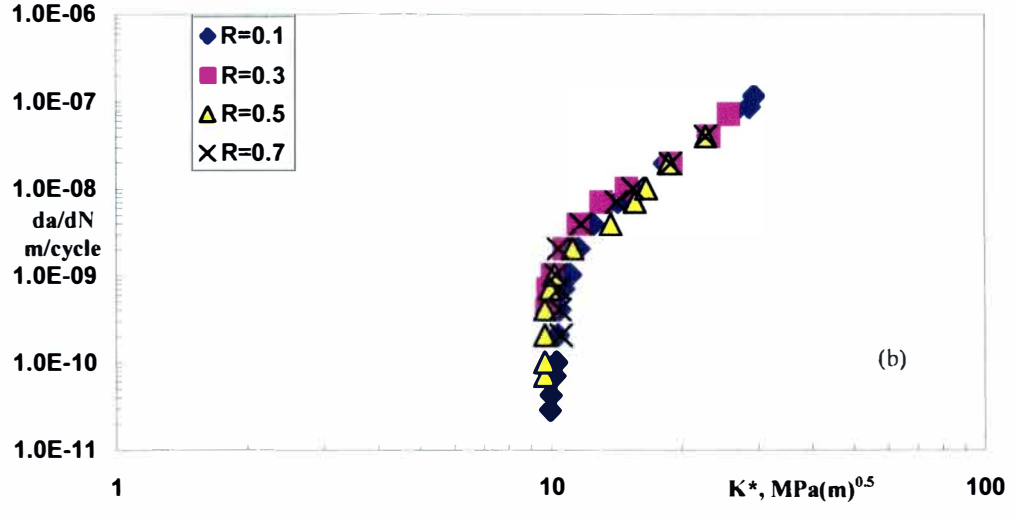

Figure 78. Fatigue crack growth data [38] of AISI 1020 steel as a function of (a) ΔK; (b) K*(using g function).

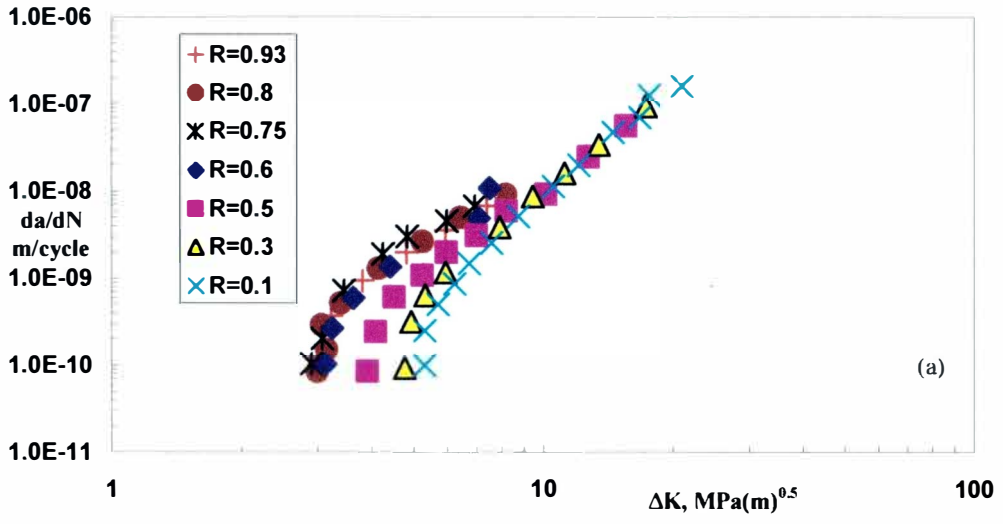

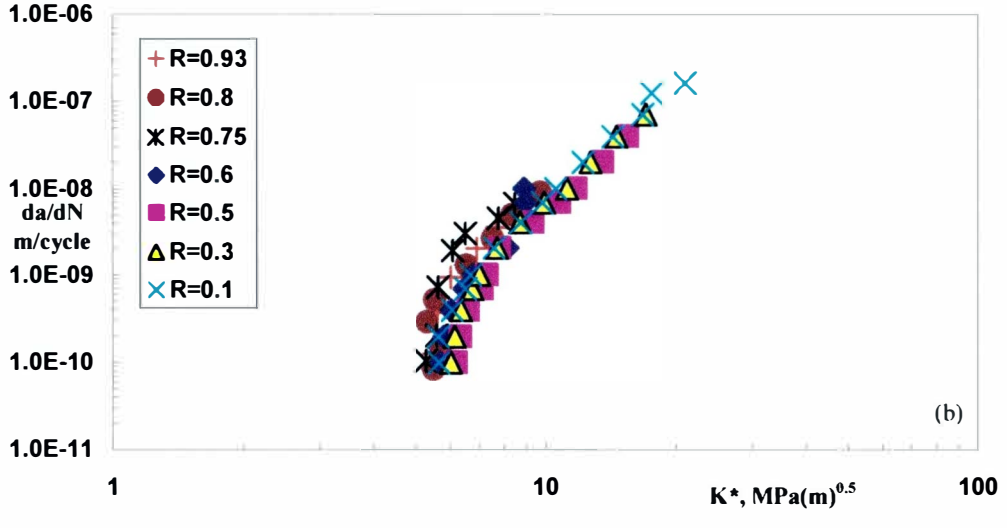

Figure 79. Fatigue crack growth data [39] of pure iron microstructure steel as a function of (a) ΔK; (b) K*(using g function).

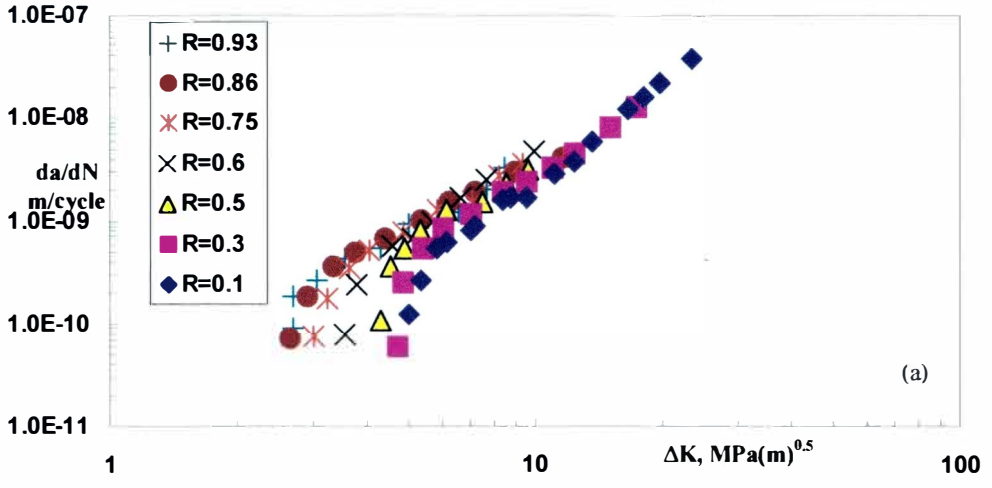

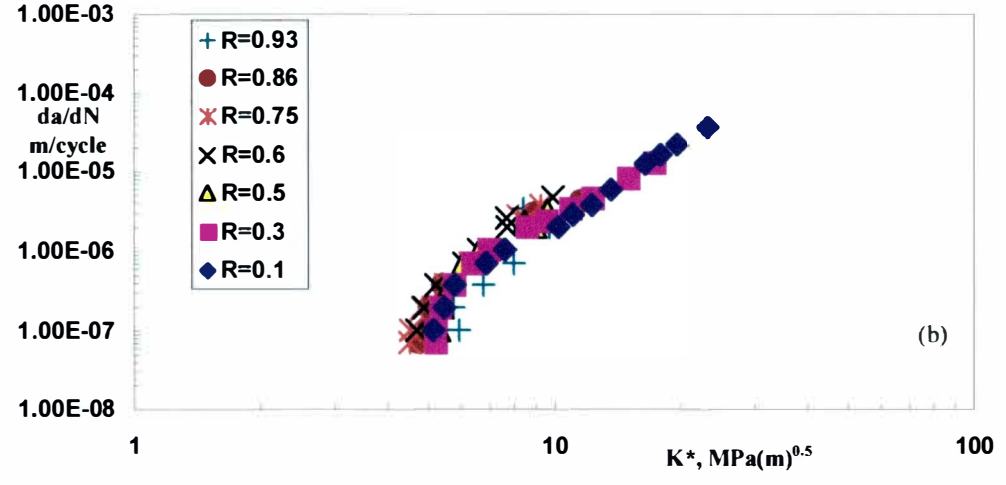

Figure 80. Fatigue crack growth data [39] of martensite microstructure as a function of (a) ΔK; (b) K*(using g function).

APPENDIX : G

CORRELATION OF EXPERIMENTAL CRACK GROWTH DATA USING MASTER CURVE APPROACH

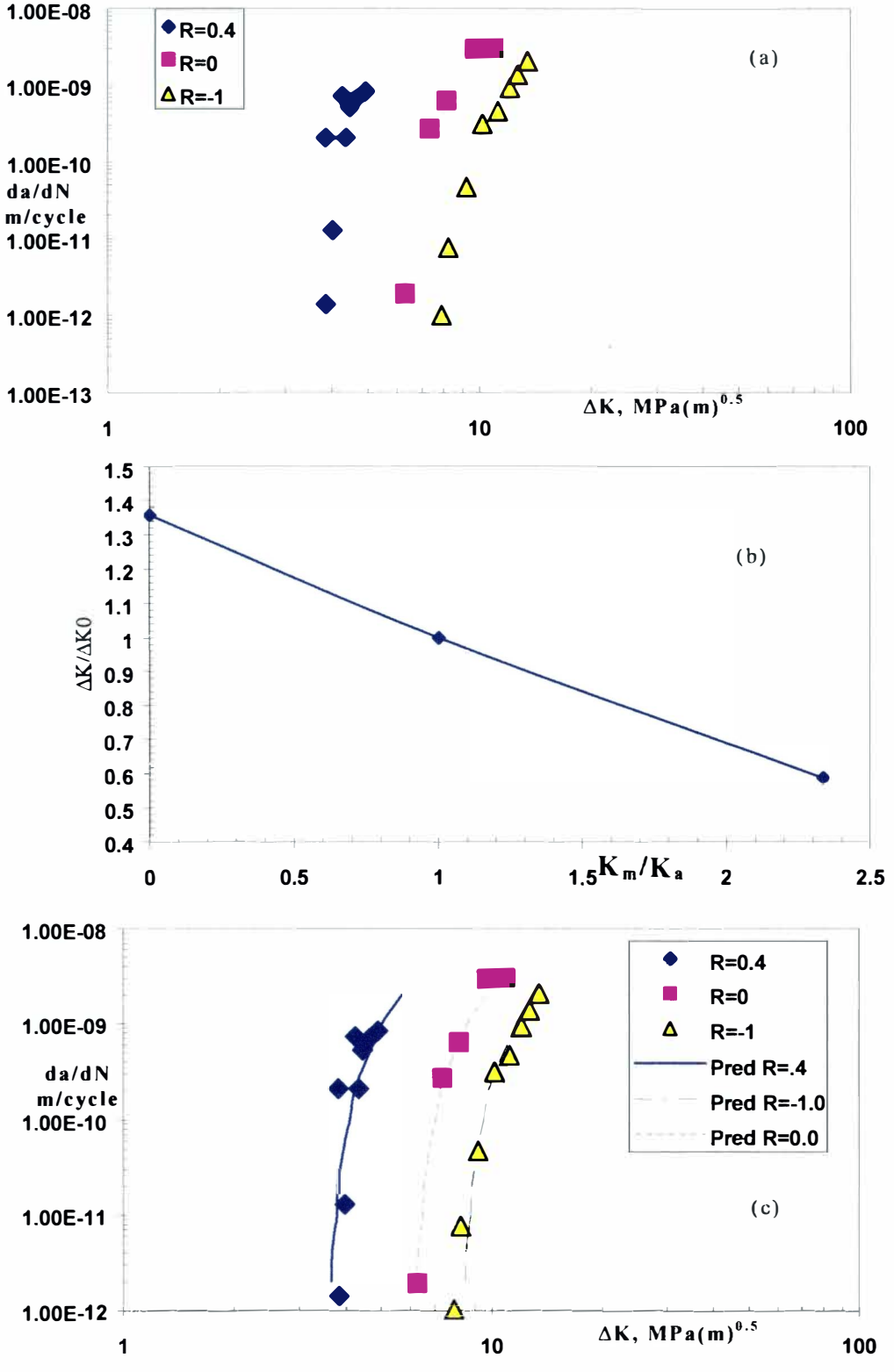

Figure 81. (a)Experimental fatigue crack growth data [35] of copper; (b)master curve of $\Delta K/\Delta K_0$ vs K_m/K_a ; (c)Predicted fatigue crack growth data compared with experimental data.

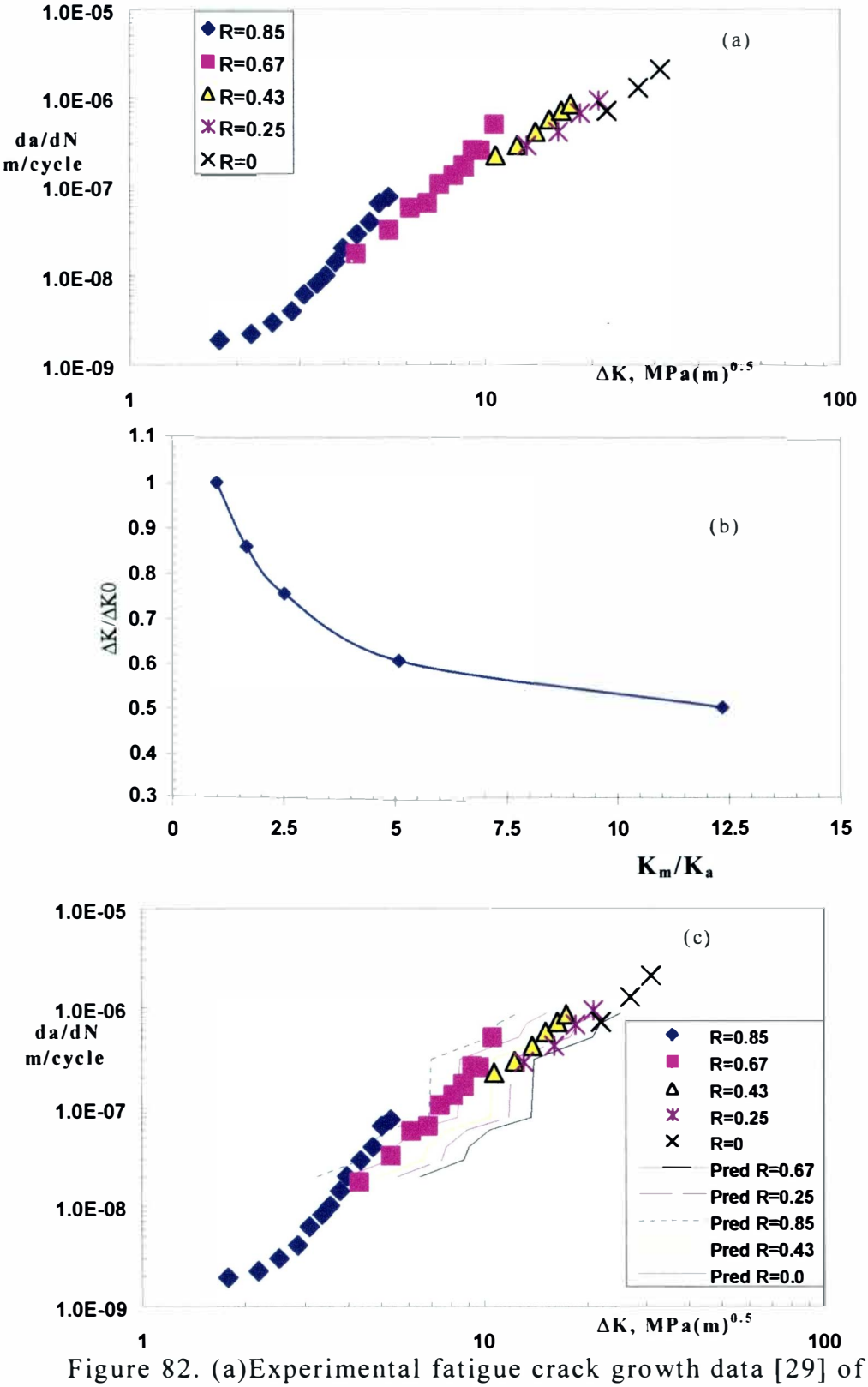

Figure 82. (a)Experimental fatigue crack growth data [29] of Ti-8-1-1; (b)master curve of $\Delta K/\Delta K_0$ vs K_m/K_a ; (c)Predicted fatigue crack growth data compared with experimental data.

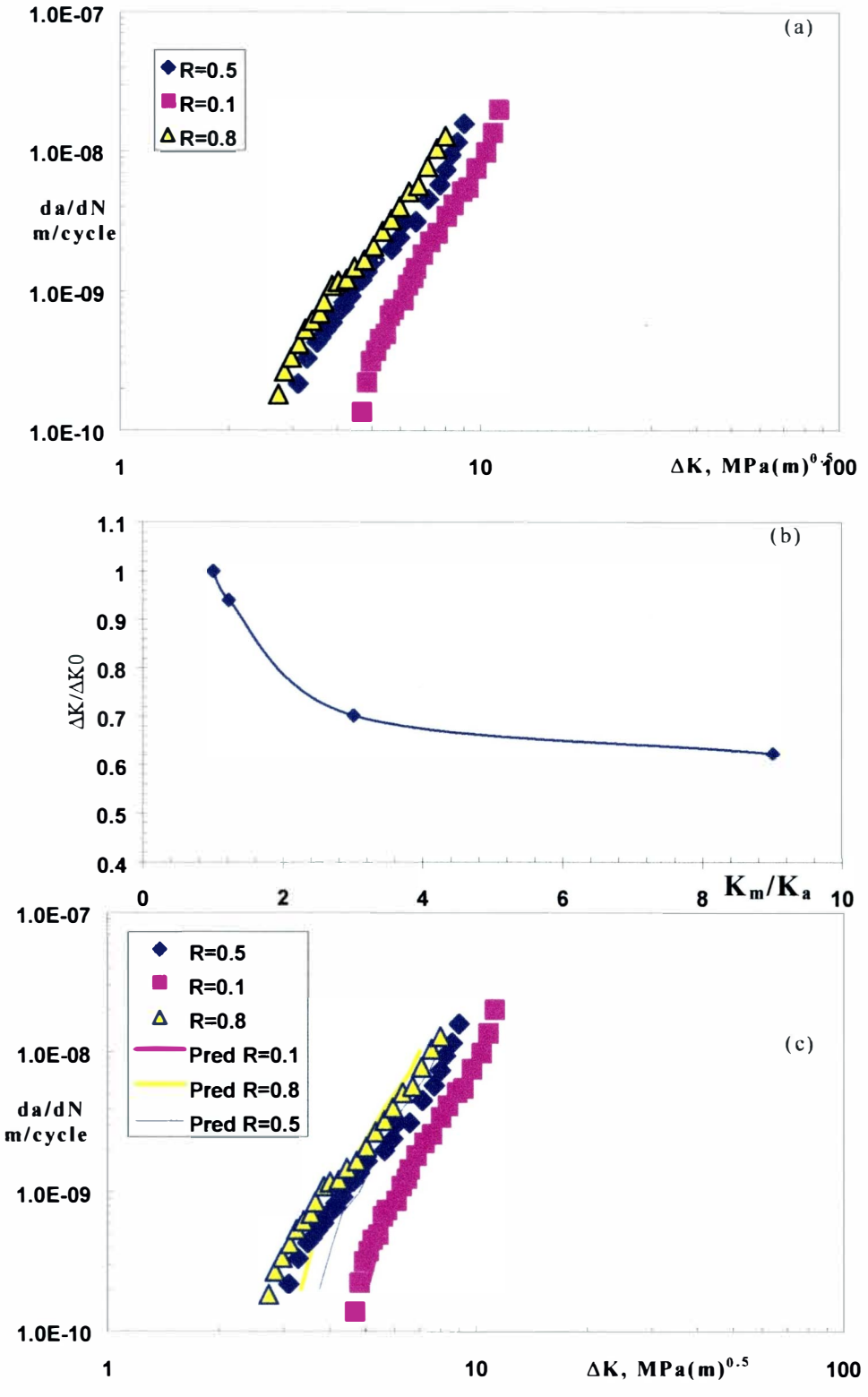

Figure 83. (a)Experimental fatigue crack growth data of [23] of Ti-6Al-4V ; (b)master curve of $\Delta K/\Delta K_0$ vs K_m/K_a ; (c)Predicted fatigue crack growth data compared with experimental data.

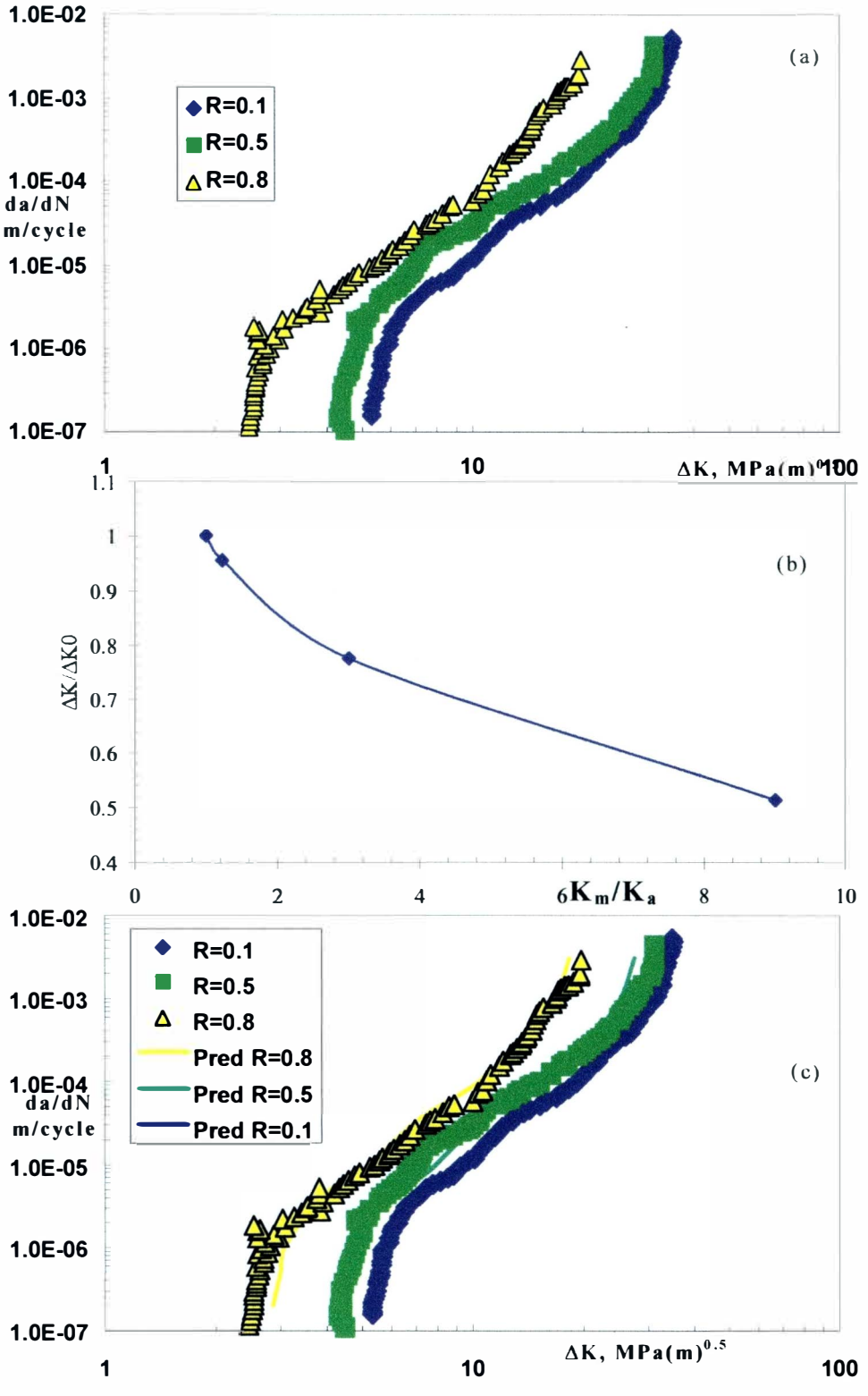

Figure 84. (a)Experimental fatigue crack growth data of [24] of Ti-10V-2Fe-3Al; (b)master curve of $\Delta K/\Delta K_0$ vs K_m/K_a ; (c)Predicted fatigue crack growth data compared with experimental data.

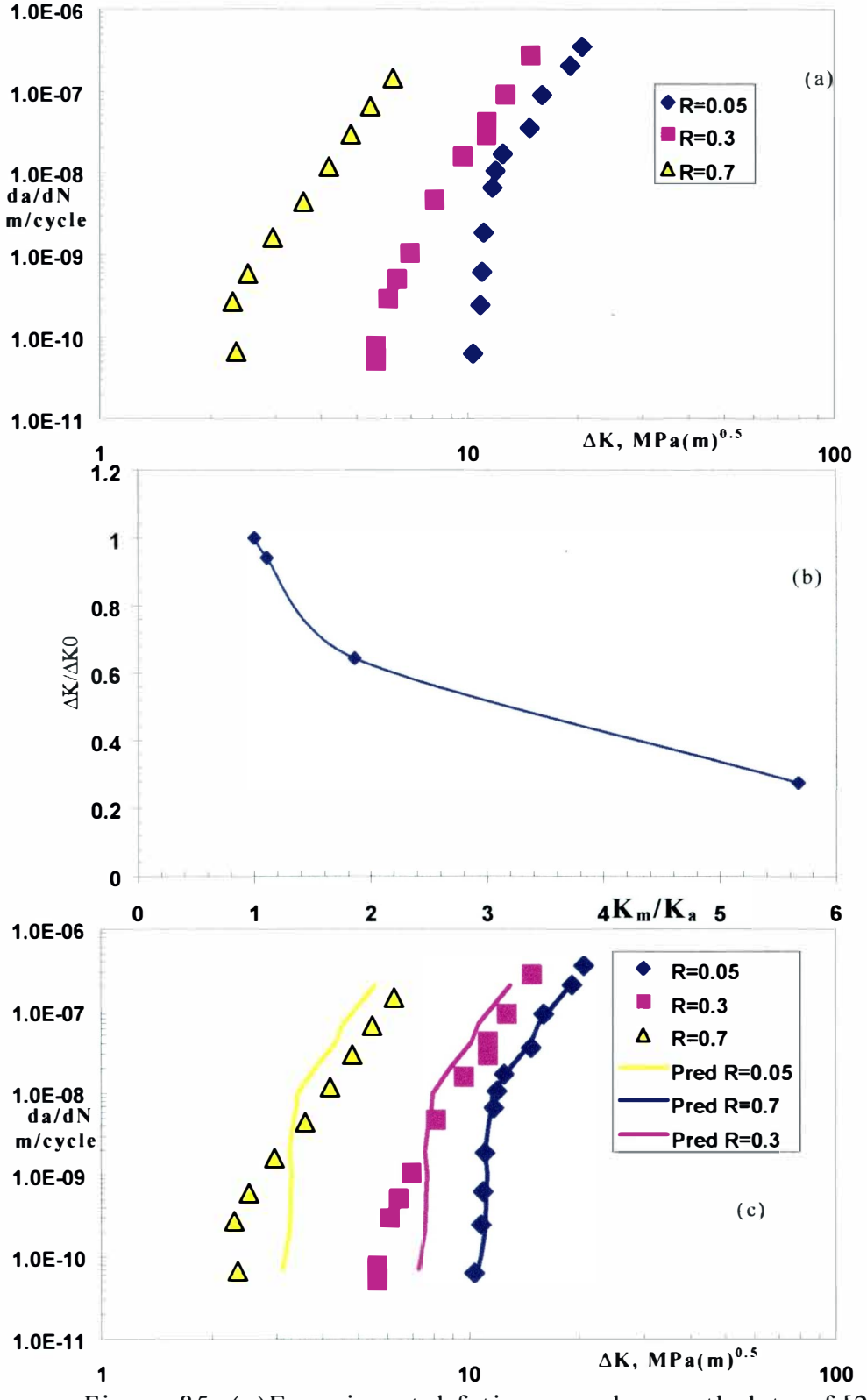

Figure 85. (a)Experimental fatigue crack growth data of [27] of spherodical cast iron; (b)master curve of $\Delta K/\Delta K_0$ vs K_m/K_a (c)Predicted fatigue crack growth data compared with experimental data.

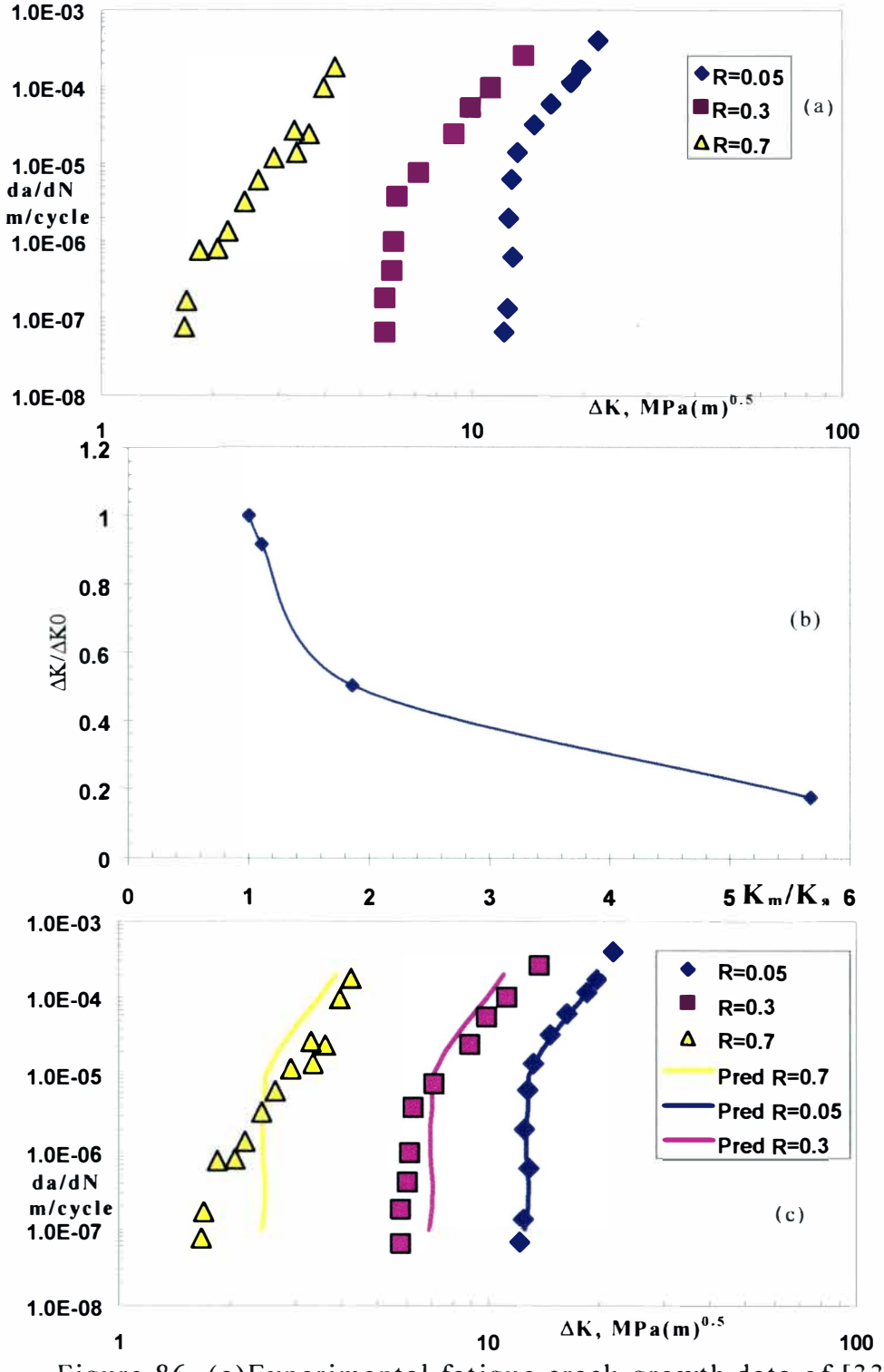

Figure 86. (a)Experimental fatigue crack growth data of [33] of ferrite microstructure; (b)master curve of $\Delta K/\Delta K_0$ vs K_m/K_a ; (c)Predicted fatigue crack growth data compared with experimental data.

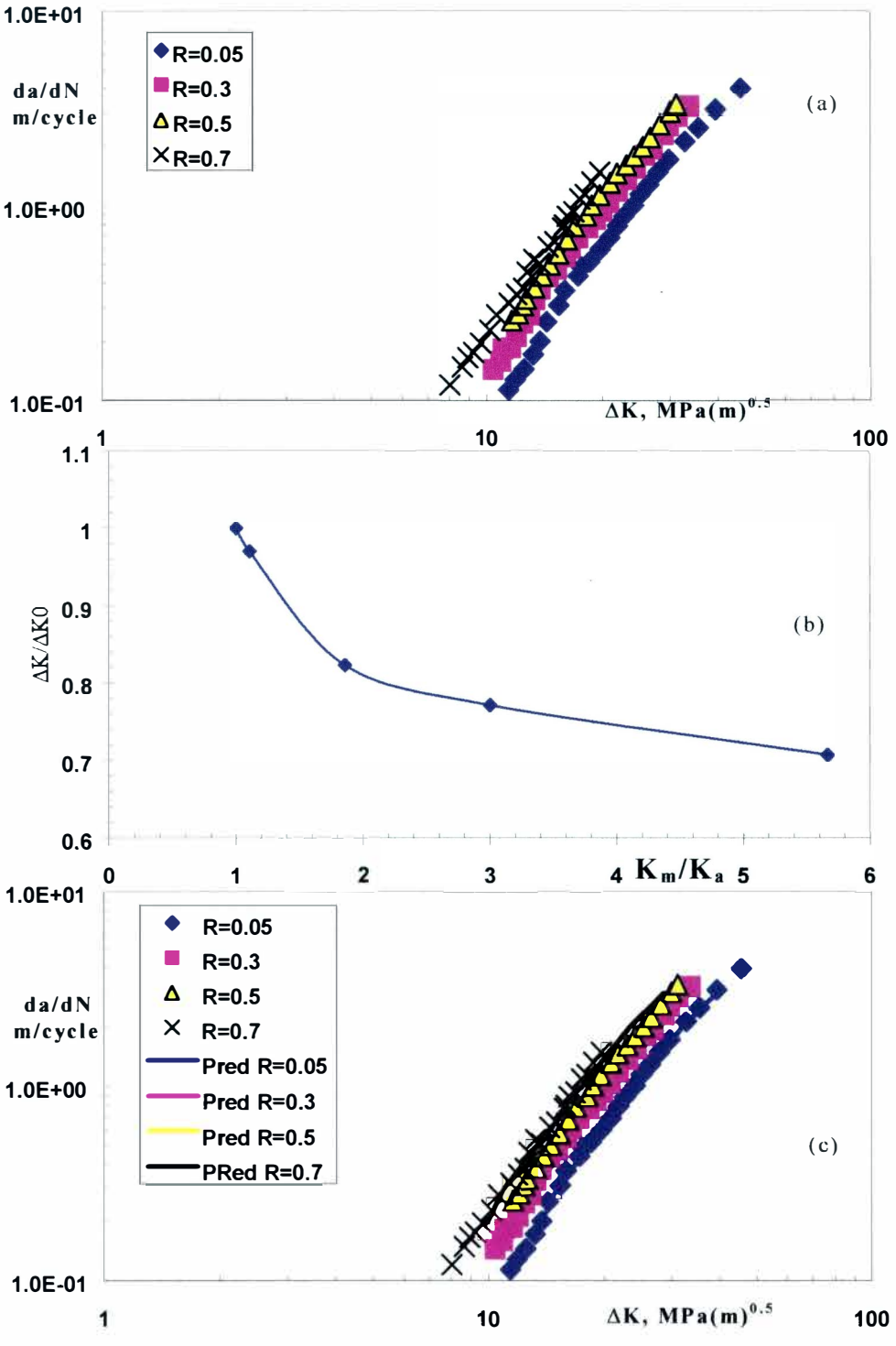

Figure 87. (a)Experimental fatigue crack growth data of [26] of 300M steel; (b)master curve of $\Delta K/\Delta K_0$ vs K_m/K_a ; (c)Predicted fatigue crack growth data compared with experimental data.

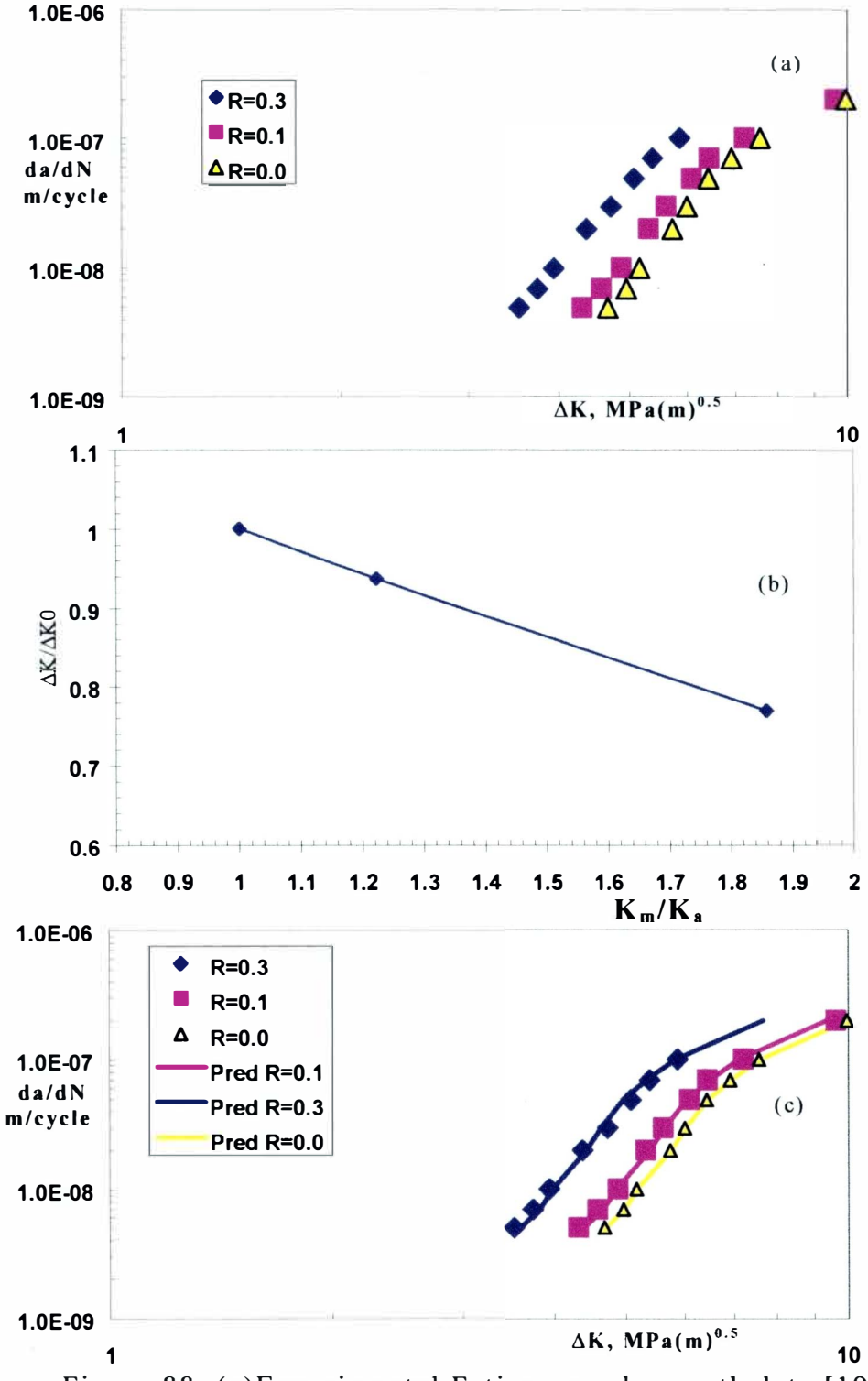

Figure 88. (a)Experimental Fatigue crack growth data [19] of 7075-T651; (b)master curve of $\Delta K/\Delta K_0$ vs K_m/K_a ; (c)Predicted Fatigue crack growth data compared with experimental data.

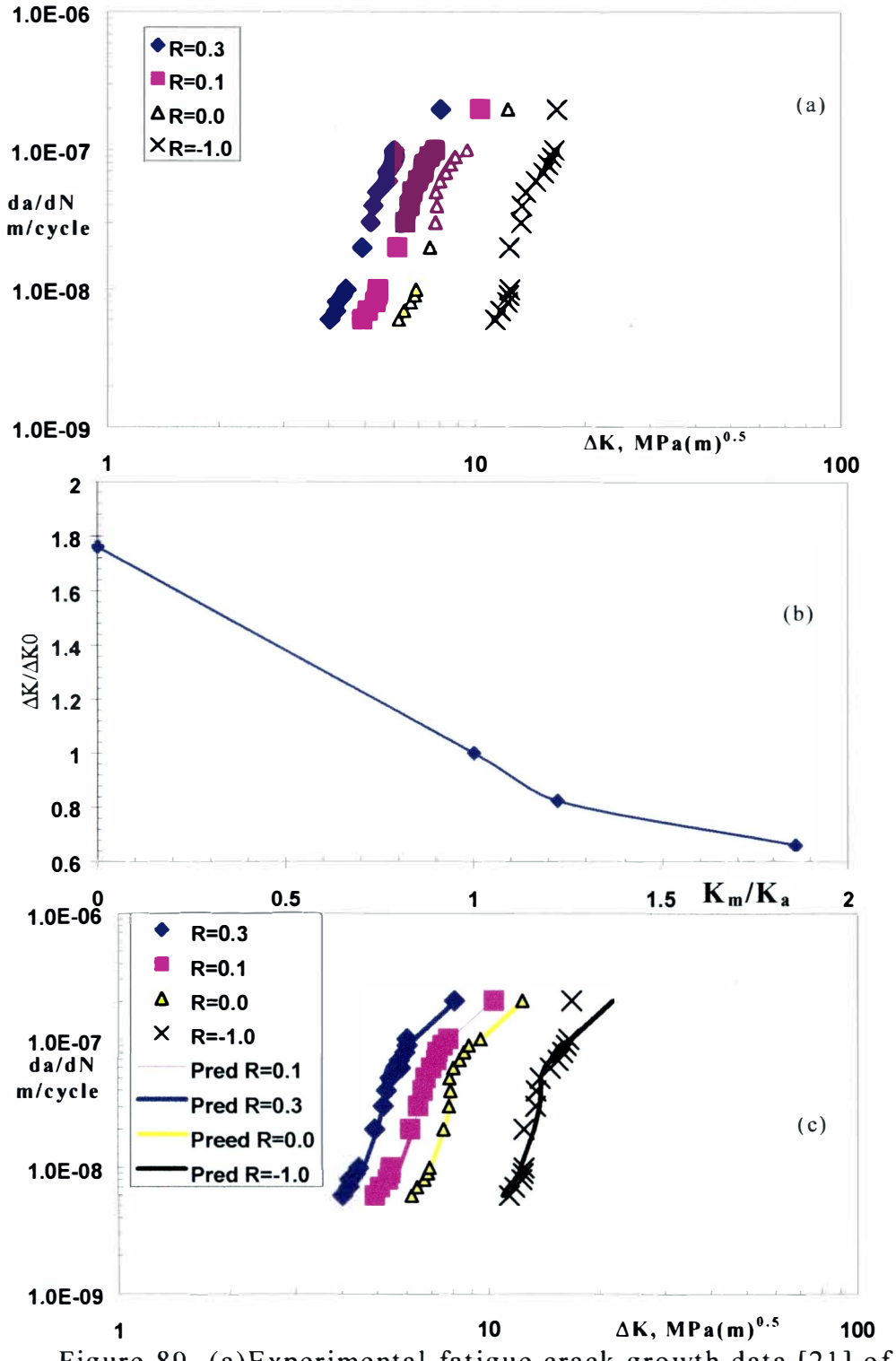

Figure 89. (a)Experimental fatigue crack growth data [21] of 7075-T7451; (b)master curve of $\Delta K/\Delta K_0$ vs K_m/K_a ; (c)Predicted fatigue crack growth data compared with experimental data.

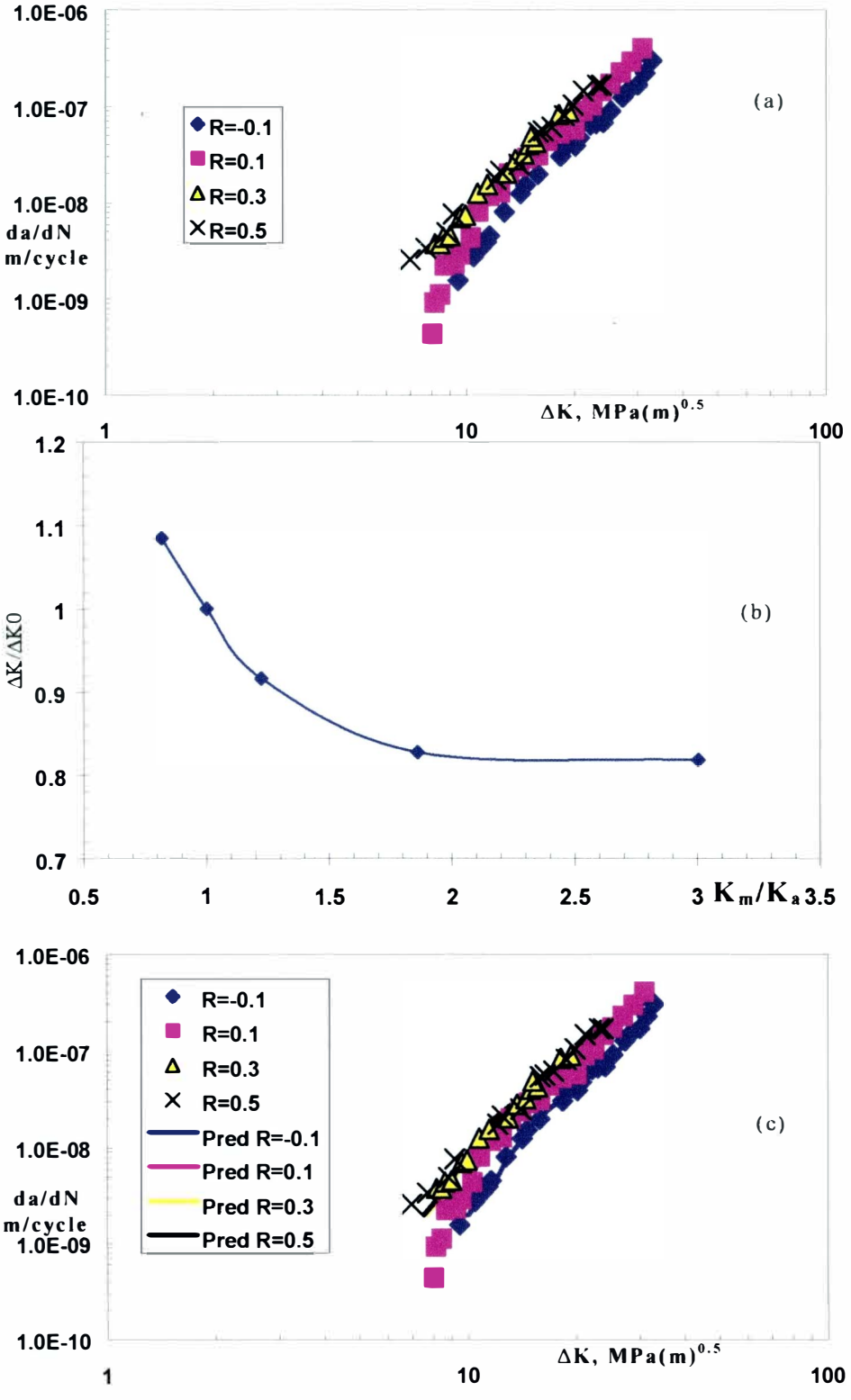

Figure90. (a)Experimental fatigue crack growth data [32] of 304 stainless steel; (b)master curve of $\Delta K/\Delta K_0$ vs K_m/K_a ; (c)Predicted fatigue crack growth data compared with experimental data.

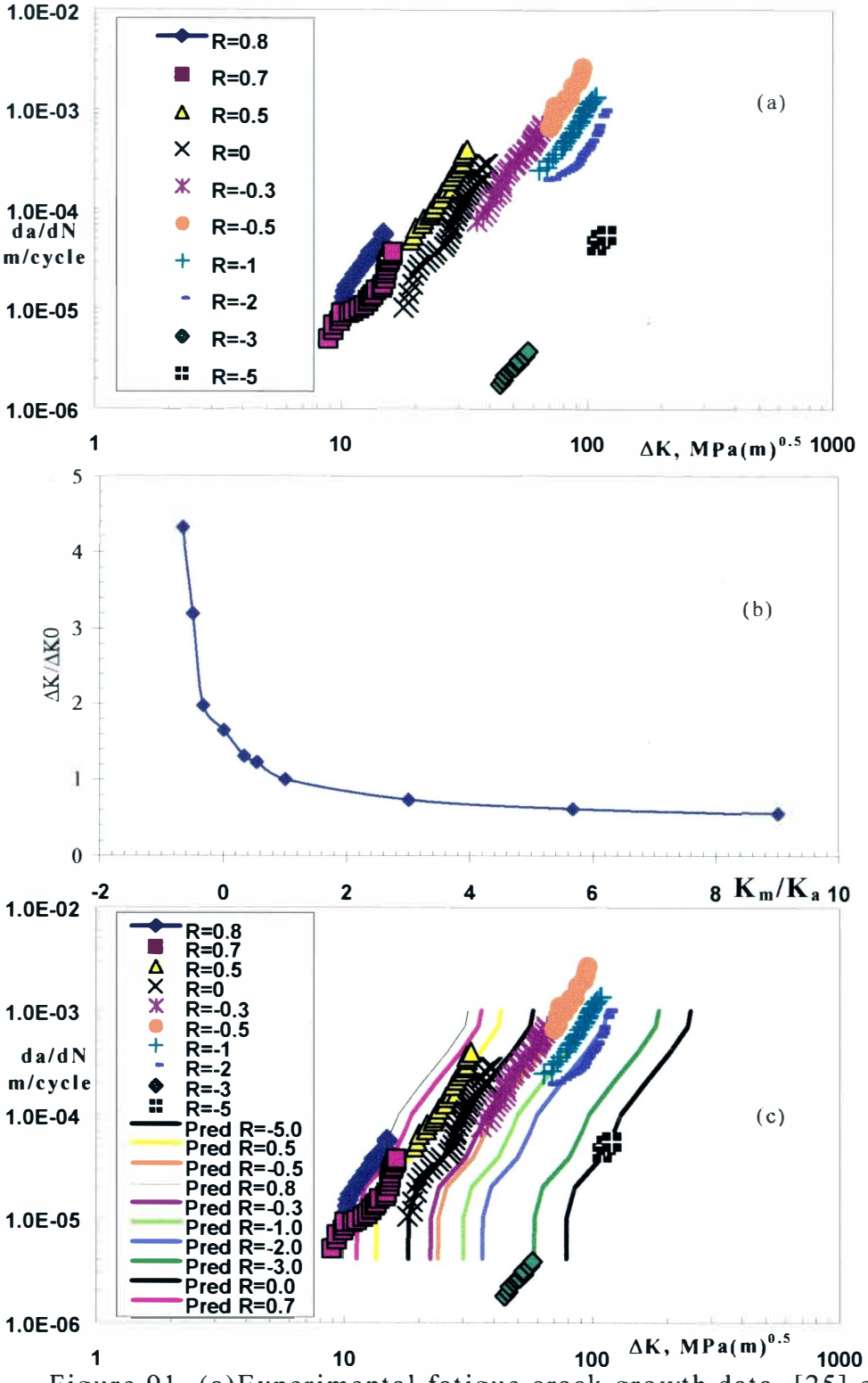

Figure 91. (a)Experimental fatigue crack growth data [25] of structural steel; (b)master curve of $\Delta K/\Delta K_0$ vs K_m/K_a ; (c)Predicted fatigue crack growth data compared with experimental data.

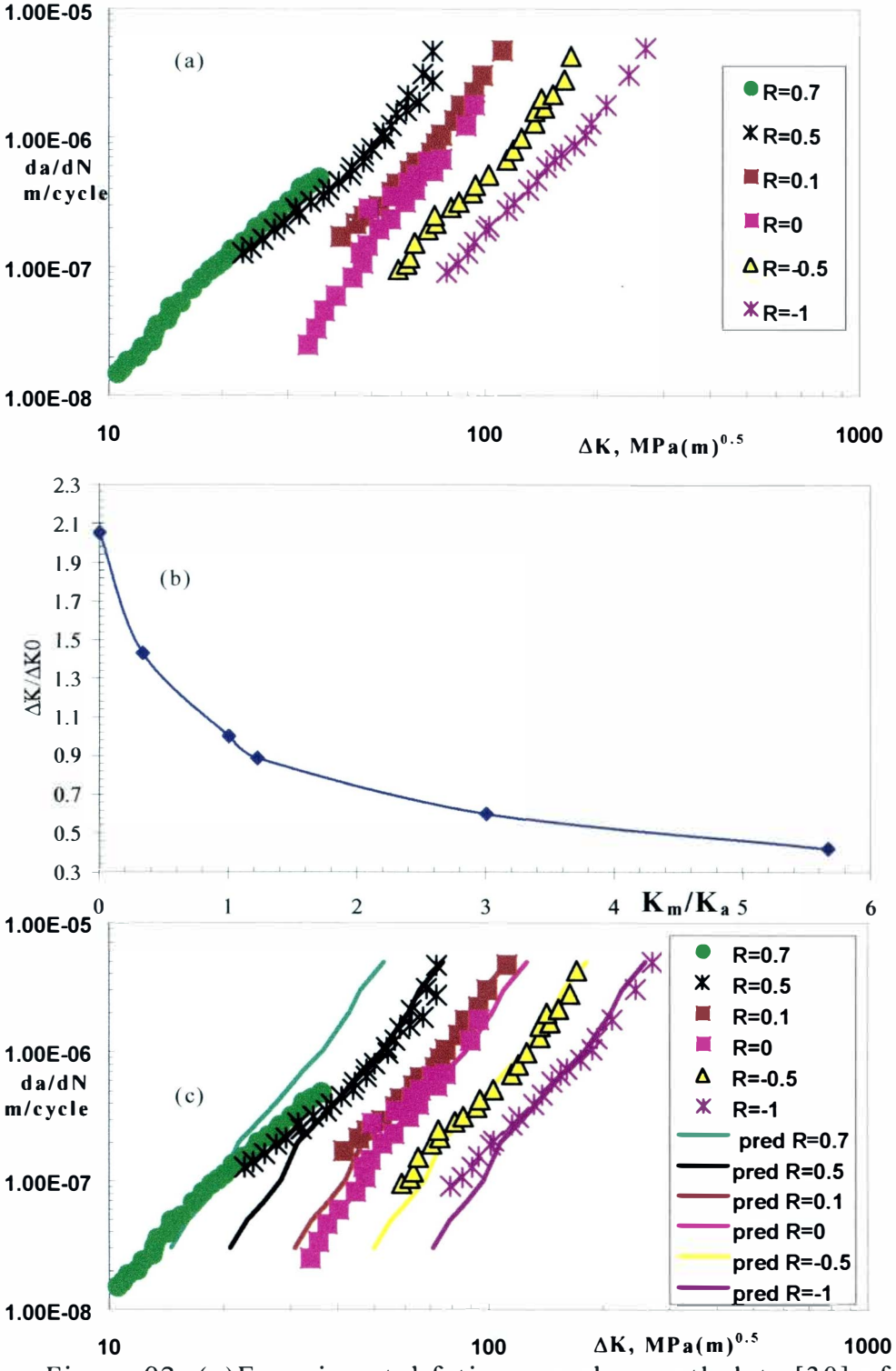

Figure 92. (a)Experimental fatigue crack growth data [30] of AISI 4340 steel; (b)master curve of $\Delta K/\Delta K_0$ vs K_m/K_a ; (c)Predicted fatigue crack growth data compared with experimental data.

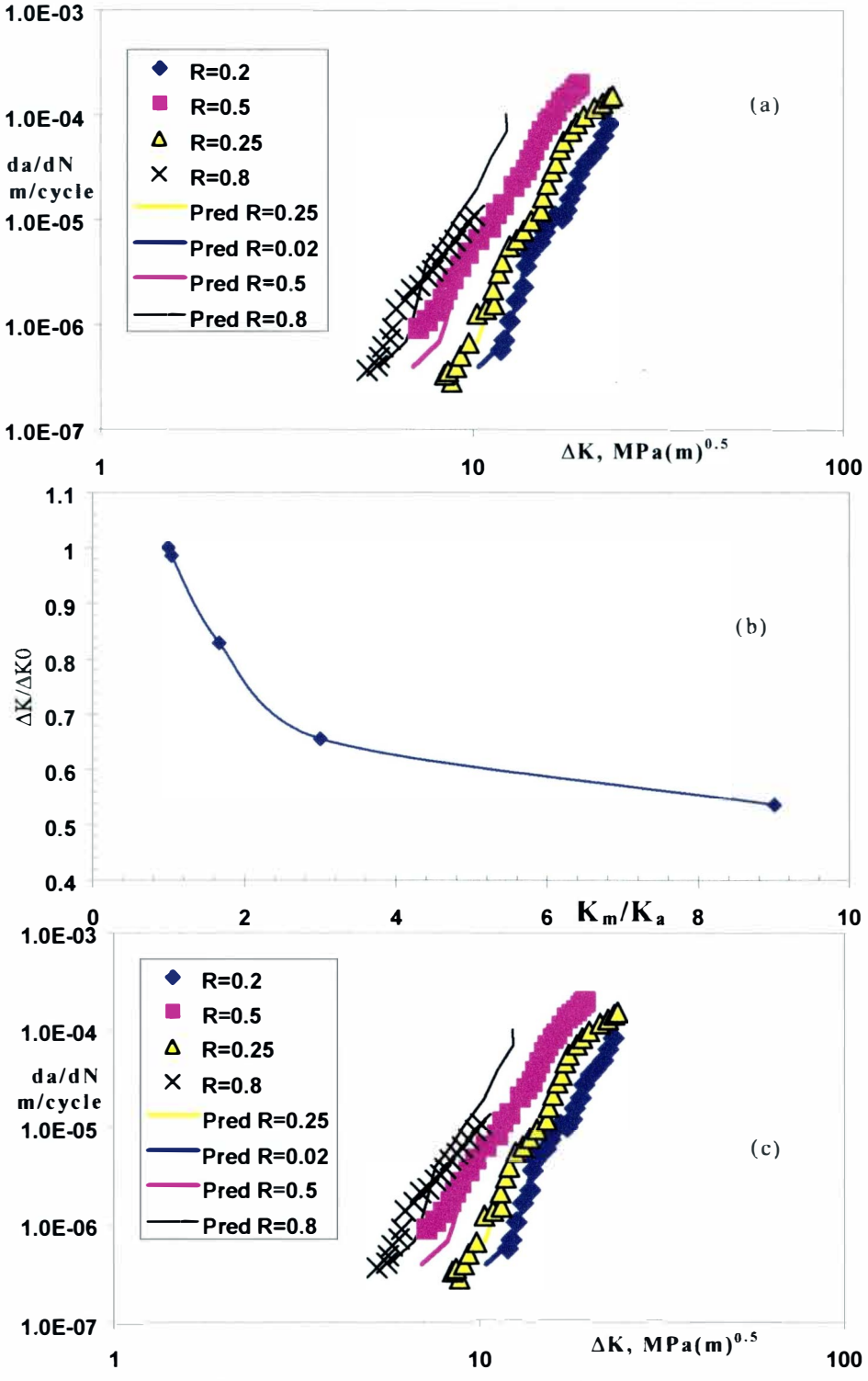

Figure 93. (a)Experimental fatigue crack growth data of [9] of Ti-6Al-4V; (b)master curve of $\Delta K/\Delta K_0$ vs K_m/K_a ; (c)Predicted fatigue crack growth data compared with experimental data.

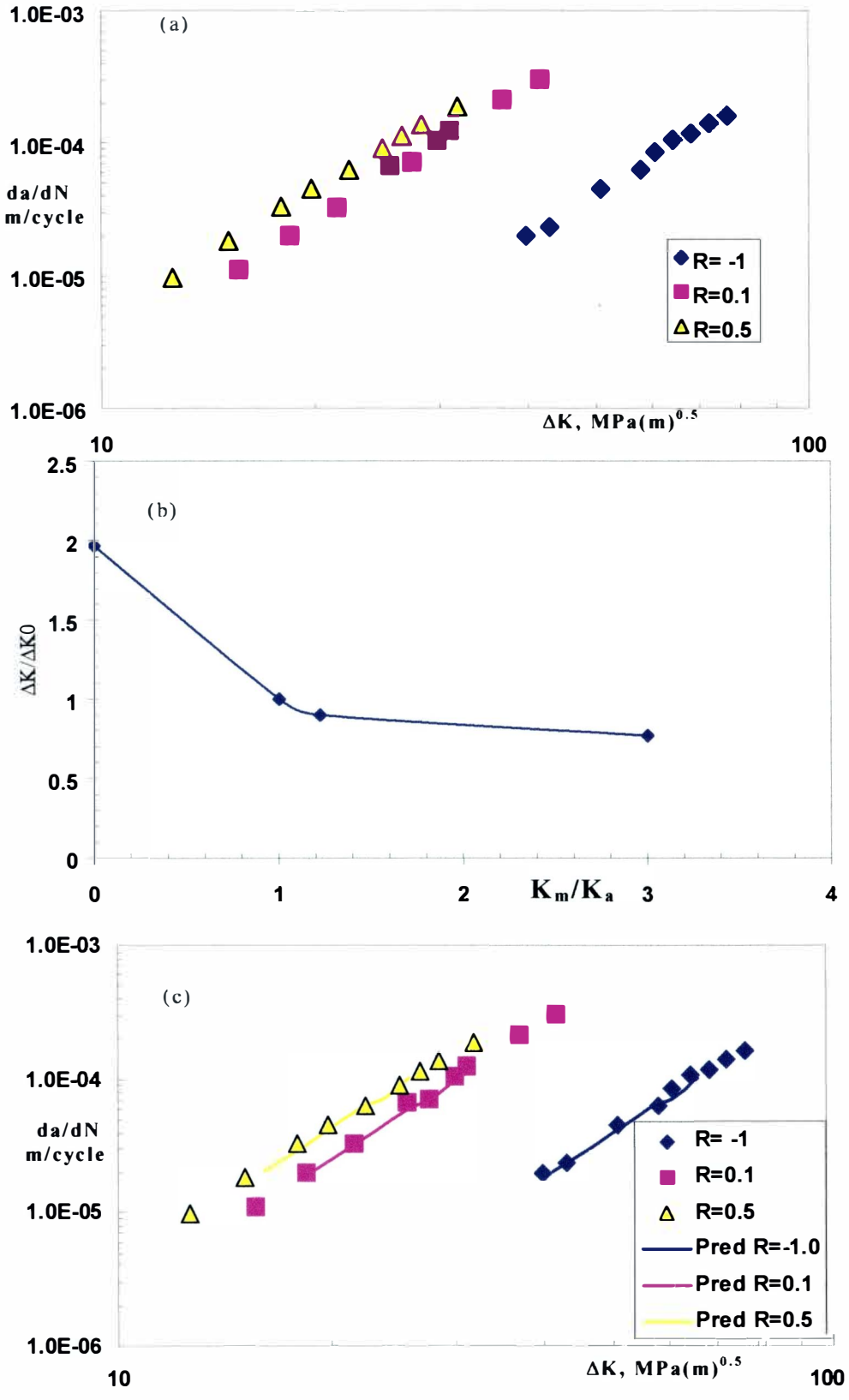

Figure 94. (a)Experimental fatigue crack growth data of [19] Udimet 720 Al; (b)master curve of $\Delta K/\Delta K_0$ vs K_m/K_a ; (c)Predicted fatigue crack growth data compared with experimental data.

APPENDIX : H

PREDICTION ACCURACY OF MASTER CURVE APPROACH

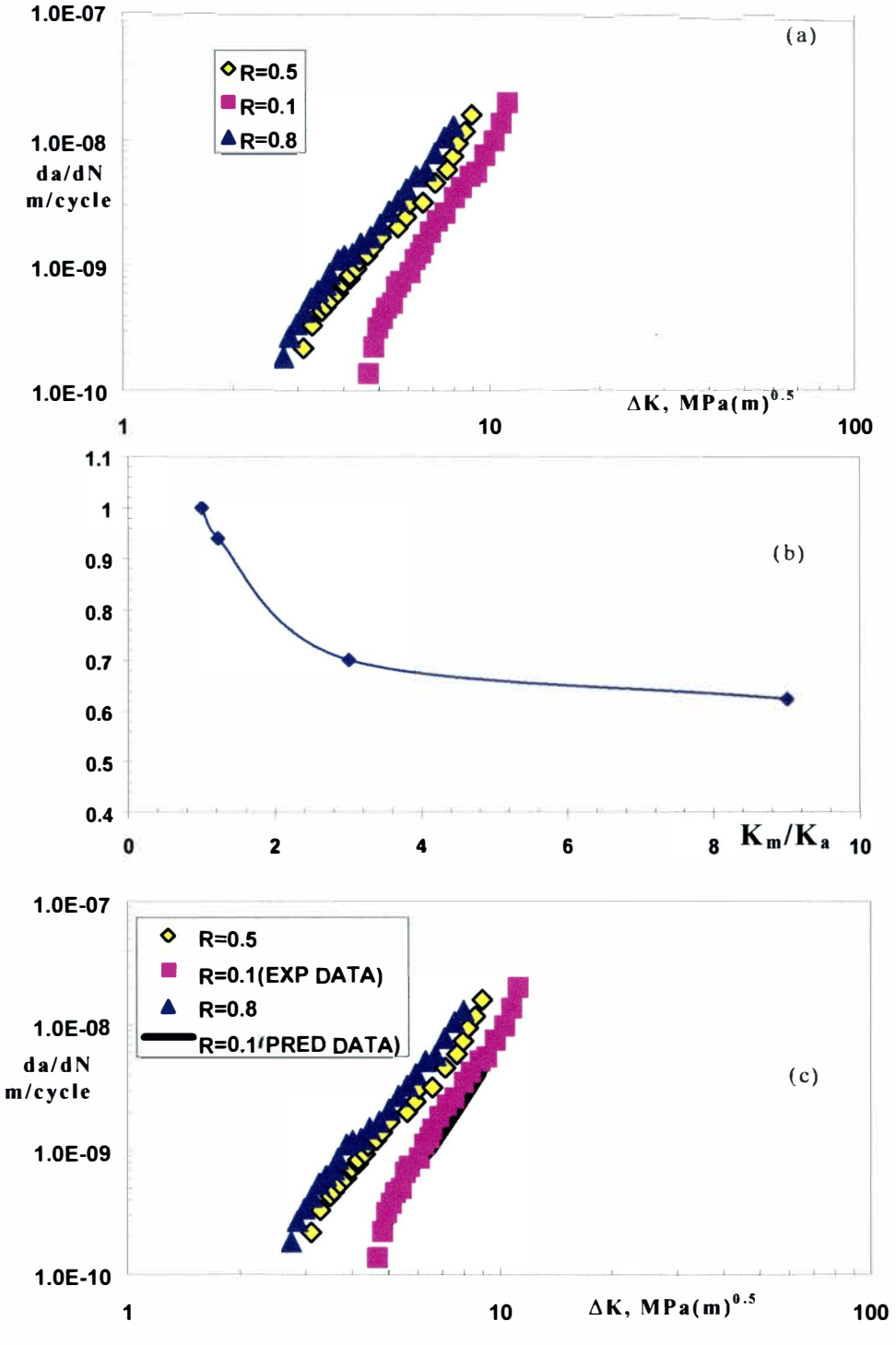

Figure 95. (a)Experimental fatigue crack growth data of [23] of Ti-6Al-4V ; (b)master curve of $\Delta K/\Delta K_0$ vs K_m/K_a ; (c)Predicted fatigue crack growth data for R=0.1compared with experimental data.

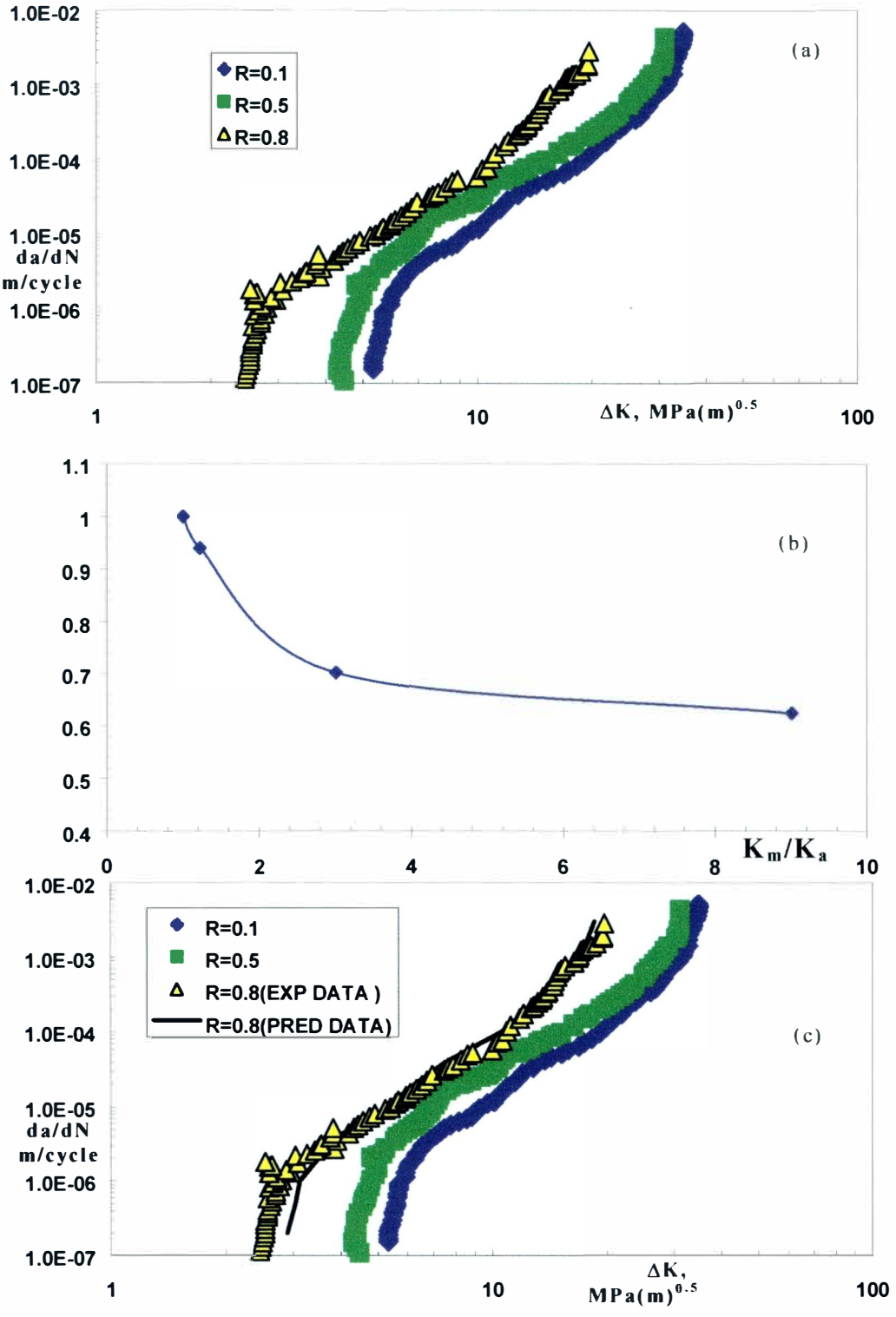

Figure 96. (a)Experimental fatigue crack growth data of [24] of Ti-10V-2Fe-3Al; (b)master curve of $\Delta K/\Delta K_0$ vs K_m/K_a ; (c)Predicted fatigue crack growth data for R=0.8 compared with experimental data.

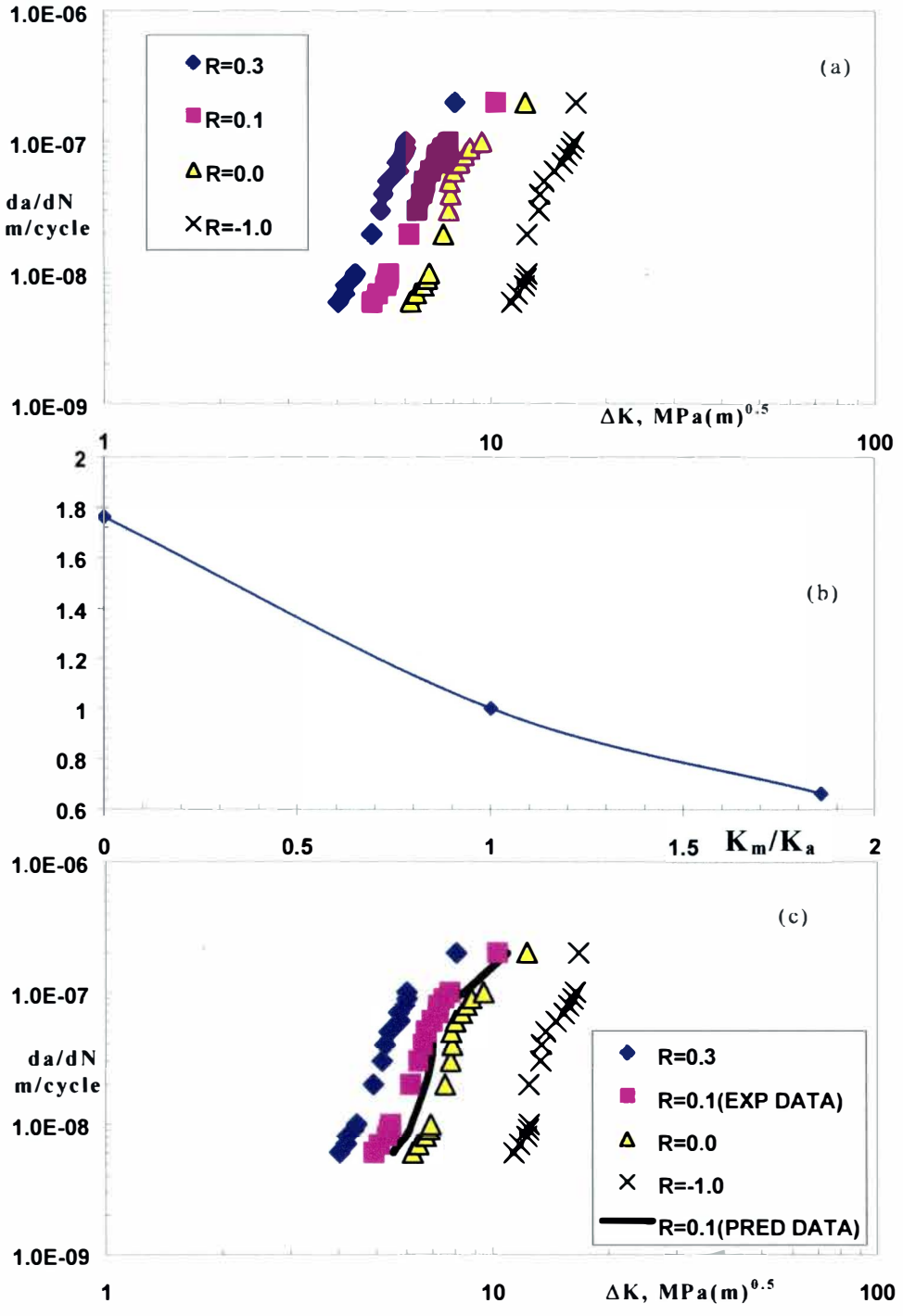

Figure 97. (a)Experimental fatigue crack growth data [21] of 7075-T7451; (b)master curve of $\Delta K/\Delta K_0$ vs K_m/K_a ; (c)Predicted fatigue crack growth data for R=0.1compared with experimental data.

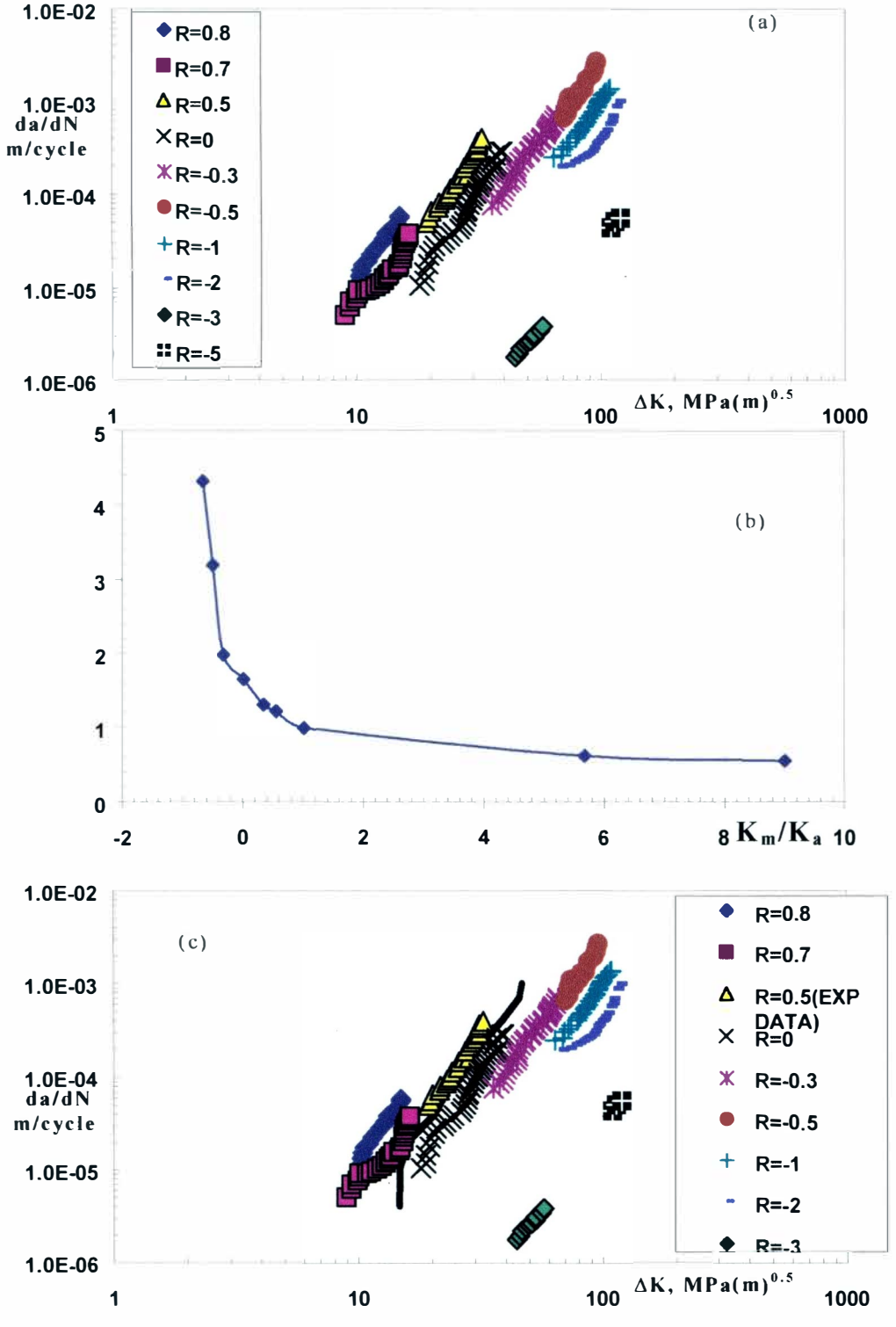

Figure 98. (a)Experimental fatigue crack growth data [25] of structural steel; (b)master curve of $\Delta K/\Delta K_0$ vs K_m/K_a ; (c)Predicted fatigue crack growth data for R=0.5 compared with experimental data.